ELUCIDATING THE FUNCTIONAL ROLE OF CCCTC-BINDING FACTOR (CTCF) IN HEPATOCELLULAR CARCINOMA

ZHANG YAJING

PhD

The Hong Kong Polytechnic University

2023

The Hong Kong Polytechnic University

Department of Applied Biology and Chemical Technology

Elucidating the Functional Role of CCCTC-binding Factor (CTCF) in Hepatocellular Carcinoma

ZHANG YAJING

A thesis submitted in partial fulfillment of the requirements for the Degree of Doctor of Philosophy

JAN 2023

CERTIFICATE OF ORIGINALITY

I hereby declare that this thesis is my own work and that, to the best of my knowledge and belief, it reproduces no material previously published or written, nor material that has been accepted for the award of any other degree or diploma, except where due acknowledgement has been made in the text.

Student Name: ZHANG Yajing

Signed:

Abstract

Hepatocellular carcinoma (HCC) is the most prevalent cause of cancer and cancer death in the world, where China accounts for more than half of new cases worldwide. Despite the advances in cancer treatments, the prognosis of HCC remains poor. Therefore, a thorough understanding of the mechanisms regarding HCC growth and metastasis is essential for the development of more effective treatments. Earlier evidence suggested that CCCTC-binding factor (CTCF), a highly conserved nuclear factor involved in the maintenance of genome architecture and transcriptional regulations, plays a role in HCC cells growth and metastasis. Furthermore, overexpression of CTCF in HCC is also associated with poor prognosis of the patients. The goal of my study is to further delineate the functional role of CTCF in HCC pathogenesis. I successfully created CTCF-knockout cell models using CRISPR/Cas9 technology. I confirmed the known growth and metastatic phenotypes of CTCF deficiency using the CTCF-knockout cell models. Transcriptomic and chromatin-immunoprecipitations sequencing (ChIP-seq) analysis identified genes regulated by CTCF. Bioinformatic analysis of CTCF-regulated genes further revealed enrichment of biological pathways related to metabolic processes. Concordantly, the rate of oxidative phosphorylation, the glycolytic flux, NAD^+/NADH ratio, and cellular ATP levels, were compromised in CTCF knockout cells, confirming a functional role of CTCF in HCC energy metabolism. Analysis of CTCF-regulated genes related to metabolic processes revealed three genes that are

implicated in the regulation of cellular NAD^+/NADH ratio, which includes fatty acid desaturase 1 (FADS1), IQ Motif Containing GTPase Activating Protein 2 (IQGAP2), and glutamic-oxaloacetic transaminase 2 (GOT2), respectively, suggesting that these genes may mediate the phenotypes of CTCF deficiency. Accordingly, a significantly reduction in cellular NAD^+/NADH ratio was observed when FADS1 and IQGAP2 was knocked down in HCC cells respectively. Furthermore, knockdown of FADS1 and IQGAP2 respectively resulted in reduced HCC cell growth, cell migration and invasion, as well as oxidative phosphorylation and glycolytic flux, to an extent similar to the knockout CTCF knockout, suggesting that the two genes are potential players in the CTCF regulatory axis for metabolic regulation. Further works are required to confirm if ectopic expression of the two gene could rescue the phenotypes of CTCF knockout. My study has discovered a novel functional role of CTCF in HCC cells in energy homeostasis, suggested a potential HCC intervention strategy via CTCF inhibition.

Publications

Papers

1) The CCCTC-binding factor (CTCF)–forkhead box protein M1 axis regulates tumour growth and metastasis in hepatocellular carcinoma. Zhang B, **Zhang Y**, Zou X, Chan AWH, Zhang R, Lee TKW, Liu H, Lau EYT, Ho NPY, Lai PBS, Cheung YS, To KF, Wong HK, Choy KW, Keng VW, Chow LMC, Chan KKY, Cheng AS, and Ko BC*. Journal of Pathology, 2017;243:418-430.

2) Unconventional tonicity-regulated nuclear trafficking of NFAT5 mediated by KPNB1, XPOT and RUVBL2. Cheung, C.Y., Huang, T.-T., Chow, N., Zhang, S., Zhao, Y., Chau, M.P., Chan, W.C., Wong, C.C.L., Boassa, D., Phan, S., Ellisman, M.H., Yates, III, J.R., Xu, S., Yu, Z., **Zhang, Y**., Zhang, R., Ng, L.L., and Ko, B.C.B* (2022). J Cell Sci 135. https://doi.org/10.1242/jcs.259280.

3) CCCTC-binding factor (CTCF) regulates proliferation and metastasis of hepatocellular carcinoma via regulating cellular energy homeostasis. **Zhang**, **Y**., Liu H., Wang Y., Pardeshi L., Wong K.H., Zhao Y.X., Chow, L.M.C., LEE, T., Wong, J., Ko B.C.B.*. (2022). Manuscript in preparation.

Patent

Mainland China Patent (# 201910562893.1) CTCF inhibitors and their applications. Ko BC, Ma C, **Zhang YJ**, Chan WC, Cheung YC.

Awards

1) Best Oral Presentation Award, 3rd ABCT Research Postgraduate Symposium in the Biology Discipline (2022), The Hong Kong Polytechnic University. “Elucidating the functional role of CCCTC-binding factor (CTCF) in hepatocellular carcinoma”, **Zhang Yajing**, Hang Liu, Yixiang Wang, Lakhansing Pardeshi, Koon Ho Wong, Yan Xiang Zhao, Larry MC Chow, Terence LEE, Jason Wong, Ben C.B. Ko*.

2) Best Poster Award in Life Science (Second Prize), The Sunney and Irene Chan Lecture in Chemical Biology（2017), The Chinese University of Hong Kong. “CTCF-FoxM1 axis regulates tumor growth and metastasis in hepatocellular carcinoma”, Bin Zhang, **Yajing Zhang**, Xiaoping Zou, Anthony WH Chan, Rui Zhang, Terence Kin-Wah Lee, Hang Liu, Larry MC Chow, Ben CB Ko*.

Acknowledgement

First and foremost, I would like to extend my heartfelt gratitude to my supervisor, Dr Ko Chi-bun, Ben, for providing me with an opportunity to study my PhD in the Hong Kong Polytechnic University. I have gained a lot under the professional guidance of my supervisor. I would like to express my gratitude to Dr. KO for his careful guidance in the process of completing this thesis. During my PhD studies, Dr. KO was conscientious and responsible, giving his support and assistance to me. I appreciate his instructive comments and useful suggestions on my thesis.

Also, I am grateful and thankful to the Prof. Chow Ming-cheung, Larry, Prof. Zhao Yanxiang and Prof. Dr. Lee Kin-wah, Terence and their lab for the kind assistant and advice for my project. I also express my appreciation to Dr. Koon-Ho Wong and Dr. Lakhansing Pardeshi from University of Macau for the transcriptome analysis. I would also like to thank Dr. Jason Wong and his lab from The University of Hong Kong for bioinformatics analysis. Special thanks to Prof. Zhang Yaojun and Dr. Wang Juncheng from Guangzhou Sun Yat-sen University Cancer Centre, for providing the HCC specimens. Grateful acknowledgement is also made to Dr. Ma Cong, Dr. Zhao Qian and Dr. Wong Tsun-ting, Clarence for their kind advice and assistance. I also owe a special debt of gratitude to Dr. Liu Hang for his kind help and encouragement during my PhD research. I gratefully acknowledge the help of all the technicians and staffs of the Department of Applied Biology and Chemical Technology.

In addition, I deeply appreciate to Dr. Huang Tingting, Dr. Zhang Rui, Dr. Chris Cheung, Dr. Chan Wing Cheung, Ricky, Mr. Wang Yixiang, Mr. Leung Ming Fai, Allen, Ms. Chau Po Ki, Mary, Mr. Liu Mingkang in Dr. KO's lab for their kind help and encouragement. I would also like to express my deep gratitude to my friends, Dr. Chen Teng, Dr. Peng Li, Dr. Li Xiaoxiao, Dr. Wang Miaomiao, Dr. Sun Wenqin, Ms. Su Xiaochun, Ms. Li Shuqi, Ms. Zhang Shuqi, Ms. Liu Yang and Ms. Wang Xiao for their kind help and enthusiastic encouragement.

Last but not the least, I am indebted to my parents for their encouragement and support during my PhD study. Thanks for being there when I needed you.

I would like to give my heartfelt thanks to all the people who have ever helped me.

Table of Content

List of Figures and Tables

List of Abbreviations

HCC	Hepatocellular carcinoma
NAFLD	Nonalcoholic fatty liver disease
TACE	Transarterial chemoembolization
HBV	Hepatitis B virus
HCV	Hepatitis C virus
NASH	Non-alcoholic steatohepatitis
CGH	Comparative genomic hybridization
RIZ1	Rb-interacting zinc finger 1
CDH1	E-cadherin
HMT	Histone methyltransferase
HAT	Histone acetyltransferase
HDAC	Histone deacetylase
PCAF	P300/CBP-associated factor
lncRNA-HEIH	lncRNA high expression in HCC
TNF-α	Tumor necrosis factor alpha
IL-6	Interleukin 6
IL-1β	Interleukin-1β
VCAM-1	Vascular cell adhesion protein 1
ICAM-1	Intercellular adhesion molecule 1
MCP-1	Monocyte chemoattractant protein 1
SLC7A11	Solute carrier family 7 member 11
PD-L1	Programmed death ligand 1
CSF1	Colony-stimulating factor 1

TAM	Tumor-associated macrophage
MDSC	Myeloid-derived suppressor cell
HSEC	Hepatic sinusoidal endothelial cell
ICR	ICAM-1-related long non-coding RNA
CSC	Cancer stem cell
MSC	Mesenchymal stromal cell
CXCL8/IL-8	C-X-C motif chemokine ligand 8
CCL2/MCP-1	C-C motif chemokine ligand 2
CXCL1-2-3/GRO	C-X-C motif chemokine ligand 1-2-3
ECM	Extracellular matrix
CAF	Carcinoma associated fibroblast
HSC	Hepatic stellate cell
TIL	Tumor-infiltrating lymphocyte
Th	T helper cells
TAM	Tumor-associated macrophage
SP	Side population
ABCG2	ATP Binding Cassette Subfamily G Member 2
EpCAM	Epithelial cell adhesion molecule
HpSC	Hepatic stem cells
TCF	T-cell factor
LEF-1	Lymphatic enhancer factor 1
MAPK	Mitogen-activated protein kinases
RTK	Receptor tyrosine kinases
JNK	c-Jun N-terminal kinase
EGF	Epidermal growth factor

VEGF	Vascular endothelial growth factor
PDGF-β	Platelet-derived growth factor-β
TGF-α	Transforming growth factor-α
PIP3	Phosphatidylinositol-3,4,5-trisphosphate
PIP2	Phosphatidylinositol-4,5-trisphosphate
PH	Pleckstrin-homology
COX-2	Cyclooxygenase 2
MMP-2	Matrix metalloproteinase 2
GSK-3	Glycogen Synthase Kinase-3
STATs	Signal transducers and activators of transcription
EGFR	Epidermal growth factor receptors
TGFA	Transforming growth factor-α
HBEGF	Heparin-binding EGF-like growth factor
BTC	Betacellulin
AREG	Amphiregulin
EREG	Epiregulin
EPGN	Epigen
AFP	Alpha-fetoprotein
NCCN	National Comprehensive Cancer Network
CT	Computed tomography
MR	Magnetic resonance
LI-RADS	Liver Imaging Reporting and Data System
HS-GGT	Hepatoma-specific Gamma-glutamyl Transferase Isoenzyme
TGF-β1	Transforming Growth Factor-β1

IGF	Insulin-like Growth Factor
HGF	Hepatocyte Growth Factor
HSP	Heat Shock Protein
GPC3	Complement C3a, Glypican-3
SCCA	Squamous Cell Carcinoma Antigen
SIRT	Selective internal irradiation therapy
EMA	European Medicines Agency
CTCF	CCCTC binding factor
APP	Amyloid β-protein precursor
5'HS4	5'DNase-hypersensitive locus 4
ICR	Imprinting control region
XCI	X chromosome inactivation
TAD	Topologically associating domain
MRD21	Mental retardation 21
SRS	Silver-russell syndrome
BWS	Beckwith-Wiedemann syndrome
CBS	CTCF/cohesin binding site
ER	Estrogen Receptor
TFF3	Trefoil factor 3
TMPRSS3	Transmembrane protease, serine 3
P2RY2	P2Y purinoceptor 2
SOCS3	Suppressor 3 of cytokine signaling
STAT3	Signal transducer and activator of transcription 3
MT	Metallothionein
TERT	Telomerase reverse transcriptase

TRF1	Telomerase repeat binding factor 1
FOXM1	Forkhead box protein M1
bFGF	Basic fibroblast growth factor
OCR	Oxygen consumption rate
FCCP	Carbonyl cyanide-4 (trifluoromethoxy) phenylhydrazone
ECAR	Extracellular acidification rate
2-DG	2-Deoxy-D-glucose
2DG6P	2-deoxyglucose-6-phosphate
CHOL	Cholangiocarcinoma
ESCA	Esophageal carcinoma
STAD	Stomach adenocarcinoma
CRISPR	Clustered Regularly InterSPaced Repeats
sgRNA	Single guide RNA
EMT	Epithelial-to-mesenchymal transition
DEG	Differentially expressed gene
OXPHOS	Oxidative phosphorylation
FADS1	Fatty acid desaturase 1
GOT2	Glutamic-Oxaloacetic Transaminase 2
IQGAP2	IQ Motif Containing GTPase Activating Protein 2

Chapter One: Introduction

1.1 Hepatocellular carcinoma

Hepatocellular carcinoma (HCC) is the most common type of primary liver cancer. Liver cancers are the third leading cause of cancer-related deaths worldwide, and ranked the sixth most common cause of incidence according to WHO report in 2020[1][2]. Chronic liver inflammation, as a result of hepatitis viral infections (HBV and HCV), alcohol abuse, aflatoxin, nonalcoholic fatty liver disease (NAFLD), and obesity, predispose the development of liver cancer [3][4]. Most HCC patients are diagnosed at an advanced stage, and the 5-year survival rate is low in most HCC patients [5]. Surgical resection and liver transplantation are currently the most effective treatment for HCC[4]. Although other intervention strategies, such as transarterial chemoembolization (TACE), chemotherapy, targeted therapy, and immune checkpoint therapy are also available, they are not effective in extending the lifespan of HCC patients. Sorafenib was the first approved targeted therapy for advanced HCC patients, despite of its low efficacy[6]. Recently, new drugs like lenvatinib, regorafenib, cabozantinib, and ramuzumab have been shown to improve clinical outcomes. Recently, immune checkpoint inhibitors are also included in the treatment of HCC [7].

1.1.1 Epidemiology and risk factors

HCC is the fifth and eighth most common cancer in men and women respectively [8]. Overall, age-adjusted incidence rates of HCC have increased three times from 1975 to 2005, rising from 1.6 per 100,000 individuals to 4.9 per 100,000 individuals[9], with the peak at the age of 70-year-old [10]. The age-adjusted mortality rate has been increasing 1.6% per year, with the highest for Asians/Pacific Islanders, followed by Hispanics, blacks, American Indians/Alaska Natives, and Whites [9]. Asia accounts for over 70% newly diagnosed liver cancers, which is equal to 75% of all those HBV infection worldwide[11]. China alone accounted for 55% of cases of HCC worldwide[12]. In China, most cases of HCC are arised from Hepatitis B virus (HBV) infection, aflatoxin intake, alcohol abuse, α-antitrypsin deficiency, or non-alcoholic steatohepatitis (NASH), whereas some unknown risk factors may also be involved[13]. HBV is one of the most important risk factors for HCC development. More than 300 million people are suffered from chronic HBV infection and about 700,000 people died each year, according to the World Health Organization[14][15]. The median survival rate for HBV-associated HCC is less than 16 months, and the five year survival rate is only about 15 to 26% [14].

1.1.2 Pathogenesis

The pathogenesis of HCC is complex and involves multiple molecular malfunctions. These include genetic and epigenetic alterations, dysregulation of inflammatory cytokines and chemokines, alternation in microenvironments, generation of cancer stem cells, and dysregulation of signaling pathways[3][16].

1.1.2.1 Genetic and epigenetic alterations

HCC development is generally considered to be a long-term process. The accumulation of diverse genetic and epigenetic alterations can lead to the activation of oncogenic genes or repression of tumor suppressor genes.

1.1.2.1.1 Genetic alterations

Genetic alterations as one of the most important mechanisms associated with the carcinogenesis of HCC. In normal hepatocytes, the accumulation of abnormal gene expression is an important factor for the development of hepatocellular carcinoma. Chromosomal amplifications, deletions, and genomic mutations are classified as genetic alterations[17]. Most frequent genetic alterations occur at chromosomal instabilities in HCC. Based on comparative genomic hybridization (CGH) data, amplifications of chromosomes 1q and 8q are frequently observed in hepatocellular carcinoma, as well as frequent losses of chromosomes 1p, 4q, 6q, 9p, 16p, 16q and 17p[18]. Both the region 1q21 and 8q24 are commonly amplified in most HCC patients,

which contain CHD1L, c-Myc and PTK2 oncogenes[19], [20]. Chromosome losses are also frequently observed in HCC. The region of 1p35-36 is deleted in most HCC patients, which contains 14-3-3σ and Rb-interacting zinc finger 1 (RIZ1) tumor suppressors[21]. The cell adhesion molecule E-cadherin (CDH1), a suppressor of cell proliferation and metastasis, is located in the 16q22 region and frequently absent in HCC[22]. In addition, mutations in CTNNB1, AXIN1, APC and P53 are frequently observed[23], [24].

1.1.2.1.2 Epigenetic alterations

Epigenetic modifications regulate chromatin structures and gene transcriptions. DNA methylation, histone modifications and lncRNAs are predominant types of epigenetic modifications. In tumor cells, hypermethylated CpG islands at the promoter region block incorporation of RNA polymerase and transcription factors, leading to the inhibition of target gene transcription. In HCC, hypermethylation of CpG islands generally occurs in the promoter regions of tumor repressor genes. SOCS-1, a suppressor of cytokine signaling that regulates the JAK/STAT signaling pathway, is silenced due to catalytic hypermethylation[25]. On the other hand, histone modifications perform a pivotal role in the regulation of chromatin structure. H3K4Me3 and H3K36Me3 represent active transcriptional markers, whereas H3K27Me3 and H3K9Me3 relate to repress transcription[26]. Histone methyltransferase (HMT), histone acetyltransferase (HAT) and histone deacetylase (HDAC) are important histone mediator enzymes. Abnormal expression of these enzymes is frequently observed in

HCC. EZH2, a histone methyltransferase of H3K27Me3, is overexpressed in HCC and high expression of EZH2 is associated with poor prognosis[26]. P300/CBP-associated factor (PCAF) is one of the HATs, which is expressed at low levels in HCC. PCAF is found to suppress HCC tumor growth both in vitro and in vivo[27]. Besides, evidences suggest that lncRNAs may play an important role in histone methylation and chromatin remodeling and gene expression at the post-transcriptional level[28][29]. Alterations of lncRNA expression have been observed in HCC. lncRNA high expression in HCC (IncRNA-HEIH) is highly expressed in HCC, and a high level of lncRNA-HEIH expression is implicated in HCC recurrence and patients poor prognosis[30].

1.1.2.2 Inflammation cytokines and chemokines

Recent studies suggested potential relationship between hepatic inflammation and HCC [17][18]. Inflammatory cytokines are the mediators for the development of liver injury. When liver was stimulated by alcohol and fatty acids, liver cells synthesize various cytokines [33] including tumour necrosis factor alpha (TNF-α)[34], interleukins IL-6 and IL-1β[21] [22], and chemokines such as vascular cell adhesion protein 1(VCAM-1), intercellular adhesion molecule 1 (ICAM-1) and monocyte chemoattractant protein 1(MCP-1)[37]–[39], etc.

1.1.2.2.1 Inflammation cytokines

TNF-α and IL-6 are well-known multifunctional cytokines induced by chronic liver infection. High serum levels of TNF-α and IL-6 have been found in chronic HBV

infected patients [40], and they are risk factors for the development of cirrhosis and HCC. IL-1β was thought to be an important regulator of HCC metastasis. It upregulates programmed death ligand 1(PD-L1) and colony-stimulating factor 1(CSF1) through the αKG/HIF1α axis, leading to the overexpression of solute carrier family 7 member 11(SLC7A11), which promotes the infiltration of tumor-associated macrophages (TAMs) and myeloid-derived suppressor cells (MDSCs)[41].

1.1.2.2.2 Inflammation chemokines

CD151 was upregulated in chronic liver disease and hepatocellular cancer, which was closely connected to VCAM-1 on hepatic sinusoidal endothelial cells (HSECs). The evidence of functional blockade of VCAM-1 and CD151 in combination suggested that CD151 mediated lymphocyte adhesion to HSECs through interaction with VCAM-1. Therefore, modulating the interaction of CD151 with VCAM-1 in endothelial cells may be an attractive and specific target for chronic inflammatory liver disease[39]. ICAM-1 expression was regulated by ICAM-1-related long non-coding RNA (ICR) through the formation of RNA double-stranded to increase its mRNA stability, leading to the modulation of cancer stem cells (CSCs) properties of ICAM-1^+ HCC cells[38]. The CXC chemokine family was the most favored chemokine family in cancer metastasis, and the MCP-1 axis was essential for the migration of mesenchymal stromal cells (MSCs) to human HCC *in vitro*. Recent study[37] identified C-X-C motif chemokine ligand 8(CXCL8/IL-8), C-C motif chemokine ligand 2(CCL2/MCP-1) and C-X-C

motif chemokine ligand 1-2-3(CXCL1-2-3/GRO) as chemotactic axis for migration of MSCs in HCC.

1.1.2.3 Tumor microenvironments

Tumor microenvironment is important for HCC metastasis and proliferation. Tumor development and malignant progression can be promoted by microenvironmental stimuli, immune cell responses and inflammatory signaling pathways. Communication exists between liver tumor cells and the stroma. The non-tumor stroma, including the extracellular matrix (ECM), carcinoma associated fibroblasts (CAFs), immune cells, and endothelial cells, generally referred as the peritumor microenvironment. The microenvironment can secrete growth factors from these cells that contribute to the proliferation of HCC by promoting processes such as angiogenesis, inflammatory response, cell proliferation and metastasis, as well as altering immune surveillance response[42]–[44]. Carcinogenesis of HCC is a multistep process. HBV or HCV infection, and alcohol consumption, etc, are the risk factors. These factors lead to chronic inflammation and injury of the liver, resulting in genetic and epigenetic mutations, and finally resulted in tumorigenesis. Sustained injury leads to an inflammatory microenvironment in the liver. Hepatic stellate cells (HSCs) and macrophages are recruited and activated in the inflammatory microenvironment and further secrete ECM members, growth factors to foster HCC angiogenesis[43]. Although the molecular mechanisms of ECM and tumor is unclear, current evidence suggests that the accumulation and proliferation of HSCs in the tumor stroma, which

are induced by PDGF-BB and the overexpression of VEGF-A , contributing to HCC angiogenesis[45]. Besides, primary HCC also results in a hypoxic microenvironment. As a result, there will be enhanced angiogenesis, and an increased blood supply to the tumor, which contribute to tumor growth and metastasis[45].

Immune cells are the most common cells in the tumor microenvironment. In response to inflammation, immune cells such as T cells, B cells, macrophages and dendritic cells will move into the tumor tissue and regulate tumor cells growth by secreting a series of cytokines[43]. CD4+ T helper cells are the most abundant tumor-infiltrating lymphocytes (TILs). T helper cells (Th) comprise both Th1-like cytokines and Th2-like cytokines. In the HCC tumor microenvironment, Th1 cytokines of IL-1β, IL-2,TNFα and IFN-γ are found to be increased and Th2 cytokines like IL-4, IL-5, and IL-10 are decreased[46]. Tumor-associated macrophages (TAMs) represent another important sub-group of invasive immune cells in the tumor microenvironment. TAMs can secrete growth factors, cytokines, and chemokines to promote tumor growth. Highly infiltrated TAMs are strongly associated with poor prognosis in HCC patients[47].

1.1.2.4 Cancer stem cells

Cancer stem cells (CSC) has been suggested as a mechanism leading to the HCC growth and metastasis. Cancer stem cells, which not only be able to undergo self-renewal, but also capable of differentiating into specific tumor cells, potentially contribute to the heterogeneity of HCCs [48]. Malignant tumor cells typically have similar features as

embryonic cells, including HCC, which exhibit high expression levels of stemness markers[49]. The tumor-specific markers and molecular mechanisms are extremely important for the diagnosis of HCC. Some populations of cells have been established as prospective cancer stem cells in HCC. Side population (SP) cells are suggested to be one of the potential hepatocellular carcinoma stem cells, which can deliver nuclear dye by pumping through ATP Binding Cassette Subfamily G Member 2 (ABCG2) transporters. One study identified that ABCG2 is expressed intrinsically in HCC tissues. The expression of ABCG2 has a significant effect on the level of drug efflux from HCC cell lines[50]. Liver CSCs are associated with drug resistance and recurrence in HCCs [51], [52]. In addition, multiple signaling pathways involved in cancer self-renewal and differentiation can be activated in SP cells[50], [53], [54]. Epithelial cell adhesion molecule (EpCAM) is another biomarker of hepatic stem cells (HpSC). A study showed that HCC growth and invasiveness were mediated by a subpopulation of EpCAM cells. EpCAM could be a new treatment for liver cancer through blocking the Wnt/catenin signaling component in HCC cancer cells [55]. Moreover, a CSC population with the CD133 phenotype was observed in HCC. CD133(+) cells have greater colony formation efficiency and higher proliferative capacity in HCC [56]. Several other putative surface markers of hepatic CSCs have been identified, including CD90, CD44, CD13 and CD24[57]–[61]. Overall, CD markers are important for early diagnosis of liver cancer, while targeting CSCs and the tumour microenvironment are expected to inhibit tumour growth.

1.1.2.5 Signaling pathways

Gene mutations in HCC resulted in the alternation of cellular signaling pathways, leading to the growth and metastasis of HCC cells and protecting them from apoptosis. Several signaling pathways are involved in the pathogenesis of HCC, including the Wnt/β-catenin pathway, Ras/Raf/MEK/ERK pathway, PI3K/AKT/mTOR pathway, JAK/STAT pathway, and EGFR pathway.

1.1.2.5.1 Wnt/β-catenin pathway

The Wnt/β-catenin pathway has been a key pathway involved in the pathogenesis of many cancers[62]. Wnt family of proteins are secretory glycolipoportiens that control embryonic development and homeostasis through signaling, mediated by the transcriptional cofactor β-catenin [63]. Mutations in the Wnt/β-catenin pathway have been found to be one of the most common genetic variants in human HCC, and abnormal activation of β-catenin signaling plays an important role in HCC pathogenesis [64]. The hallmark of the Wnt/β-catenin pathway dysregulation is the translocation and accumulation of β-catenin in the nucleus. β-catenin, encoded by the CTNNB1 gene, plays a role in cell adhesion and intercellular signaling by interaction with E-cadherin, N-cadherin or Axin/APC degradation complex and T-cell factor (TCF)/lymphatic enhancer factor-1 (LEF-1) transcription factor. The canonical Wnt signaling pathway, in the absence of Wnt ligands, β-catenin is phosphorylated by the “disruption complex” (composed of axin, APC, CK1 and GSK3β), resulting in ubiquitination by β-TrCP-

targeted proteasomal degradation. The deficiency of β-catenin in the nucleus caused the repressor complexes containing TCF/LEF and TLE/Grouche to bind to the target genes, which suppressed genes activities. However, when Wnt ligands bind to Frizzled receptors and LRP co-receptors, LRP receptors were phosphorylated by CK1 and GSK3β, causing the recruitment of Dvl proteins to the plasma membrane and the accumulation of hypophosphorylated β-catenin at the cytosol allowing its translocation to the nucleus. As a result, β-catenin modulated the expression of target genes by interacting with transcription factors of the TCF/LEF family[63], [65]–[67].

A couple of genetic alterations induced aberrant β-catenin, which contributed to the pathological organization and development of HCC, including CTNNB1 mutation[68]–[70], AXIN1 deficiency[71], GSK-3β phosphorylation[72], E-cadherin alteration[73], long noncoding RNAs overexpression[74], and TBX3 upregulation[75] respectively. Gain-of-function CTNNB1 mutations occurred in approximately 30% of HCCs[76] , while loss-of-function of negative regulators of the pathway could be observed, comprising AXIN1 and AXIN2 genes (<5%)[64]. In addition, the genetic alterations in TERT promoter, TP53, and HBV integrations were all closely associated with CTNNB1 in the development of HCC[77], [78]. In one study, β-catenin mutations were found in 9/22 (41%) cases of HCCs, but no APC mutations were found, indicating that β-catenin mutations activation of the Wnt signaling pathway promoted the hepatocellular carcinogenesis associated with HCV infection[79]. Moreover,

inflammation deranged lipid metabolism and aberrant oxidative stress have been found to be involved in the abnormal expression of the Wnt signaling pathway, resulting in the development of chronic liver diseases such as NAFLD and liver fibrosis[80], [81]. In conclusion, it was shown that activating and inactivating mutations of CTNNB1 played an important role in liver tumorigenesis by activating the WNT-β-catenin pathway.

1.1.2.5.2 Ras/Raf/MEK/ERK pathway

The Ras/Raf/MEK/ERK signaling cascade is an important signaling pathway for mitogen-activated protein kinases (MAPKs) signaling, and played a key role in the pathogenesis of HCC[82]–[84]. MAPK is a serine/threonine protein kinase in eukaryotes, which is involved in gene transcriptions, protein synthesis, cell growth, apoptosis, and differentiation[85], [86]. Four core protein kinases are involved in the Ras/Raf/MEK/ERK signaling pathway, namely Ras, Raf, MEK and ERK. Among them, Ras, Raf and MEK have several gene members. Ras consists of three members, Ki-Ras, N-Ras and Ha-Ras. Raf also has three components, A-Raf, B-Raf and Raf-1. And MEK has five gene family members，including MEK1, MEK2, MEK3, MEK4 and MEK5. The MAPK signaling pathway can be activated by receptor tyrosine kinases (RTK) and G protein-coupled receptors, in order to transfer the signal to the nucleus. In this pathway, four core protein kinases of Ras, Raf, MEK and ERK, are phosphorylated to regulate further gene transcription. Previous studies found MARKs pathways are implicated in HCC development, including the ERK, c-Jun N-terminal kinase (JNK),

ERK5, and p38 respectively. A major signaling pathway in MAPKs is the Ras/Raf/MEK/ERK cascade reaction. In brief, three processes are involved in the pathway. Activated Ras can recruit and activate the protein kinase Raf. Raf then phosphorylates and activates MAPK/ERK kinase (MEK1 o/MEK2). MEK subsequently phosphorylates and activates mitogen-activated protein kinase (MAPK) [87]–[91].

The Ras/Raf/MEK/ERK pathway was one of the most significant cellular signals for hepatocellular carcinoma development. This pathway convey extracellular signal to the nucleus by the activation of ligand-tyrosine kinase receptor, followed by the activation of serine threonine kinases of the Ras and Raf families via specific phosphorylation process[83], [85], [92]–[94]. It has been reported that Ras protein is a key regulator for normal cell growth [95]. Ras mutations are found in 30% of HCC cases[96], and in most of the HCCs, Raf kinase are found to be overexpressed. [97]. Many of the the ligands that are overexpressed in HCC, including epidermal growth factor(EGF), vascular endothelial growth factor (VEGF), platelet-derived growth factor-β (PDGF-β) and transforming growth factor-α (TGF-α), transactivate receptor tyrosine kinase, leading to the activation of Ras/Raf/MEK/ERK pathway[98]. The JNK pathway cooperates with the ERK pathway through activation of the JNK transcription factor c-Jun to ensure cell cycle progression[99]. JNK pathway affects HCC cell invasion and metastasis. Inhibitors of JNK mitigate growth of human HCC xenograft[100]. p38

MAPK pathway can induce apoptosis of hepatocytes by regulating the distribution of inflammatory cytokines like IL-1β, IL-6 and TNF-α, and increased ROS activity[101].

1.1.2.5.3 PI3K/AKT/mTOR pathway

The phosphatidylinositol 3-kinase /the serine-threonine protein kinase /mammalian target of the rapamycin (PI3K/Akt/mTOR) signaling pathway is activated in many cancers including HCC. The PI3K/AKt/mTOR pathway is critical for the regulation of many cellular processes, including cell cycle, apoptosis, cell survival, and protein synthesis. Dysregulated receptor tyrosine kinase (RTK) may activate PI3K/AKt/mTOR pathway [102]–[105].

PI3K is a member of the intracellular lipid kinase family, which catalyzes the production of phosphatidylinositol-3,4,5-trisphosphate (PIP3) from phosphatidylinositol-4,5-trisphosphate (PIP2). AKT is a serine/threonine kinase which is recruited to the plasma membrane through PIP3 via its pleckstrin-homology (PH) structural domain and is activated by phosphorylation at Thr308 and Ser473. PDK1, a 3-phosphocreatine-dependent protein kinase, phosphorylates Thr308, whereas Ser473 is phosphorylated by an unidentified kinase, commonly referred to as PDK2. Activated AKT is translocated to the nucleus and activated mTOR and downstream targets[103], [104]. PTEN is a tumor suppressor that could dephosphorylate PIP3 to PIP2[106], [106]–[108]. It is reported that P-AKT is found in 71.5% (143/200) of HCC tissues, and

its expression is positively correlated with tumor grade and the presence of intrahepatic metastases. The expression of P-mTOR is detected in 47.5% (95/200) of HCC. On the contrary, PTEN protein expression is negatively correlated with p-AKT and p-mTOR[106]. Activation of PI3K/AKt/mTOR pathway in HCC is a promoting factor for tumor angiogenesis, mainly caused by the activation of cyclooxygenase 2 (COX-2), and upregulation of HIF-1α and VEGF expression, induced by hypoxia [109]–[111]. Meanwhile, transcriptional activation of NF-κB and up-regulation of matrix metalloproteinase 2 (MMP-2) expression promotes tumor cell metastasis[105][106]. Moreover, activated PI3K/Akt/mTOR signaling pathway upregulates major cell cycle proteins like p70s6k-related CDK4, to promote cell proliferation and differentiation in HCC[84][107]. Several targeted therapeutics of the PI3K-Akt pathway were currently in clinical use for the treatment of cancers, including PI3K-mTOR inhibitors, PI3K inhibitors, and Akt inhibitors respectively [105]. Glycogen Synthase Kinase-3(GSK-3) is a famous substrate of Akt. Upregulation of GSK-3β is associate with poor prognosis in HCC patients. Depletion of GSK-3β can decrease mTORC1 activity, glycolytic ability and tumor growth in HCC[115][116]. In summary, the PI3K/AKt/mTOR pathway has an impact on the development and metastasis of HCC.

1.1.2.5.4 JAK/STAT pathway

The JAK-STAT pathway, discovered in 1994 by Darnell[117] et al, is an extremely efficient signaling pathway that transmits extracellular signals to the nucleus through the activation of receptor tyrosine kinase signaling and the transcription activator target

genes, eventually triggering biological effects. The JAKs family is a family of non-receptor tyrosine kinases with four family members, which are JAK1, JAK2, JAK3 and TYK2, respectively. JAK1, JAK2 and TYK2 are expressed in most tissues, while JAK3 is exclusively expressed in lymphoid tissues[117]. The signal transducers and activators of transcription (STATs) are a subclass of cytoplasmic proteins that are downstream substrates of JAKs. There are 7 family members, including STAT1, STAT2, STAT3, STAT4, STAT5a, STAT5b and STAT6. Under physiological conditions, the JAK-STAT signaling pathway plays a crucial role in cell growth, differentiation, tissue and organogenesis, and immune defense[118]. Upon aberrant activation of the JAK/STAT3 signaling pathway, cytokines bound to specific receptors and transactivated JAKs. Activated JAKs could further phosphorylate tyrosine STAT transcription factors. As STATs are translocated into the nucleus, SOCS proteins could direct targets of STAT and act as negative feedback inhibitors to silence the signaling cascade[119], [120]. STAT was highly expressed in many malignant cells and STAT3 is considered an oncogene that contributes to hepatocarcinogenesis and progression through cell proliferation, differentiation, and apoptosis[118], [119]. It has been shown that the introduction of HCV core protein leads to increased expression of IL-6, gp130, and Stat3, which in turn regulates c-myc and cyclin D1 that were downstream of the Stat3 signaling pathway[121]. A JAK2-specific inhibitor, AG490 inhibits STAT3 signaling and reduces the size and number in a rat model of HCC [122]. Moreover, treatment of HCC cell lines with a combination of Ras and Jak/Stat inhibitors resulted in

apoptosis[123]. Together, these data suggested that JAK/STAT inhibitors are a potential treatment for hepatocellular carcinoma.

1.1.2.5.5 EGFR pathway

Epidermal growth factor receptors (EGFR) are members of the tyrosine kinase involved in cell cycle progression, differentiation and tumorigenesis processes in cancers[124]–[126]. There were four members in the family, including EGFR/ErbB1/HER1, ErbB2/HER2/Neu, ErbB3/HER3 and ErbB4/HER4. Several ligands transactivate EGFR, including EGF, transforming growth factor-α (TGFA), heparin-binding EGF-like growth factor (HBEGF), betacellulin (BTC), amphiregulin (AREG), epiregulin (EREG) and epigen (EPGN)[127], [128], respectively. Multiple pathways interacted with EGFR signaling, such as ERK/ MAPK, PI3K/AKT, SRC, JNK and JAK-STAT pathways, to regulate cell growth, differentiation, apoptosis, and metastasis[129], [130]. Compared to adjacent tissues, EGFR and ErbB3 are overexpressed in HCC. Highly expressed EGFR and ErbB3 have a poor prognosis in HCC patients[131]. Interestingly, over-expression of EGFR in HCC does not have a positive correlation with EGFR gene copy number. Activation of EGFR is also associated with drug resistance to sorafenib in HCC[132], [133]. A study showed that HCC-derived EGFR mutants are sensitive to EGFR-tyrosine kinase inhibitor erlotinib [134]. In addition, another study showed that gefitinib attenuated hepatocellular carcinoma cell growth and induced apoptosis by inhibiting EGFR[135], [136].

1.1.3 Diagnosis

HCC is very difficult to be diagnosed at its early stage, as most HCC cases do not have obvious symptoms. Therefore, the tumor is usually diagnosed at inoperable advanced stage, and the prognosis of HCC is very poor. Early screening for liver cancer by measuring serum alpha-fetoprotein (AFP) level and by liver ultrasound in every 6 to 12 months are recommended in high-risk groups in the National Comprehensive Cancer Network (NCCN) guidelines[137]. Current diagnosis of HCC does not require liver biopsy of the patient. Definitive diagnosis of HCC can be made when the tumor is larger than 1 cm in diameter with typical imaging features present on contrast-enhanced examinations, through dynamic computed tomography (CT) or magnetic resonance (MR) [138]. However, there are two situations where patients are advised to have a biopsy to confirm a diagnosis of liver cancer, including patients with typical lesion features without liver disease, and patients with typical lesions with cirrhosis[138]. A Liver Imaging Reporting and Data System (LI-RADS) has been developed by the American College of Radiology to reduce variability in the interpretation of liver lesions and to standardize the reporting of CT and MR information. LI-RADS assigned imaging results into 5 categories, which allows radiologists to categorize individual observations based on the level of HCC. Thus, LR-1 represents a well-defined benign tumor, whereas LR-5 represents definitive HCC[139]. Despite the fact that serum alpha-fetoprotein (AFP) level is a useful marker for detection and monitoring of HCC, up to 30% of patients with advanced HCC will not show an increase in AFP level [140].

Several other serum proteins have been shown to be potential tumor markers for early diagnosis of HCC. These include Hepatoma-specific Gamma-glutamyl Transferase Isoenzyme (HS-GGT), Transforming Growth Factor (TGF)-β1, Insulin-like Growth Factor (IGF)-II, Hepatocyte Growth Factor (HGF), Heat Shock Proteins (HSPs), Complement C3a, Glypican-3 (GPC3), Squamous Cell Carcinoma Antigen (SCCA)[141]. Nevertheless, pathological assessment in combination with biomarkers may result in a high sensitivity and specificity for early diagnosis and prognosis of HCC. Moreover, recent studies indicated that dysbiosis, leaky gut and bacterial metabolites could promote the HCC development[142]–[144]. Therefore, the microbiome could be a potential diagnostic tool and new therapeutic target for HCC treatment in the future.

1.1.4 Treatments

Multiple options are available for the treatment of HCC, depending on the stage of the cancer and the overall health status of the patient. At the early stages, treatment options such as partial liver resection, liver transplantation, and ablation will be available. Tumor resection should be considered as the primary treatment option for any patient with HCC[145]. Whereas in the advanced stages, the aim of cancer treatments is to prolong the life of the patient. At this stage, transarterial chemoembolization (TACE) or /and chemotherapy will be the options [145][146]. In addition, selective internal irradiation therapy (SIRT) is usually recommended for patients with large tumors who are not suitable for TACE in intermediate- or advanced-stage stages[147]. Sorafenib is

targeted therapeutic which can suppress new blood vessel formation and tumor growth and has been approved for its use in HCC treatment. Sorafenib has some advantages in HCC treatment, but limited[148]. Recently, targeted therapy using a combination of atezolizumab and bevacizumab is found to be more effective than sorafenib in HCC treatment. The treatment has been approved by the European Medicines Agency (EMA) at the end of 2020 and was recommended as the standard of care for the first-line treatment of patients in advanced HCC[149]–[151]. It is also recommended that if atezolizumab plus bevacizumab fails, approved drugs such as sorafenib, lenvatinib, regorafenib, cabozantinib, and ramucirumab, can be used as a second line treatment [147], [152]–[155]. The 5-year survival rates have been effectively improved with combination treatments for HCC patients[156][157].

1.2 CCCTC-binding factor (CTCF)

1.2.1 Functional roles of CTCF

CCCTC binding factor (CTCF) is a highly conserved nuclear factor which is composed of 11 zinc finger DNA binding domains[158]. CTCF is originally discovered as a "multivalent factor" that binds specific binding sites at the proximal region of the c-myc promoter of the chicken, mouse and human [159]. Subsequently, more than 13,800 CTCF binding sites were found in the human genome[160]. CTCF involves in a variety of regulatory functions, including transcriptional regulation, insulation, imprinting, and X chromosome inactivation[158]–[162]. CTCF also plays an essential role in early embryonic development in mice[163].

CTCF is required for transcriptional activation of the amyloid β-protein precursor (APP)[164], and extracellular deposition of aggregated amyloid β-protein is a hallmark of Alzheimer's disease[165]. The nuclear factor binding site APBβ is the predominant activation domain of the APP proximal promoter, and it can recognize GCCGCTAGGGGT sequence[164]. CTCF has already been characterized as the nuclear factor that binds APBβ to upregulate APP gene expression through transforming growth factor-β (TGF-β)[162], [166], [167]. In addition to being involved in activating transcription, CTCF also regulates some genes in transcriptional repression manner. CTCF is known to play a role in transcriptional repression at the

chicken lysozyme silencer gene and c-myc gene[159], [168], [169]. When CTCF binds to the c-myc promoter, it may recruit histone deacetylase (HDAC) complexes to condense chromatin structures and thereby to repress gene transcription[170]. In addition, genes such as TERT, FOXA1, BCL6 and PAX6 are also transcriptionally repressed by CTCF[171]–[174].

Apart from its role in transcriptional regulation, CTCF also acts as a chromatin insulator protein, which prevents interactions between promoters and nearby enhancers. CTCF was originally discovered as an insulating element at the 5'DNase-hypersensitive locus 4 (5'HS4) from the chicken β-globin locus[175]. Subsequently, CTCF was also identified as an insulator in mouse and human IGF2/H19 (insulin-like growth factor 2) locus[176]. CTCF can bind to several sites in the imprinting control region (ICR) which is located on the maternal allele between IGF2 and the enhancer, to silence IGF2 expression by blocking the enhancer[176][177]. Conversely, when the ICR is methylated on the paternal allele, the CTCF binding sites would be block and activate the expression of IGF2[176][177]. The cohesin protein complex, which is composed of Smc1, Smc3, Scc1(Rad21) and Scc3, is essential for normal chromosome segregation and post replication DNA repair [172][173]. The DNA-binding sites of cohesins largely overlaps with those of CTCF[180]. Evidence showed that cohesin combines with CTCF to insulate the promoter from distant enhancers and to modulate the transcription of the H19/IGF2 motif[181]. CTCF also plays an essential role in genome architecture. CTCF

was found to be a candidate trans-acting factor for X chromosome selection, involved in X chromosome inactivation (XCI)[182]. In the period of XCI, CTCF can incorporate both active and inactive X-chromosomes and directly interact with Tsix, Xite and Xist non-coding RNAs. CTCF is targeted by Tsix and Xite non-coding RNAs, recruits to X-inactivation center, resulting a homologous X chromosome pairing[183], [184].

Topologically associating domains (TADs) played a role in regulating the long-range regulation of gene expression[176][177]. Alterations in TADs may result in undesired promoter/enhancer communications, causing activation of oncogenes or repression of tumor suppressors[187]. Hi-C analysis showed that the TAD boundaries are enriched in CTCF binding sites[188]. CTCF can facilitate the establishment of a stable topology during cell differentiation[189]. Some chromatin loops may be lost or formed by recruiting CTCF, for the further transcriptional regulation[189]. Moreover, cohesins could catalyze the folding the genome into a loop anchored by CTCF[190], [191]. Loss of core cohesin subunit SCC1 caused the reduction of TADs, and depletion of CTCF resulted in an apparent reduction in CTCF-anchored loops[184][185]. Taken together, CTCF is a multifunctional protein that is involved in transcriptional regulation, enhancer blocking, imprinting and the formation of three-dimensional chromatin structures.

1.2.2 The role of CTCF in diseases

Abnormal expression of CTCF and dysregulation of CTCF are implicated in the pathogenesis of a variety of diseases. CTCF frameshift mutations with c.375dupT and c.1186dupA is associated with autosomal dominant mental retardation 21 (MRD21) [194]. Abnormal association of CTCF with the IGF2-H19 locus is associated with Silver-russell syndrome (SRS)[195] or Beckwith-Wiedemann syndrome (BWS)[196]. Hypermethylation and hypomethylation in CTCF binding sites are associated with some cancers, such as ovarian cancer, testicular germ cell tumors, bladder cancers colorectal cancers[197], [198], [199]–[206]. Besides, some zinc finger domains mutations of CTCF are observed in prostate cancer[207], [208], endometrial cancer[209] and Wilms' tumor[202], [210]. CTCF H345R mutation and R377C mutation are identified in prostate cancer and endometrial cancer, respectively[207]–[209]. In Wilm's tumor, two CTCF missense zinc finger mutations, R339W and R448Q, are identified [202], [210]. Among these mutations, the CTCF R377C mutation is one of the cancer hotspots in endometrial cancer, which presents a statistically significant mutation. Moreover, studies suggested that CTCF/cohesin binding sites (CBSs) are frequently mutated in different cancers, including gastric cancer[211] and skin cancers[212].

CTCF may play a dominant role in the pathogenesis of breast cancer. Evidence suggested that CTCF act as a transcriptional regulator, complexing with co-factors like

Estrogen Receptor (ER) and TP53 at the unmethylated CpG region to regulate the expression of MYC and Bax genes[213][214]. Therefore, CTCF is involved in increasing myc level to promote cell growth while attenuating Bax level to againt apoptosis. CTCF also can insulate enhancer activity to regulate neighbor genes trefoil factor 3 (TFF3) and transmembrane protease, serine 3 (TMPRSS3), by binding to the trefoil factor (TFF) locus in breast cancer cells[215]. CTCF can bind to both boundaries of TFF1, which is the target of ER. Knockdown of CTCF leads to alterations in epigenetic markers, as evidenced by an increase in H3K27M3 and a decrease in H3K4M1 and H3K4M2 [213]. The study suggested a role for CTCF in establishing the responsiveness of this genome towards estrogen, involved in regulating the transcription of the ER[215]. Besides, CTCF involved in the organization of chromatin structure. Estrogen stimulation affect ER binding sites and induce the depletion of CTCF, causing specific ER-ER looping in P2Y purinoceptor 2(P2RY2) in MCF-7 cells[215]. P2RY2 is involved with several functions, which include cell proliferation and apoptosis. Specific ER-ER looping in P2RY2 may alter cell growth in breast cancer cells. Collectively, CTCF may play a role in the pathogenesis of breast cancer, including transcriptional regulation, insulation, and the organization of chromatin structures.

Recently, several studies suggested that CTCF also plays an important role in the pathogenesis of HCC. Suppressor 3 of cytokine signaling (SOCS3), a negative

regulator of the IL6/JAK/STAT3 signaling pathway, can prevent progressive transformation of cells and foster apoptosis by interfering with signal transducer and activator of transcription 3 (STAT3) phosphorylation[216]. A study showed that SOCS3 expression in HCC is inversely proportional to EZH2 and is reliant on the state of methylation of its promoter. Moreover, it was found that methylation of the SOCS3 promoter is associated with CTCF expression[217]. In addition, knocking down CTCF resulted in a reduction in the recruitment of EZH2 to the SOCS3 promoter, which suggested that CTCF may be responsible for the silencing of SOCS3 in HCC[217]. Moreover, CTCF may play an important role in transcriptional regulation through regional organization of chromatin structure in HCC. Findings revealed[218] that the metallothionein (MT) family members had a significant reduction in HCC, and CTCF binding sites were positioned at two loci in the MT gene clusters. Upon CTCF knockout, an increased level of MTs was observed in Huh7 and HepG2 cells, and alterations of H3K4me3 and H3K9me3 were detected by 3C and ChIP[218]. This result suggested that CTCF may alter the transcriptional activity of genes by modifying chromosomal loops in HCC. In addition, several CTCF missense mutations were identified in HCC patients from TCGA, including D328Y, Q418R, R470H and M504I (http://www.cbioportal.org). Nevertheless, these mutations were not significant in HCC.

These discoveries demonstrated the different functional roles of CTCF in different cell types. However, the functional significance of CTCF and its binding sites in HCC

remains unclear. Therefore, a thorough comprehension of the mechanisms of HCC progression and metastasis is fundamental to the development of efficacious treatments for this deadly disease.

1.3 Aim of the study

Previous studies in our lab [219] showed that CTCF expression is highly upregulated in a subpopulation of HCC, and CTCF overexpression is correlated with a more unfavorable prognosis in HCC patients. In HCC cell models, depletion of CTCF using shRNA resulted in reduced expression of telomerase reverse transcriptase (TERT), telomerase repeat binding factor 1 (TRF1), and forkhead box protein M1 (FOXM1), which was associated with the inhibition of growth and metastasis of HCC cells[219]. In addition, knockdown of CTCF expression profoundly inhibited cell growth and metastasis *in vitro* and *in vivo*[219]. Therefore, the aim of my current study is to gain a better understanding on how CTCF regulates tumor growth and metastasis in HCC.

.

Chapter Two: Materials and Methods

2.1 Cell lines and HCC specimens

Transformed primary human hepatocytes (PHH) were from Applied Biological Materials Inc (Canada). Human hepatocytes (PHH15062, PHH16057, PHH15052) were obtained from Cytes Biotechnologies SL (Spain). PLC5, Hep3B cells were from American Type Culture Collection. Huh7 cells were from the Health Science Research Resources Bank (Japan). HepG2.2.15 cells were from Z. Y. Tang of Fudan University and A. L. Huang of Chongqing Medical University, PR China, respectively. Thirty pairs of HCC specimens and adjacent tissues were obtained from the laboratory of Professor Zhang Yaojun at the Sun Yat-sen University Cancer Centre, Guangzhou, China. PHH were growth in Enhanced Primary Human Hepatocytes Media Kit (Matrix Applied Biological Materials Inc) in cell culture vessels coated with Applied Cell Extracellular (Matrix Applied Biological Materials Inc). PLC5, Hep3B, HepG2 and Huh7 Cells were cultured in DMEM growth medium (Gibco, #12100046) supplemented with 10% heat inactivated fetal bovine serum (Gibco BRL, Grand Island, NY, USA). The cells were cultured in 100 U/mL penicillin and 100 μg/mL streptomycin (Thermo Fisher, #15140122), and in a humidified incubator at 37°C with 5% CO2. All cells were authenticated by short tandem repeat profiling analysis.

2.2 Plasmids, reagents and antibodies

Lentivirus plasmid pLenti-CRISPRv2-Cas9 was purchased from Addgene. pLKO.1-puro vector was a gift from Prof. Terence Lee's lab. ViaFect™ Transfection Reagent (#E4982) was from Promega. Gibco™ Opti-MEM™ I Reduced Serum Medium (#31985070), B-27™ Supplement (50X, #12587010), N-2 Supplement (100X, #17502048) were from Gibco. Human recombinant epidermal growth factor (#354052) was purchased from Corning. Human basic fibroblast growth factor (#PHG0266) was from Life Technologies Limited. Methyl cellulose (#M0512) was from Sigma. PrimeScript RT Master Mix, SYBR Premix Ex Taq II kits and RNAiso Plus (#9109) were from Takara. Alexa Fluor™ 568 Phalloidin (#A12380) and MitoTracker™ Red FM (#M22425) were from Invitrogen. TransDetect® Annexin V-FITC/PI Cell Apoptosis Detection Kit (FA101-01) was fromTransgene. Senescence β-Galactosidase Staining Kit (#9860) was from CST. NAD/NADH-Glo Assay kit (#G9071), Glucose Uptake-Glo™ Assay Kit (#J1341) and Lactate-Glo™ Assay Kit(#J5021) were purchased from Promega. CellTiter-Glo® Luminescent Cell Viability Assay kit was a gift from Dr Wong Tsun-ting, Clarence's lab.CTCF antibody (#3418) was from CST. β-actin (#A5316) was from Sigma.

2.3 CTCF sgRNA CRISPR/Cas9 system

LentiCRISPRv2 is a vector system in which the plasmid contains two expression cassettes, hSpCas9 and chimeric guide RNA[220], [221]. This vector can be digested

with BsmBI where an annealed pair of oligos can be cloned into a single guide RNA scaffold. The oligos were designed according to the target site sequence (20bp) and required to be flanked by a 3bp NGG PAM sequence at the 3' end. The sgRNA of CTCF was designed from Benchling online tool (https://www.benchling.com/crispr).

CTCF sgRNA CRISPR/Cas9 Lentivector sequence: GAGCAAACTGCGTTATACAG

2.4 Lentivirus packaging and transduction

The lentiviral structure pLenti-V2-puro expressing Cas9 and gRNA was originally from Feng Zhang's laboratory (Addgene,[220], [222]). For lentivirus packaging, HEK293FT cells were transfected with with 10 μg CTCF sgRNA CRISPR/Cas9 vector, 10.5 μg of pLP1, 10.5 μg of pLP2 and 9.0 μg pVSVG, using calcium phosphate transfection. After 48h-72h of transfection, medium containing the lentivirus was collected. For cells transduction, medium containing the lentivirus was mixed with 8μg/ml hexadimethrine bromide (Polybrene) and incubated with HCC cells. After two days, cells were replaced with fresh medium containing 5μg/ml puromycin (Gibco) , for selection of cells with target gene integration.

2.5 DNA Transfection

Cells were transfected with DNA vector by using ViaFect™ Transfection Reagent (Promega). Cells were seeded one day before transfection. Cells were 70%-80% confluent on the day of transfection, with around 25-30 $\times 10^4$ adherent cells in each well of a 6-well plate. 1-3μg of plasmid DNA was added to the Opti-MEM medium and

mixed well. DNA was mixed with ViaFectTM Transfection Reagent in a 3:1 ratio. The mixture was incubated at at room temperature for 15-30 mins before adding to the cells.

2.6 RNA extraction, reverse transcription and RT-PCR analysis

Total RNA was extracted from cells using RNAiso Plus (Takara) Reagent according to the manufacturer's instruction. cDNA was synthesized from RNA by the PrimeScript RT Master Mix (TaKaRa). cDNA was mixed with SYBR Premix Ex Taq II kits (TaKaRa), followed by quantitative polymerase chain reaction (qPCR) analysis using Applied Biosystems QuantStudio 7 Flex Real-Time PCR System (University Research Facility in Life Sciences of The Hong Kong Polytechnic University, Hong Kong). PCR was conducted using the following cycle parameters: 95°C for 2 mins, followed by 95°C for 30s for 40 cycles, with final extension step at 60°C for 30s. Melting curve analysis was conducted by heating the samples to 95°C for 15s, followed by 60°C for 1mins.

Primers used in the Real-time PCR experiments were below:

CTCF:
Forward: 5’-GTGTTCCATGTGCGATTACG-3’
Reverse: 5’-TCATGTGCCTTTTCAGCTTG-3’

β-Actin
Forward: 5’-CTCTTCCAGCCTTCCTTCCT-3’
Reverse: 5’-AGCACTGTGTTGGCGTACAG-3’

FADS1

Forward: 5’-CTGTCGGTCTTCAGCACCTCAA-3’

Reverse: 5’-CTGGGTCTTTGCGGAAGCAGTT-3’

IQGAP2

Forward: 5’-TTCAGTCCTGGTTCCGAATGGC-3’

Reverse: 5’-TGTTCGCTCTCAACAGTGACTGT-3’

GOT2

Forward: 5’-CCAAGGCTTTGCCAGTGGTGAT-3’

Reverse: 5’-AGTGAAGGCTCCTACACGCTCA-3’

shRNA used in the experiments were below:

shCon	CAACAAGATGAAGAGCACCAA
shFADS1	GTCCGCTTCTTCCTCACTTAT
shIQGAP2	GCATTCACGCACTGAGTTTGT
shGOT2	GCTACAAGGTTATCGGTATTA

Primers used in the validation of On-and off-target effects in CRISPR knockout CTCF cells:

On-target(sg-CTCF)

Forward: 5’-TTGGCTTTGGAGGCTTCATATTACCAACC-3’

Reverse: 5’-GTTTCAGGTGGTTAAAGTGGGGG-3’

Off-target-1

Forward: 5’-ACCCTCCATCTTTCCACTCCAG-3’

Reverse: 5’-AGAAGCAAGAGGAGGCGGAG-3’

Off-target-2

Forward: 5’-CGCAGCATTATGTCCTCAAGGTTC-3’

Reverse: 5’GAATGTTTAACTTGTCAAAACTGAGGATCACAGAG-3’

Off-target-3

Forward: 5’CTGCAAACCTGTACAGCAGGTG-3’

Reverse: 5’AGGGTCCCTACAGGTCCTTTC-3’

Off-target-4

Forward: 5’-GACTTCTAGGCTTTCCCTCGTG-3’

Reverse: 5’-GCACAGCATAGTGGAAATAAGCAGGAG-3’

Off-target-5

Forward: 5’-CAGAAGATCTCGTGTCTAGCCAA-3’

Reverse: 5’-GCATCATAATGAGCTCCACCACAC-3’

Off-target-6

Forward: 5’-CAACTCATCGTATGAATGCATGTGCATTTTTGG-3’

Reverse: 5’-CATCAGAGAAATCCAAATCCAAACCACAATGAG-3’

Off-target-7

Forward: 5’-CACGTGCATATGTCTCTATGGTGG-3’

Reverse: 5’-CAGAGAAATGCACATCAAAACCACAGTGAG-3’

Off-target-8

Forward: 5’-CCCAGATCTTCCTGGCCCTA-3’

Reverse: 5’-AATTCTCTGAATTCCCCTGGCGC-3’

Off-target-9

Forward: 5’-GGACCACTTATTTAAAACTGCCCTTCCTAC-3’

Reverse: 5’-GCGTTATGTCTTTCTAGGAGACCTTGC-3’

Off-target-10

Forward: 5’-CCTGTGTGTTATCAGCCTGTGG-3’

Reverse: 5’-CCTAGCCTAAGGTCCCTGGAA-3’

2.7 Western blotting analysis

Cell were lysed by SDS protein lysis buffer. Protein concentration was determined by using the BioRad Protein Assay Kit (BioRad). 20 μg of protein was mixed with 6x SDS loading dye and denatured at 100 °C for 10 mins. Each sample was resolved on 5% stacking and 8-12% resolving polyacrylamide gel (SDS-PAGE) at 130V, then transferred to a nitrocellulose membrane or PVDF membrane at 110V for 100 mins. 5% non-fat milk contained 0.1% Tween 20 in TBS was used for blotting the membrane at room temperature for 1 hour. Membrane was incubated with appropriate concentration of the primary antibody for overnight at 4 °C. After washing, secondary antibody was added and incubated at room temperature for 1 hour. Blots were developed with ECL reagent (Millipore) and images were detected by ChemiDoc MP Imaging System (Bio-Rad).

2.8 Cell proliferation assay

Cells transfected with lentivirus containing sgCTCF or shRNAs were seeded in triplicates in a 24-well plate. Cell proliferation was measured by counting cells number over a period. Cells were trypsinized, stained by trypan blue, and counted using a hemacytometer.

2.9 Colony formation assay

Cells were seeded onto a 6-well plate and incubated with culture medium containing puromycin. After 7-10 days, colonies will be fixed with 100% methanol for 20 mins followed by staining using 0.5% crystal violet for 20 mins at room temperature. Cells were washed three times with PBS and air dried. Colonies containing over 50 cells were counted. Each assay was done in triplicate.

2.10 Soft agar assay

Soft agar containing bottom and top agar was prepared. Bottom agar was prepared as 0.6% agar by mixing $\frac{1}{3}$ volume of agar (1.8%), $\frac{1}{2}$ volume of medium (2x DMEM + 20% FBS), and ddH_2O. Mixture was incubated at 42°C for 10 mins. 2 mL of bottom agar was plated in each well and was allowed to set for 30 min in room temperature. Top agar (0.45%) was prepared by mixing $\frac{1}{2}$ agar (1.8%) and $\frac{1}{2}$ medium (DMEM + 10% FBS +1% PS), and the mixture was kept in 42°C for 10 mins. Subsequently, cells suspended in regular growth medium (DMEM + 10% FBS +1% PS) were mixed with the top agar, followed by laying on top of the bottom agar. After 2 weeks, the plate was stained with 0.5 % crystal violet at room temperature. Colonies were counted under a microscope.

2.11 Sphere formation assay

Serum-free medium containing DMEM/F12 medium supplemented with 20 ng/ml human recombinant epidermal growth factor (EGF), 10 ng/ml human recombinant

basic fibroblast growth factor(bFGF), N2 and B27 (thermo fisher), 100 units/mL penicillin, 100 μg/ml streptomycin, and 0.25% methylcellulose (Sigma, USA) was used for cancer cell sphere culture. Cells were cultured at a density of 1000 cells/mL. After 1 weeks, spheres over 100 μm in diameter were counted.

2.12 Cell migration and invasion analysis

Cell migration analysis was performed using a Transwell system (8-μm pore size; Millipore). Forty thousand cells were seeded on top of the Transwell chamber in serum-deficient cultures. DMEM supplemented with 10% FBS was added to the basal compartment for use as a chemical attractant. After 16 hours of cell migration, cells on the top of the chamber were scraped and removed. Cells migrated to the bottom side of the chamber were fixed with methanol for 15 minutes, stained with 0.5% crystal violet, photographed and counted. Invasion analysis was conducted in a manner similar to the migration assay, excepted that the chamber was pre-coated with Matrigel (Corning). Migration and invasion assays were performed in triplicate and were repeated three times.

2.13 Cell cycle analysis

6 x 10^5 cells were collected, washed with PBS, and fixed in 70% ethanol at -20°C overnight. After fixation, cells were washed with PBS for three times, and were resuspended in 470 μL of PBS and 5 μL of 10 mg/mL RNase (treated with boiling), followed by incubation at 37°C for 20 mins. Subsequently, 25 μL of 1 mg/mL PI

staining buffer was added. After 10 mins, cells were analyzed by BD Accuri C6 Flow Cytometer (The University Research Facility in Life Sciences (ULS) of The Hong Kong Polytechnic University, Hong Kong).

2.14 Apoptosis analysis

3.5 x 10^5 cells were collected and washed twice with cold PBS. 100 μL of annexin V binding buffer, 5 μL of Annexin V-FITC and 5 μL of PI (Transgene, # FA101) were mixed with cells, followed by incubation for 15 mins. After incubation, 400 μL of Annexin V binding buffer was added to the cells, and subjecte to analyzed by BD Accuri C6 Flow Cytometer (The University Research Facility in Life Sciences (ULS) of The Hong Kong Polytechnic University, Hong Kong).

2.15 Senescence β-Galactosidase Staining

Senescence β-galactosidase staining kit (CST, #9860) was used to detected β-galactosidase activity. Cells were fixed by 1 ml of fixative solution for 10-15 mins at room temperature. Cells were washed twice with 1x PBS, and 1 ml of the β-galactosidase staining solution was added to each well, followed by incubation at 37°C overnight in a dry incubator. On the next day, cells were examined under a microscope for. Blue cells, signifying positivity for β-galactosidase activity, were counted.

2.16 Seahorse XF Cell Mito Stress Test

Cellular oxidative phosphorylation activity was determined by the oxygen consumption rate (OCR) of the cells, using Mito Stress Test kit from Agilent Seahorse according to description. Modulators of the electron transport chain, including oligomycin, carbonyl cyanide-4 (trifluoromethoxy) phenylhydrazone (FCCP), rotenone, and antimycin. Briefly, cells were plated in Seahorse XF microplate and incubated at 37°C overnight. On the next day, cells were changed to Seahorse XF DMEM medium containing 1 mM pyruvate, 2 mM glutamine, and 10 mM glucose (pH 7.4). As the measurement proceeds, modulators of the electron transport chain, including oligomycin, carbonyl cyanide-4 (trifluoromethoxy) phenylhydrazone (FCCP), rotenone, and antimycin, was added sequentially to the microplate. Microplate was measured using Agilent Seahorse XFe24 Extracellular Flux Analyzer (The University Research Facility in Life Sciences (ULS) of The Hong Kong Polytechnic University, Hong Kong).

2.17 Glycolysis stress test

Glycolysis stress assay was determined by measuring the extracellular acidification rate (ECAR) using Agilent Seahorse XF Cell Glycolysis Stress Test kit (Agilent Seahorse). Cells were plated in the Seahorse XF cell culture microplate and incubated at 37°C for overnight. On the next day, cells were changed to Seahorse XF DMEM medium containing 2 mM glutamine. ECAR was first determined in the absence of glucose, followed by the injection of glucose, oligomycin and 2-Deoxy-D-glucose (2-DG),

respectively, using Agilent Seahorse XFe24 Extracellular Flux Analyzer (The University Research Facility in Life Sciences (ULS) of The Hong Kong Polytechnic University, Hong Kong).

2.18 F-actin staining analysis

Cells were seeded for overnight. On the next day, cells were fixed with 4% paraformaldehyde (PFA) for 15 min at room temperature. After washing, 0.1% Triton X-100 was added to the fixed cells for 5 minutes to permeablize cells. After PPS wash, 5 nM of AlexaFluor 568 phalloidin (Invitrogen), a high affinity F-actin probe coupled with AlexaFluor 568 dye, was incubated with cells at room temperature for 60 minutes. After rinising, cells were observed by Opera Phenix High-Content Screening System (PerkinElmer) and analyzed by Harmony High-Content Imaging and Analysis Software (PerkinElmer).

2.19 Determination of NAD^+/NADH ratio

The ratio of NAD^+/NADH in cells was determined by the NAD+/NADH-Glo assay kit according to manufacturer's instruction. Briefly, the fluorescein detection reagent was prepared as described in the protocol.20,000 cells in 50 μl PBS were lysed by adding 50 μl of base solution containing 1% DTAB (alkali-treated samples). 50 μl of each sample was taken for acid treatment. Subsequently, 25 μl of 0.4 N hydrochloric acid was added to the well and incubated at 60°C for 15 minutes. After equilibration to room

temperature for 10 minutes. 25 µl of 0.5 M Tris base was added to each acid-treated cell well to neutralize the acid, and 50 µl of HCl/Tris solution was added to the alkali-treated sample. To carry out NAD+/NADH measurement, an equal volume of NAD+/NADH-Glo assay reagent was added to each well, followed by incubation for 30-60 minutes at room temperature. Subsequently, luminescence was taken using luminometer.

2.20 Glucose uptake assay

The glucose uptake rate was determined by the Glucose Uptake-Glo Assay kit according to manufacturer's instruction. The method was based on the detection of 2-deoxyglucose-6-phosphate (2DG6P) in cells. Briefly, 7000 cells were seeded onto a 96-well plate and incubated overnight with culture medium. Next day, removed cells medium and washed with 100µl PBS twice. 50µl of 1mM 2-deoxyglucose (2DG) was added per well, shaked briefly, and incubated 10 minutes at room temperature. Followed by adding 25µl of stop buffer and 25µl of neutralization buffer. 2DG6P detection reagent was prepared as described in the protocol. Each well was added 100µl of 2DG6P Detection Reagent and incubated for 1 hours at room temperature. Subsequently, recorded luminescence value with the luminometer.

2.21 Lactate secretion assay

The lactate production was examined by the Lactate-Glo Assay kit according to manufacturer's instruction. The method was based on detection of L-Lactate in cells

medium. Briefly, 7000 cells were seeded onto a 96-well plate and incubated overnight with pyruvate-free and 3% dialyzed serum medium. Next day, diluted cells medium by removing 2 µl into 98 µl PBS. Then transferred the 50 µl of diluted sample to a new 96-well plate. Lactate detection reagent was prepared as described in the protocol. Each well was added 50 µl of lactate detection reagent and incubated for 1 hours at room temperature. Subseqeuntly, luminescence was taken using luminometer.

2.22 Cellular ATP assay

Cellular ATP production was determined by the CellTiter-Glo Luminescent Cell Viability Assay kit. The medthod was based on the determination of ATP present in viable cells. Briefly, 7000 cells were seeded onto a 96-well plate and incubated overnight. CellTiter-Glo dection reagent was prepared as described in the protocol. Next day, 50 µl of CellTiter-Glo dection reagent was added to each well, incubated for 1 hours at room temperature. Subseqeuntly, luminescence was taken using luminometer.

2.23 RNA-sequencing

Total RNAs were extracted from cells and subjected to whole transcriptome shotgun sequencing (RNA-seq) analysis. RNA-seq was conducted by Novogene. The quality of the raw reads was checked using the Fastqc program. After removing the index and adapter sequences, high-quality trimmed reads were mapped against the human

reference genome (GRCh38 p12 Gencode v30) using Hisat. Gene expression levels indicated by FPKM {Trapnell:2010kd} were calculated using StringTie.

2.24 Differential expression analysis

The analysis was conducted with the help from Dr. Lakhansing Pardeshi from the University of Macau. Differential expression analysis was performed by comparing two groups two groups (with two biological replicates per group) using the DESeq R package (1.18.0). DESeq presents statistical procedures to determine differential expression in numerical gene expression data using a model based on a negative binomial distribution. An adjustment was made to the resulting P-values using Benjamini and Hochberg's method to control for false discovery rates. Genes with fold change greater than 1.5 and adjusted P-value < 0.05 were classified as differentially expressed.

2.25 GO and KEGG enrichment analysis of differentially expressed genes

Gene Ontology (GO) enrichment analysis of differentially expressed genes was evaluated and performed using the Metascape online tool (https://metascape.org/gp/index.html#/main/step1). GO term enrichment assigned genes to a predefined set of bins depending on their functional characteristics, under the terms biological process (BP), cellular component (CC), and molecular function

(MF), respectively. KEGG(http://www.genome.jp/kegg/), which categories DEGs to understand high-level functions and utilizes of the biological system, was performed using KOBAS software(http://kobas.cbi.pku.edu.cn).

2.26 Chromatin Immunoprecipitation (ChIP)

Chromatin immunoprecipitation assay was performed with the help of Dr. Liu Hang from The Hong Kong Polytechnic University. Cells were fixed by adding 270 µl of 37% formaldehyde to 10 ml of culture medium and incubated for 15 min at room temperature. Subsequently, 625 µl of glycine (2M) was added. After 5 mins, cells were washed twice with 10 mL of cold PBS containing 1 mM PMSF. Cells were scraped with ice-cold PBS and centrifuged at 1000 rpm for 8 min at 4°C. After removing the supernatant, 420 µl of SDS lysis buffer was added to the cell pellet, followed by incubation on ice for 10 min. Lysates were then re-suspend to 1 ml for ultrasonication of genomic DNA into 200 to 500 bp. Subsequently, the DNA was centrifugated in 13000 rpm for 10 minutes at 4°C, followed by the addition of 10-fold excess of ChIP dilution buffer (1620 µl). 60 µl of the diluted supernatant was reserved as input control in subsequent sequencing reactions. 60 µl mixture of salmon sperm DNA and 50% protein G agarose slurry was added to the rest of the diluted samples to remove non-specific binding. Subsequently, 4 µg of CTCF antibody (or IgG antibody) was added to the supernatant. On the next day, salmon sperm DNA and 50% protein G agarose will be added and incubated at 4°C for 1 hr with rotation, followed by centrifugation for 3 min and removal of the

supernatant. The immunocomplex consisted of protein G agarose, antibodies, and chromatins was washed three times with wash buffers and twice with Tris-EDTA (TE) buffer. Subsequently, 600 µl of elution buffer was added to the agarose. Reverse cross-linking was carried out by the addition of 24 µl of 5 M NaCl to 600 µl of the consolidated eluate, followed by heating at 65°C overnight. Proteinase K (10 mg/ml) was added to the samples and incubated at 55°C overnight. An equal volume of chloroform was added to each sample, followed by incubation for 20 min at 20°C. Afterwards, samples were centrifuged for 10 min to remove the supernatant. 2 µl of glycogen and 700 µl of isopropanol was added, and samples were incubated at -20°C for overnight. After centrifugation at 13,000 rpm for 20 min at 4°C, supernatant was removed. DNAs were pelleted by the addition of 1ml of cold 70% ethanol followed by centrifugation at 13000 rpm for 10 minutes. DNA pellet was air-dried and dissolved in TE buffer.

Chapter Three: Results

3.1 Expression of CTCF in clinical HCCs

3.1.1 CTCF expression across TCGA pan-cancer cohort

My earlier study showed that CTCF is overexpressed in a sub-group of clinical HCC from local cohort, and the overexpression is associated with a poorer prognosis [219]. To further determine if CTCF overexpression is a HCC-specific event, or it represents a general phenomenon among different cancer types, CTCF expression level in a pan-cancer cohort in the TCGA database was obtained and analyzed with University of ALabama at Birmingham CANcer Data Analysis Portal (UALCAN) [223]. It was found that CTCF is expressed at a lower level in normal livers, as indicated from the normal liver tissues from the cholangiocarcinoma (CHOL) and hepatocellular carcinoma (LIHC) groups compares to other normal tissues in other tumor groups (Figure 3.1–1). Moreover, in agreement with our study, CTCF was significantly overexpressed in LIHC. Moreover, the analysis also showed that, comparison to the adjacent normal tissues, CTCF is also significantly overexpressed in CHOL, esophageal carcinoma (ESCA), and stomach adenocarcinoma (STAD) (Figure 3.1–1). Together, these data suggested that CTCF play differential roles in the pathogenesis of different cancers. Further to the analysis earlier, this analysis suggested that CTCF may play specific pathogenic role in tumors of liver origin, including CHOL and LIHC.

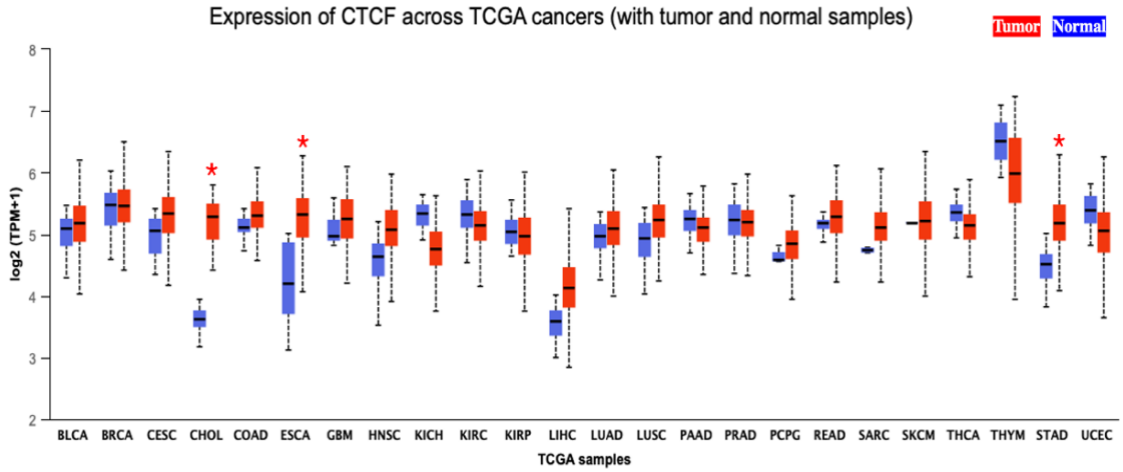

Figure 3.1–1 Expression of CTCF in TCGA Pan-cancer cohort. (Blue: normal; red: cancer)

Validation of the expression levels of CTCF in TCGA normal and different cancers. TCGA, The Cancer Genome Atlas; BLCA: Bladder urothelial carcinoma; BRCA : Breast invasive carcinoma; CESC : Cervical squamous cell carcinoma; CHOL : Cholangiocarcinoma; COAD : Colon adenocarcinoma; ESCA : Esophageal carcinoma; GBM : Glioblastoma multiforme; HNSC : Head and Neck squamous cell carcinoma; KICH : Kidney chromophobe; KIRC : Kidney renal clear cell carcinoma; KIRP : Kidney renal papillary cell carcinoma; LIHC: Liver hepatocellular carcinoma; LUAD : Lung adenocarcinoma; LUSC : Lung squamous cell carcinoma; PAAD : Pancreatic adenocarcinoma; PRAD : Prostate adenocarcinoma; PCPG : Pheochromocytoma and Paraganglioma; READ : Rectum adenocarcinoma; SARC : Sarcoma; SKCM : Skin cutaneous melanoma; THCA: Thyroid carcinoma; THYM : Thymoma; STAD : Stomach adenocarcinoma; UCEC : Uterine corpus endometrial carcinoma; TPM, transcripts per million.

3.1.2 Expression of CTCF in Liver Hepatocellular Carcinoma

The correlation between CTCF expression and clinical features of LIHC was analyzed further using the TCGA database. Heightened CTCF expression of is significantly associated with poor overall survival of HCC patients (Figure 3.1–2). These data are consistent with my earlier findings from a cohort of HCC patients from this locality [219].

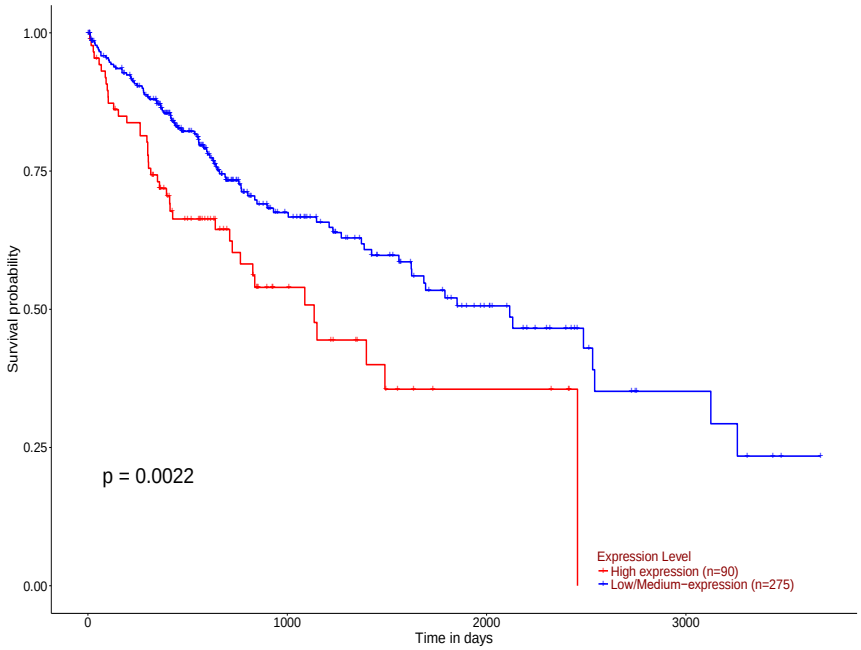

Figure 3.1–2 CTCF expression in HCCs and its prognostic significance.
Kaplan–Meier analyses of CTCF expression in HCC and overall survival suggested that the survival of the patients who had high CTCF expression was significantly shorter; P = 0.002. High expression with TPM values above upper quartile (red) and Low/Medium expression with TPM values below upper quartile (blue).

3.1.3 Expression of CTCF in primary hepatocytes and HCC cell lines

Western blotting and real-time quantitative PCR (RT-qPCR) analysis was conducted to evaluate CTCF expression in primary hepatocytes and HCC cell lines, respectively. To the best of my knowledge, IHC study has demonstrated the CTCF expression in the normal tissue as shown in previous study[219]. To obtain a more comprehensive understanding of CTCF expression in normal hepatocytes, three primary hepatocytes from independent donors, and a transformed primary hepatocyte cell lines were analyzed. In addition, four HCC cell lines were selected for the analysis of CTCF expression. These include HepG2, Hep3B, Huh7 and PLC5 cells respectively. Western blot analysis suggested that CTCF is almost undetectable in the three primary hepatocytes, while there is a very lower level of expression in the transformed primary hepatocyte cell line. On the other hand, it is highly expressed in all HCC cell lines (Figure 3.1–3A). RT-qPCR analysis of these cells showed similar pattern of CTCF expression (Figure 3.1–3B).

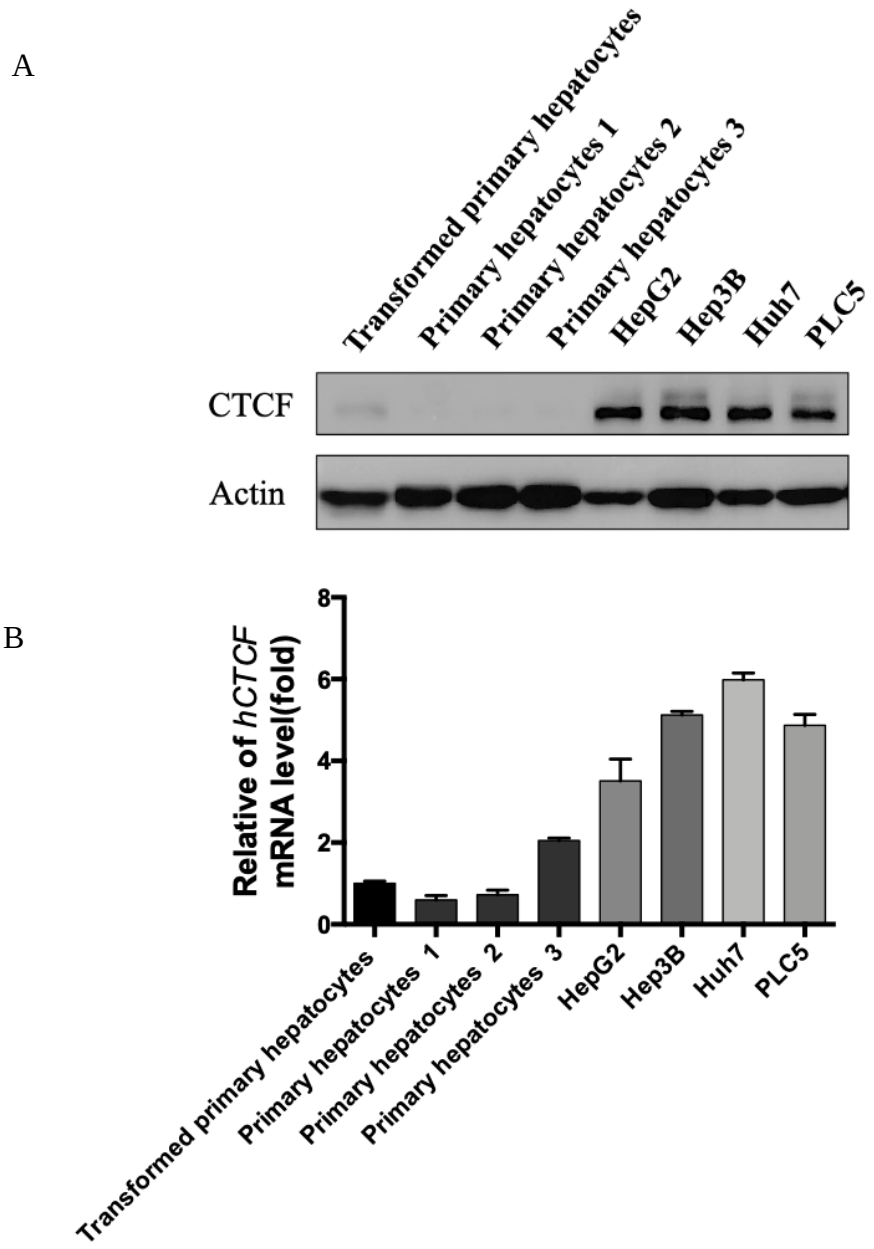

Figure 3.1–3 CTCF expression level in primary hepatocytes and HCC cells.
(A)Western blot analysis of CTCF was carried out in representative primary hepatocytes and HCC cell lines (upper panel), with β-actin serving as a loading control (lower panel). (B) qRT-PCR analysis of CTCF expression in the indicated primary hepatocytes and HCC cell lines. The relative expression of CTCF mRNA was normalized against β-actin mRNA.

3.1.4 Expression of CTCF in clinical HCC specimens

My earlier study showed that CTCF is overexpressed in a subpopulation of HCC from a local patient cohort[219]. To determine if such association remains valid in wider Chinese patients' population, thirty pairs of the clinical HCC specimens were obtained from the Sun Yat-Sen University Cancer Center, Guangzhou, China, for analysis of CTCF expression. Western blot analysis showed that 10 out the 30 HCC cases (33.33%) examined showed an increase in CTCF level of more than 2 folds, when comparing the tumoral to the adjacent non-tumoral liver tissues (Figure 3.1–4). Taken together, the finding from the TCGA data set, and HCC specimens from Hong Kong and Guangzhou, suggested that the overexpression of CTCF in clinical HCCs may play a role in its tumorigenesis.

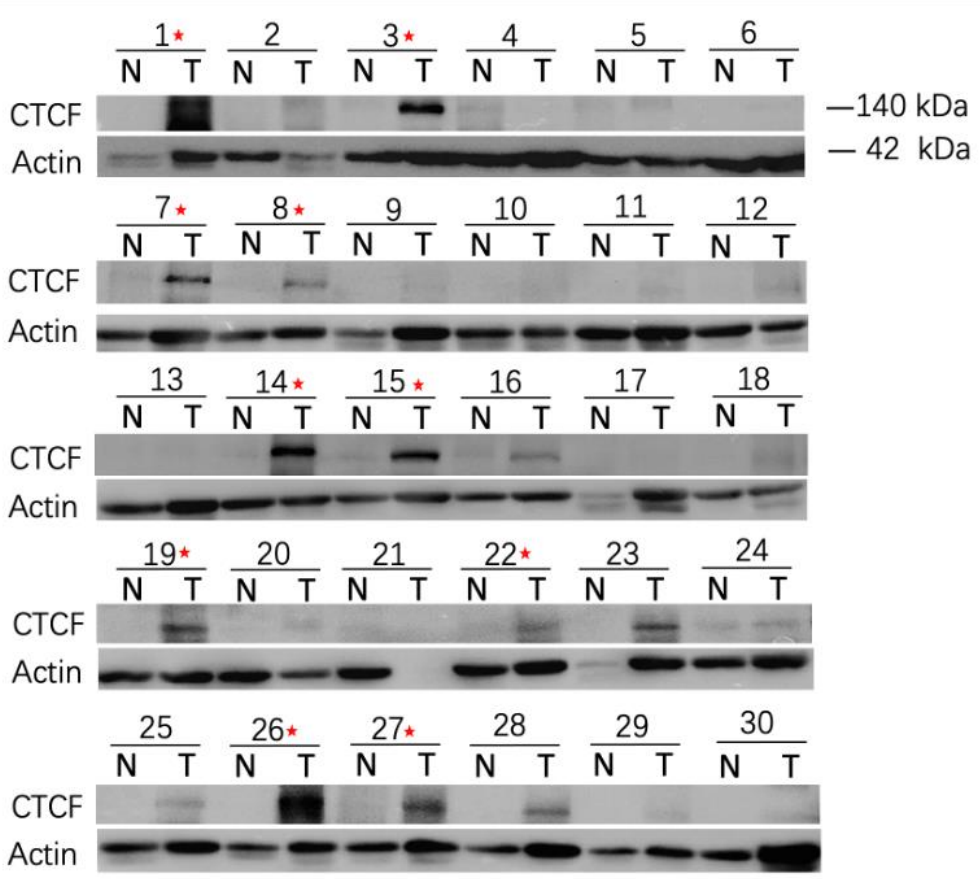

Figure 3.1–4 Expression of CTCF protein in clinical HCCs and adjacent nontumorous normal liver tissue.

Western blot analysis of CTCF in 30 pairs of HCCs. β-actin was served as a loading control (T: HCC; N: adjacent nontumoral liver; *, specimen with CTCF overexpression.)

3.2 CTCF knockout in HCC cells

3.2.1 Knockout of CTCF in HCC cells using CRISPR/Cas9 system.

My earlier study has shown that shRNA-mediated gene knockdown of CTCF inhibited HCC cell growth and metastasis[219]. Nevertheless, recent studies suggested that shRNA may exert non-specific effects of on cells, such as an inhibitory effect on the cell growth[224], [225]. Therefore, I decided to interrogate the role of CTCF in HCC using Clustered Regularly InterSPaced Repeats (CRISPR)/Cas9 gene knockout strategy, which is believed to generate gene knockout in a more specific and precise manner [221], [226]. The CRISPR/Cas9 system I used was consisted of a lentiviral packaging vector that simultaneously expresses mammalian-optimized Cas9 nuclease and single guide RNA (sgRNA) [222]. To this end, a sgRNA sequence targeting exon 3 of the CTCF gene was designed (sgCTCF) and cloned downstream of the U6 promoter of the vector. Vector without the sgRNA insert was used as a control. The vectors were packaged into lentiviral particles independently, followed by transduction into Huh7 and PLC5 cells, respectively. Stable population of lentiviral transduced cells were obtained by puromycin selection. CTCF knockout PLC5 cells (PLC5-KO) and CTCF knockout Huh7 cells (Huh7-KO), and their respective control cells, Huh7-C and PLC5-C cells, were obtained. Western blot analysis showed that CTCF was successful knockout from these cells (Figure 3.2–1).

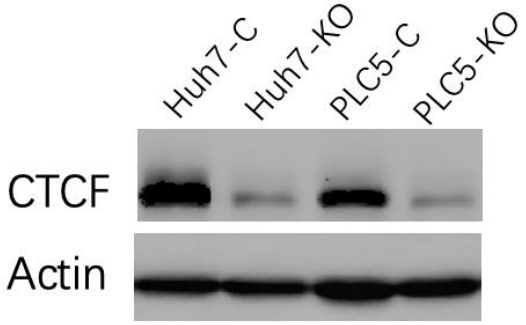

Figure 3.2–1 Expression of CTCF in CTCF knockout cells.

Western blotting analysis showing the expression of CTCF from Huh7-KO and PLC5-KO cells respectively, compares to Huh7-C and PLC5-C cells. β-actin (Actin) was used a loading control. Huh7-C, control Huh7 cells; Huh7-KO, CTCF knockout Huh7 cells; PLC5-C, control PLC-5 cells; PLC5-KO, CTCF knockout PLC5 cells.

3.2.2 Evaluation of the on- and off-target activity of CTCF sgRNA.

CRISPR/Cas9 gene targeting will lead to targeted gene excision and repair, creating insertions and deletions (indels), resulting in frame shift mutation and gene inactivation [221], [226]. However, studies suggested CRISPR/cas9 gene targeting may also result in aberrant genomic mutations due to non-specific targeting sgRNA sequence and experimental conditions[227]–[230]. Accordingly, the on-targeted and off-targeted activity of CTCF sgRNA used in this study were evaluated. The sequence of the CTCF sgRNA was analyzed by COSMID[231](https://crispr.bme.gatech.edu) to identify potential off-target genomic loci. Subsequently, the top ten potential off-target loci (Table 3.2-1) as well as the targeted loci were amplified by PCR, followed by DNA sequencing analysis to confirm the targeted and off-targeted activity the CTCF sgRNA in PLC5-KO and Huh7-KO cells respectively. A 87% indels in the CTCF locus was identified in the PLC5-KO cells, while no indels can be found from the predicted off-target loci (Figure 3.2–2A, Figure 3.2–3A). On the other hand, there was a 90% indels in the CTCF locus in the Huh7-KO cells, and a 3% indels was found in two predicted loci respectively (Figure 3.2–2B, Figure 3.2–3B). Together, these data suggested that CTCF sgRNA demonstrates target specificity in general, despite a minor non-specific targeting activity.

The indels in the CTCF locus of Huh7-KO and PLC5-KO cells were analyzed in more details. We found premature termination codons was introduced in exon at four and

five codons downstream of the CTCF sgRNA PAM sequence in Huh-7 KO and PLC5-KO cells respectively (Figure 3.2–4). Taken together, these results suggested that CTCF sgRNA effectively knockout CTCF expression by introduction of premature stop codon in exon 3 the coding sequence, resulting in a null mutation.

Table 3.2-1 The table of top 10 predicted off-target genomic loci of CTCF sgRNA.

Target No.	Sequences	Query type	Mismatch	Chromosome Position	Score
On-target	GAGCAAACTGCGTTATACAGAGG	No indel	0	Chr16:67611459-67611481	0
Off-target-1	GAGCAAACTGGTTATAAAGAGC	Del 10	2	Chr1:109470616-109470637	25.21
Off-target-2	GAGCAAACTGGTCATACAGATG	Del 10	2	Chr13:98031383-98031404	22.51
Off-target-3	GACAAACTGCTTTATACAATGG	Del 18	2	Chr10:31803027-31803048	7.46
Off-target-4	GAGGAAACTGAGTTATATAGAGG	No indel	3	Chr5:51020023-51020045	4.87
Off-target-5	GAGAAACTGCATTAGACAGAGG	Del 17	2	Chr14:41634381-41634402	3.78
Off-target-6	AGCAAACTGCTTTTTACAGTGG	Del 20	2	Chr20:45008605-45008626	3.33
Off-target-7	AGCAAACTGCTTTCTACAGTGG	Del 20	2	Chr4:30480811-30480832	3.33
Off-target-8	GAGAAACTGCTTGATACAGTGG	Del 17	2	Chr1:11176699-11176720	2.78
Off-target-9	GAGGAAACTGAGGTATACAGAGG	No indel	3	Chr12:89908491-89908513	1.97
Off-target-10	GAGGAAACTGAGGTATACAGAGG	No indel	3	Chr16:27524485-27524507	1.97

On-target: CTCF sgRNA; Del: deletion.

A

PLC5-KO	Indels (%)	KO-Score	R Squared
On-target	87	79	0.87
Off-target 1	0	0	1
Off-target 2	0	0	1
Off-target 3	0	0	0.92
Off-target 4	0	0	1
Off-target 5	0	0	1
Off-target 6	0	0	1
Off-target 7	0	0	1
Off-target 8	0	0	1
Off-target 9	0	0	1
Off-target 10	0	0	1

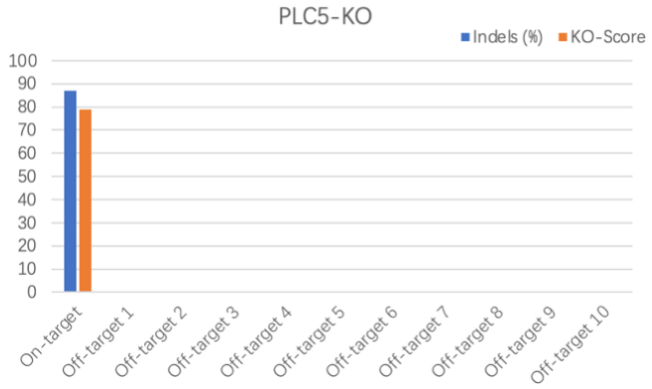

B

Huh7-KO	Indels (%)	KO-Score	R Squared
On-target	90	51	0.95
Off-target 1	0	0	1
Off-target 2	0	0	0.99
Off-target 3	0	0	1
Off-target 4	0	0	0
Off-target 5	0	0	1
Off-target 6	0	0	0.99
Off-target 7	3	3	0.95
Off-target 8	0	0	1
Off-target 9	0	0	1
Off-target 10	0	0	0.99

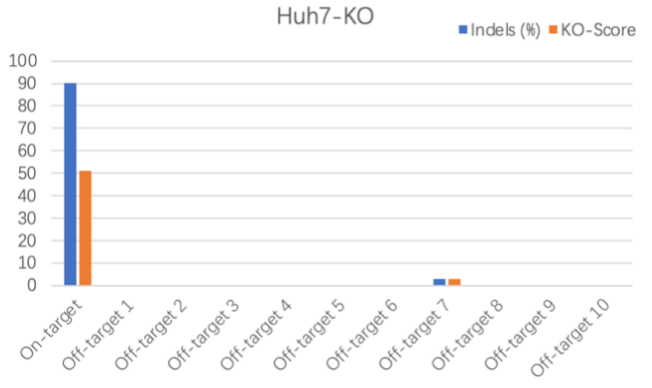

Figure 3.2–2 Summary of indels analysis of CTCF knockout cells.

On-target and off-target effects of the sgRNA in (A) PLC5-KO cells and (B) Huh7-KO cells.

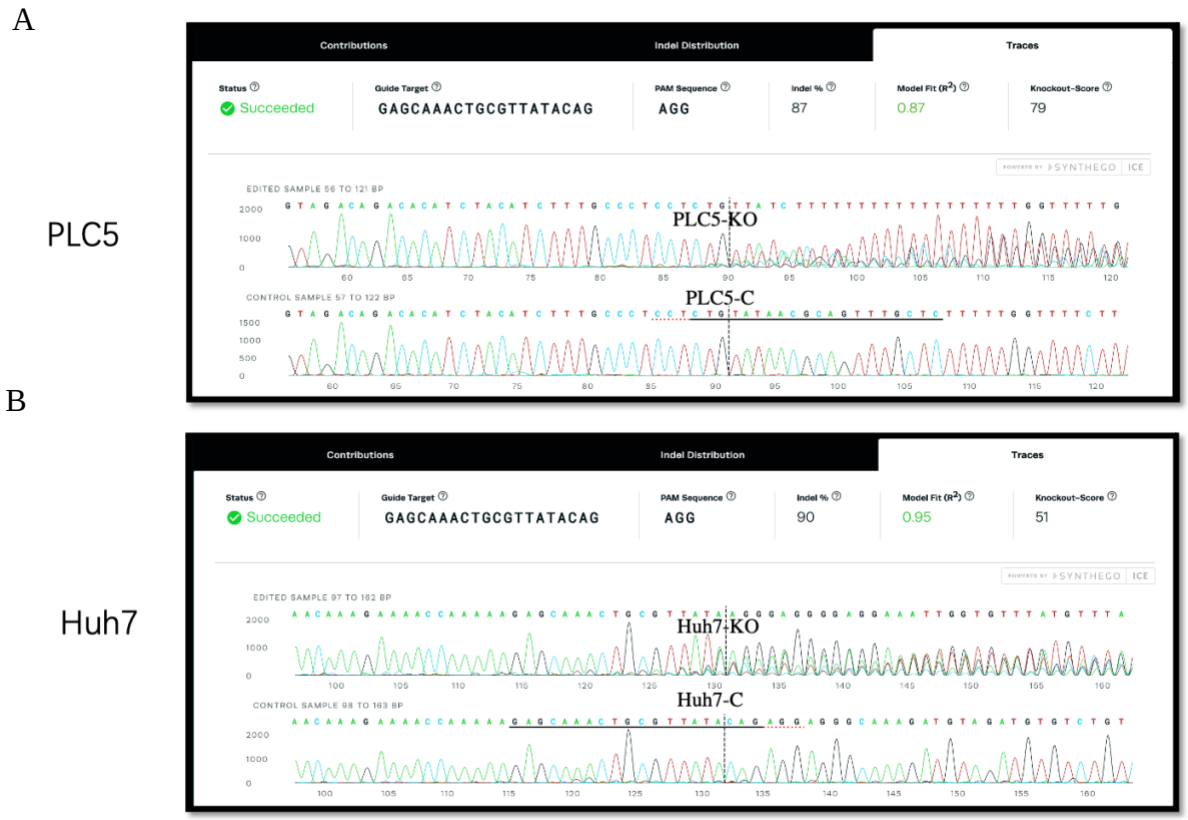

Figure 3.2–3 DNA sequencing analysis of CTCF locus in CTCF knockout cells.

DNA sequence analysis of the CTCF sgRNA targeting locus in (A) PLC5-KO and PLC5-C, and (B) Huh7-KO and Huh7-C cells.

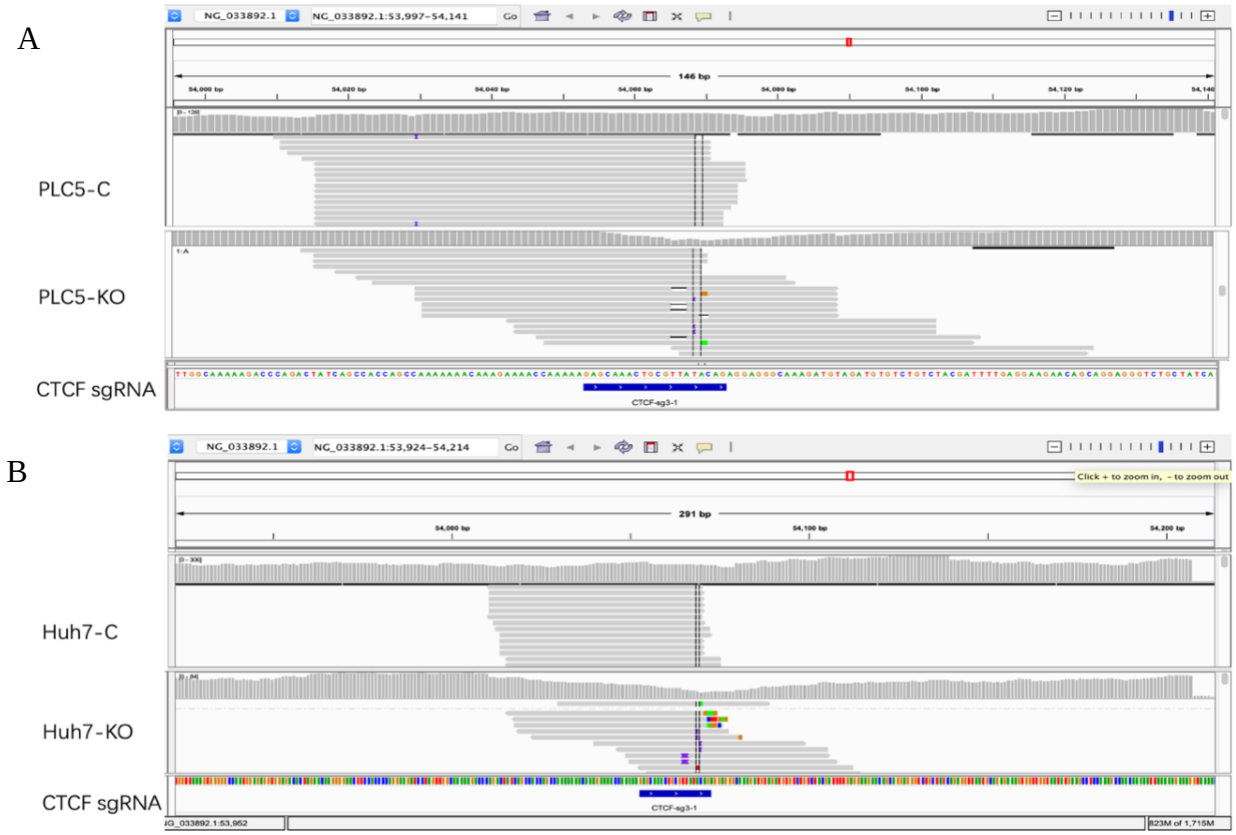

Figure 3.2–4 Transcriptomic analysis of CTCF knockout cells.

Summary of genomic aberrations at the CTCF sgRNA-targeted loci of the (A) PLC5-KO and (B) Huh7-KO cells. The position between the dotted lines indicated the Cas9 edited location. CTCF-sg3-1: sgRNA for CTCF.

3.2.3 Effect of CTCF knockout on HCC cells growth

Cell proliferation assay was conducted to evaluate the effect of CTCF knockout in of HCC cell growth. CTCF knockout cells (PLC5-KO and Huh7-KO) showed a significant reduction in proliferation over a period of 5 days, comparing to control cells (PLC5-C and Huh7-C) (Figure 3.2–5A). Similarly, colony formation assay revealed that cell colonies formed by PLC5-KO and Huh7-KO cells are reduced both in size and number comparing to the PLC5-C and Huh7-C cells respectively (Figure 3.2–5B). In addition, soft agar assay revealed a significant reduction in cell colonies in CTCF knockout cells (Figure 3.2–5C). Together, these findings suggested that CTCF regulates tumor cell growth and tumorigenicity.

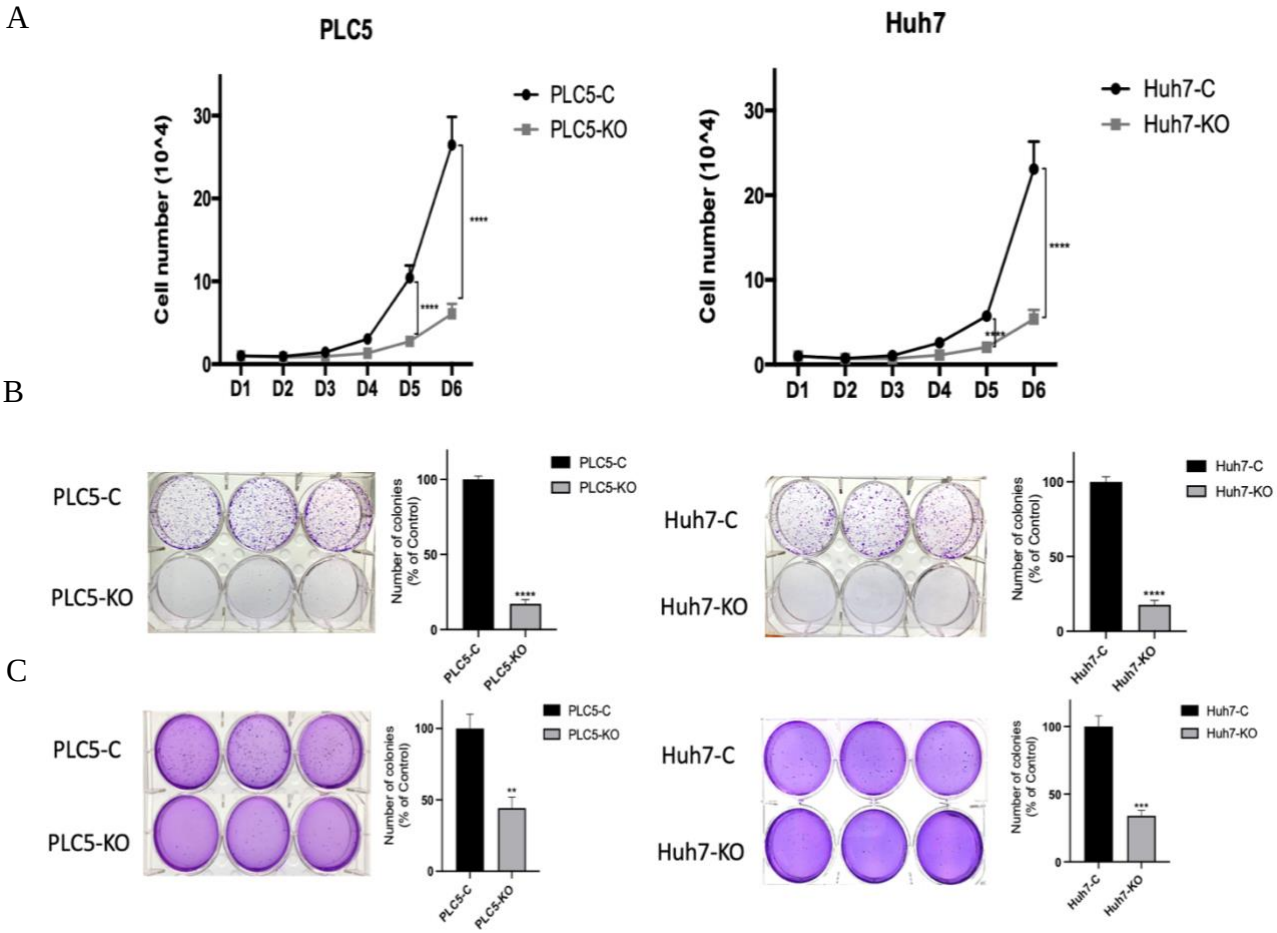

Figure 3.2–5 Proliferation and growth of CTCF knockout HCC cells.

(A) Cell proliferation of PLC5-KO and Huh7-KO cells compared with their respective control cells (PLC5-C and Huh7-C). 10,000 cells were counted daily after trypsinization and trypan blue staining. ****, $p<0.0001$, ***, $p<0.001$ by student's t test. (B) Colony formation assay was conducted by culturing cells for 7 days in the presence of 5 µg/mL puromycin. Colonies were stained using 0.25% crystal violet. (C) Soft agar assay was conducted by growing cells for 14 days in the presence of 5 µg/mL puromycin. Colonies were stained with 0.25% crystal violet.

3.2.4 Effect of CTCF knockout on tumor spheres formation in HCC cells.

To further determine if CTCF regulates stemness of HCC cells, sphere formation assay was conducted. CTCF knockout (PLC5-KO and Huh7-KO) and control (PLC5-C and Huh7-C) cells were cultured under stem cell culture conditions to allow the formation of tumor spheroids. Similar to the colony formation assay, CTCF knockout cells showed a significant reduction in the formation of spheroid number and size (Figure 3.2–6), suggesting that CTCF may play a role in the maintenance of stemness in HCC cells.

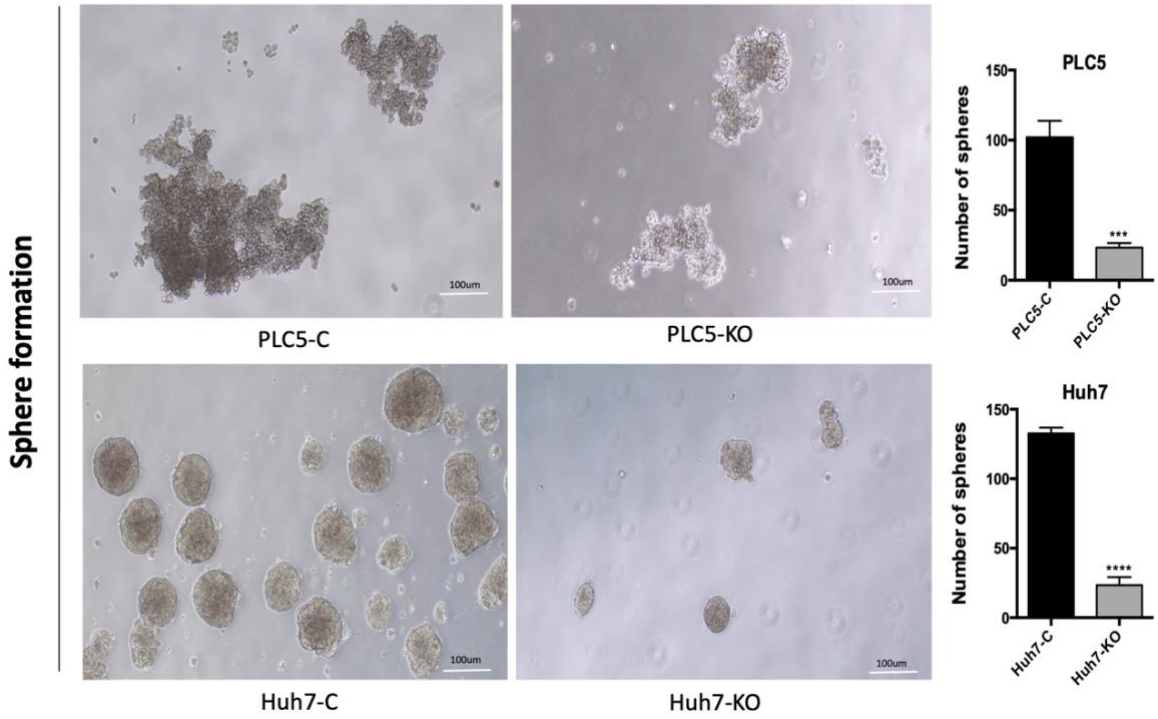

Figure 3.2–6 CTCF regulates tumor sphere formation.

CTCF knockout (PLC5-KO and Huh7-KO) or control (PLC5-C and Huh7-C) cells were maintained in stem cells culture medium for 7 days. Spheres with size > 100 mM were counted. ****, $p<0.0001$, ***, $p<0.001$ by student's t test.

3.2.5 Effect of CTCF knockout in cell senescence of HCC cells.

Microscopic inspection of the Huh7-KO and PLC5-KO cells revealed flattened and enlarged cell morphology, resembling cellular senescence. β-Galactosidase staining revealed that a significant increase β-galactosidase-positive (blue) cell population in the Huh7-KO and PLC5-KO cells compare with Huh7-C and PLC5-C cells (Figure 3.2–7), suggesting that cells undergo cellular senescence in the absence of CTCF.

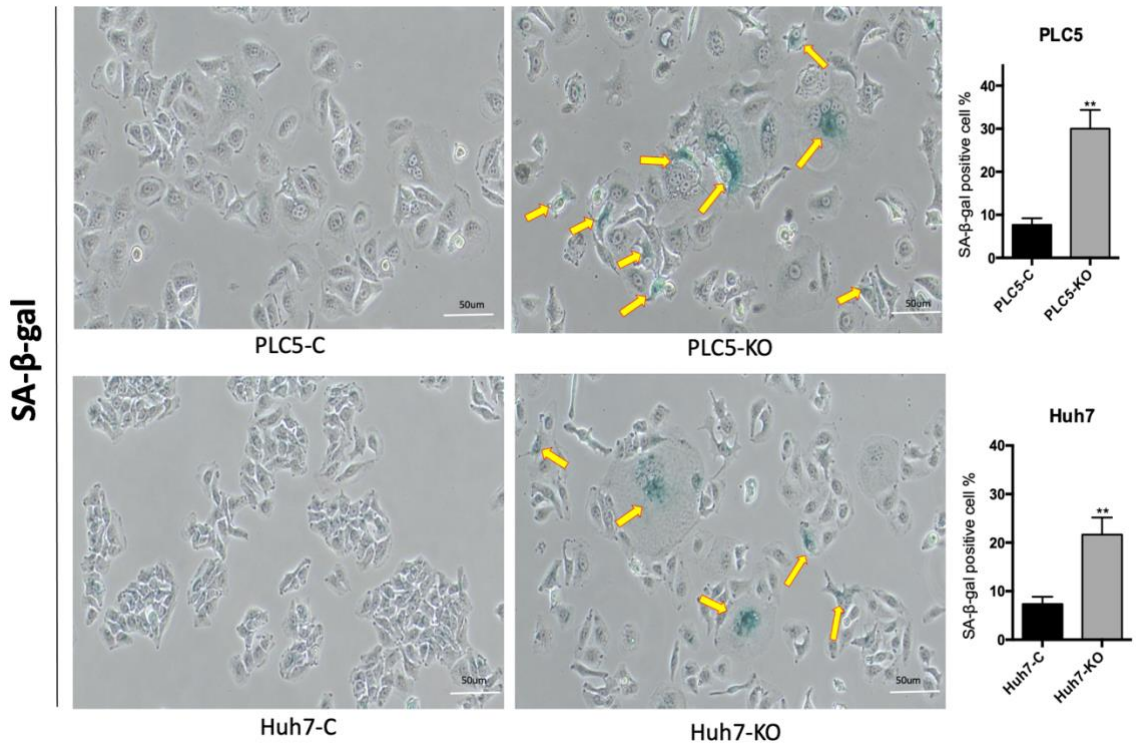

Figure 3.2–7 Effect of CTCF knockout induced cell senescence of HCC cells.
Left, β-Galactosidase (SA-β-gal) staining was conducted in PLC5 (PLC5-C and PLC5-KO) and Huh7 (Huh7-C and Huh7-KO) cells. Arrows indicated SA-β-gal positive staining. Three independent experiments were performed. Representative images were shown. Right, quantification of SA-β-gal positive cells. For each condition, 200 cells were counted. **, $p < 0.01$.

3.2.6 Cell cycle analysis in CTCF knockout cells

Next, cell cycle analysis was conducted to determine if the observed cell growth phenotypes are associated with defects in cell cycle progression. The analysis revealed that cell cycle distribution was altered in CTCF knockout cells, characterized by a G1 phase and S phase arrest PLC5-KO and Huh7-KO cells respectively (Figure 3.2–8).

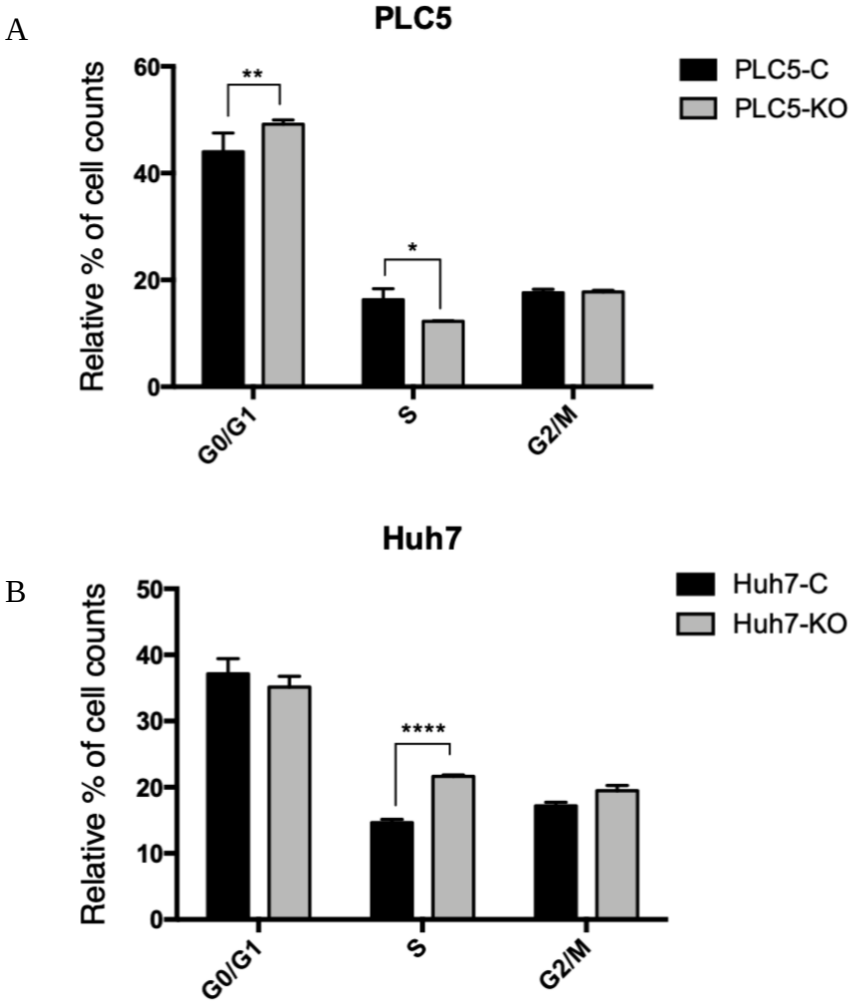

Figure 3.2–8 Cells cycle distributions in CTCF knockout HCC cells.

Cell cycle analysis of CTCF knockout cells was analyzed by fluorescence activated cell sorting analysis. Each condition was performed in triplicate. (A) PLC5-C vs PLC5-KO cells; (B) Huh7-C vs Huh7-KO cells. ****, $p < 0.0001$; **, $p<0.01$; *, $p<0.05$.

3.2.7 Analysis of apoptosis in CTCF knockout cells.

To determine if cell growth inhibition and senescence is associated with enhanced cell death, cells were analyzed for apoptosis using FACS analysis. Interestingly, CTCF knockout in both PLC5 and Huh7 cells did not result in a significant increase in cells undergoing apoptosis (Figure 3.2–9). Together, these data suggested that CTCF regulates HCC cell growth, but CTCF knockout did not compromise cell survival.

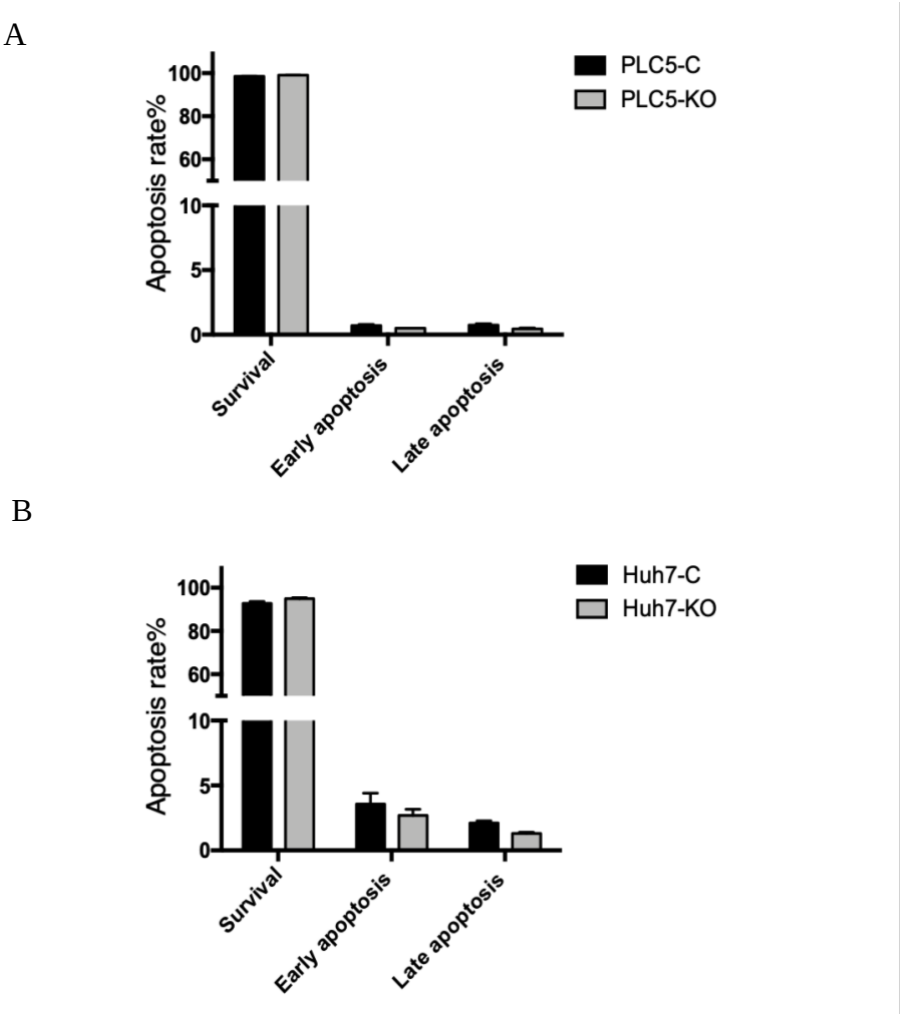

Figure 3.2–9. Analysis of apoptotis in CTCF knockout HCC cells.

FACS analysis of annexin V and propidium Iodide (PI) stained cells, (A) PLC5-C vs PLC5-KO cells; (B) Huh7-C vs Huh7-KO cells. *, $P<0.05$.

3.2.8 CTCF regulates motility and invasiveness of HCC cells

My previous study showed that shRNA knockdown of CTCF resulted in prominent inhibition of HCC cell motility and invasiveness via regulating FOXM1 expression [232]. Similarly, knockdown of CTCF in squamous cell carcinoma cells and gastric cancer cells compromised their motility and invasiveness [233][234]. To determine if CTCF knockout compromised HCC cells mobility and invasiveness, trans-well migration and invasion assays were conducted. I found that, similar to the shRNA knockdown [232], CTCF knockout significant mitigates cell mobility and invasiveness in both PLC5 and Huh7 cells (Figure 3.2–10).

Alternation in cell motility and invasiveness is often associated with alternation of epithelial-to-mesenchymal transition (EMT). EMT is mainly regulated by transcription factors belong to the SNAIL, TWIST and ZEB families[235], where it bestowed cells with metastatic and invasive properties, stemness features, resistance to cell death, and immunosuppression properties [235], [236]. Therefore, change in EMT markers in CTCF knockout cells were evaluated. As shown in Figure 3.2–11, the expression of epithelial cell marker, E-cadherin and β-Catenin in Huh7 cells was significantly reduced upon the knockdown of CTCF, whereas mesenchymal marker vimentin was induced. On the other hand, in PLC5 cells, knockout of CTCF resulted in increased expression of epithelial cell marker ZO-1, and a slight increase in the expression of mesenchymal marker Snail. Together, these findings suggested that CTCF did not

result in a consistent change in EMT markers in the HCC cell lines examined, and therefore CTCF might not regulate cell motility and invasiveness via regulating EMT pathways.

On the other hand, cell movement was regulated by dynamic changes of F-actin filaments, where stress fiber formation is associated with cell migration [237]–[239]. To determine if CTCF regulates cellular organization of F-actin, cellular actin cytoskeletons of CTCF knockout (PLC5-KO and Huh7-KO) and control (PLC5-C and Huh7-C) cells were visualized by phalloidin staining. No difference in the intensity of phalloidin staining nor the organization of phalloidin was observed（Figure 3.2–12), suggesting that CTCF does not regulate HCC cells motility and invasiveness via regulating actin organization.

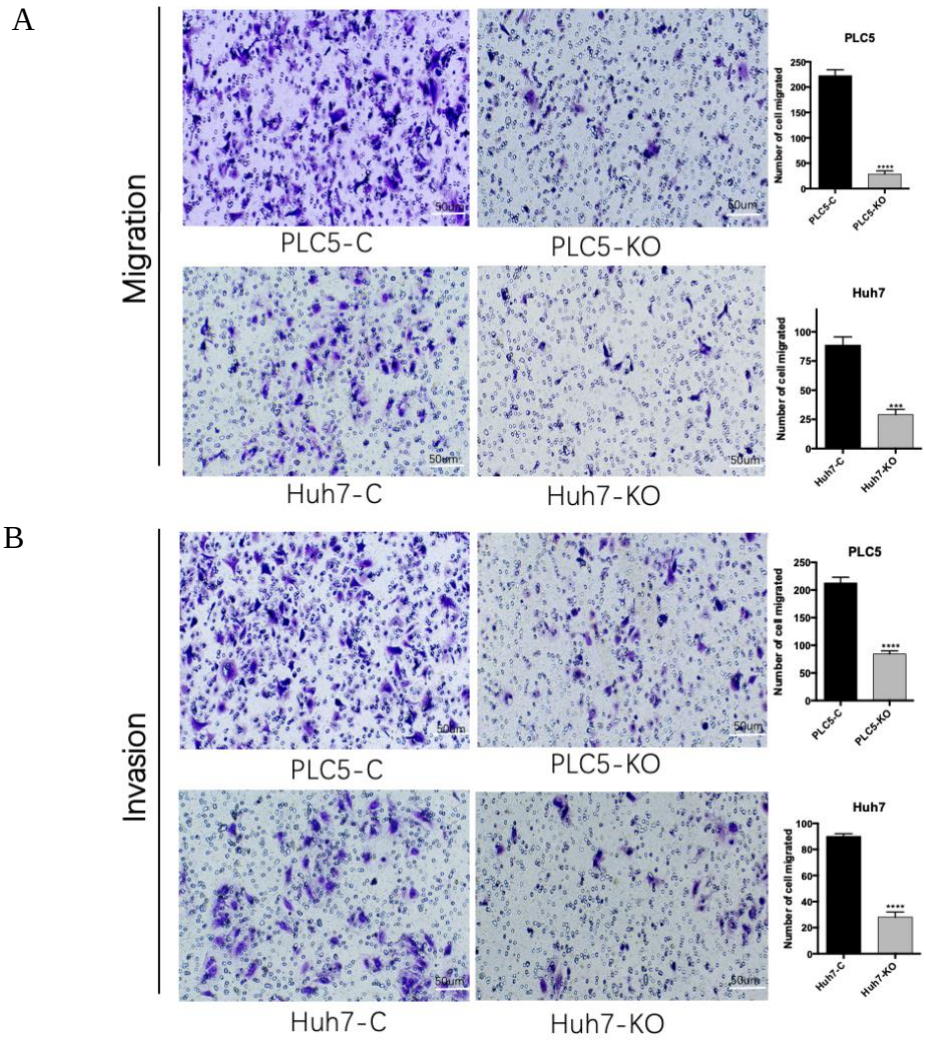

Figure 3.2–10 Regulation of HCC cells motility and invasiveness by CTCF.

HCC cells were allowed to migrate in transwell for 16 hours. (A) Left, representative pictures of cell migration assay. Right, quantification of cells migrated across the transwell. Each condition was repeated in triplicate. In each experiment, three randomly chosen fields were counted. (B) Left, representative pictures of cell invasion assay. Right, quantification of cells invaded across the transwell. Each condition was repeated in triplicate. In each experiment, three randomly chosen field were counted. Bars represent mean ± SD; ****, $p < 0.0001$; ***< 0.001.

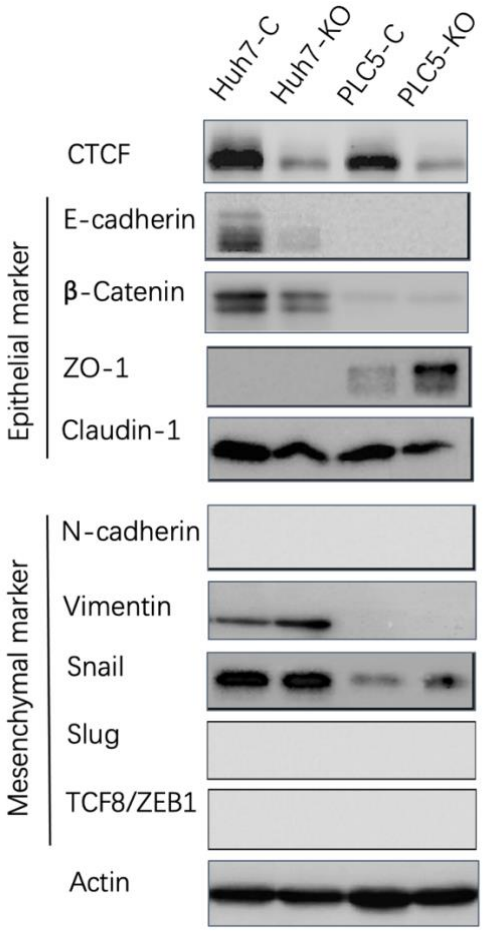

Figure 3.2–11. Western blot analysis of EMT makers in deletion CTCF cells.

Western blot analysis of the EMT makers in CTCF knockout HCC cells. Epithelial makers contain E-cadherin, β-Catenin, ZO-1, Claudin-1. Mesenchymal makers including N-cadherin, vimentin, snail, slug, ZEB1.

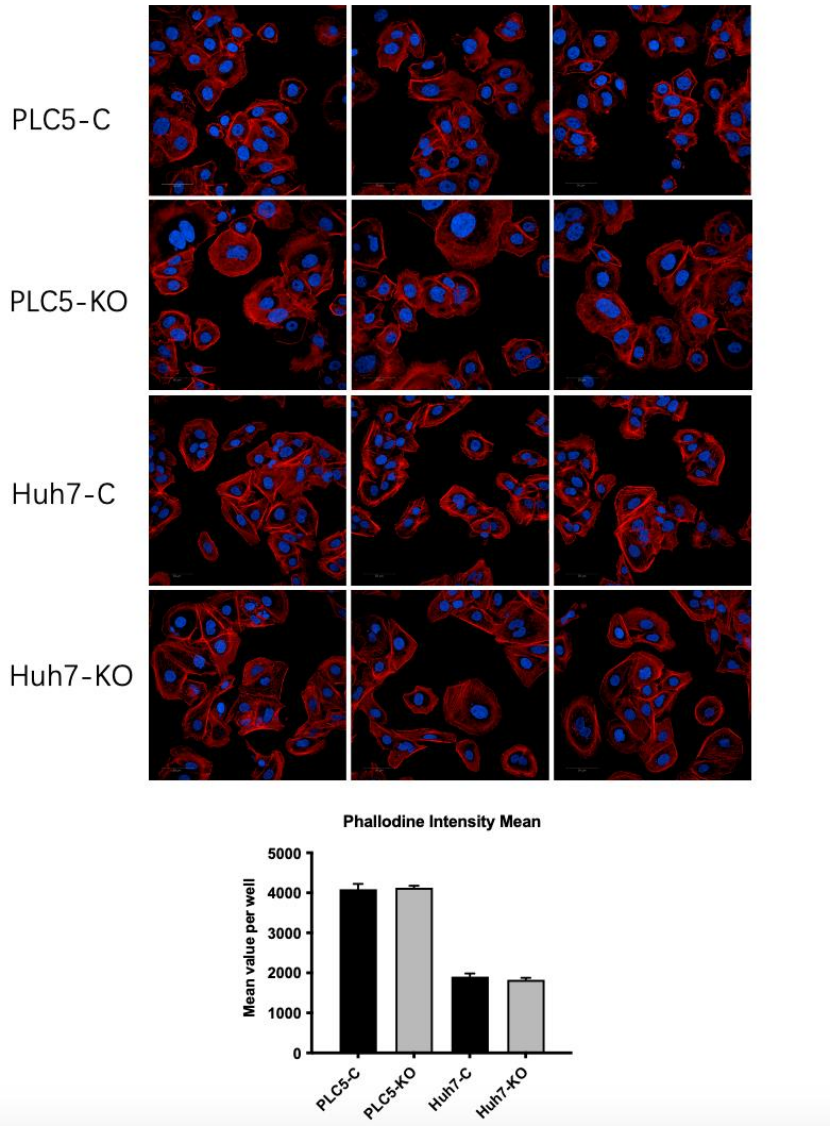

Figure 3.2–12. CTCF does not regulate actin cytoskeletons in HCC cells.

F-actin organization in PLC5 and Huh7 cells were visualized by Phalloidin staining analysis. Quantification of phalloidin intensity was present as mean value per well. Data are presented as mean ± SD, *$p < 0.05$.

3.3 Elucidation on mechanism of CTCF-dependent HCC growth.

3.3.1 Transcriptomic analysis on CTCF knockout cells

To further elucidate how CTCF regulates growth and metastasis of HCC cells, the transcriptional output of PLC5-KO and PLC5-C cells, and Huh7-KO and Huh7-C cells, were compared using genome-wide RNA sequencing analysis. Sample distance analysis (Figure 3.3–1A) revealed that gene expression profiles of biological repeats of treatment (n=2) are highly correlated with a median R value of 0.999. Principal component analysis (PCA) showed that biological repeats are generally more similar to each other than to different treatments (Figure 3.3–1B). Differentially expressed genes (DEGs) were identified using DESeq2 (Figure 3.3–2A). The results are summarized in volcano plots (Figure 3.3–2B) using fold changes in gene expression of more than 1.5, log2 (fold change) and statistical q value of less than 0.05 (-log10 q-value) as cutoffs (dotted vertical lines) for DEGs. Accordingly, PLC5-KO and Huh7-KO exhibited 2,081 DEGs (1382 up-regulated and 699 down-regulated) and 2,564 DEGs (1327 up-regulated and 1237 down-regulated) respectively (Figure 3.3–2A).

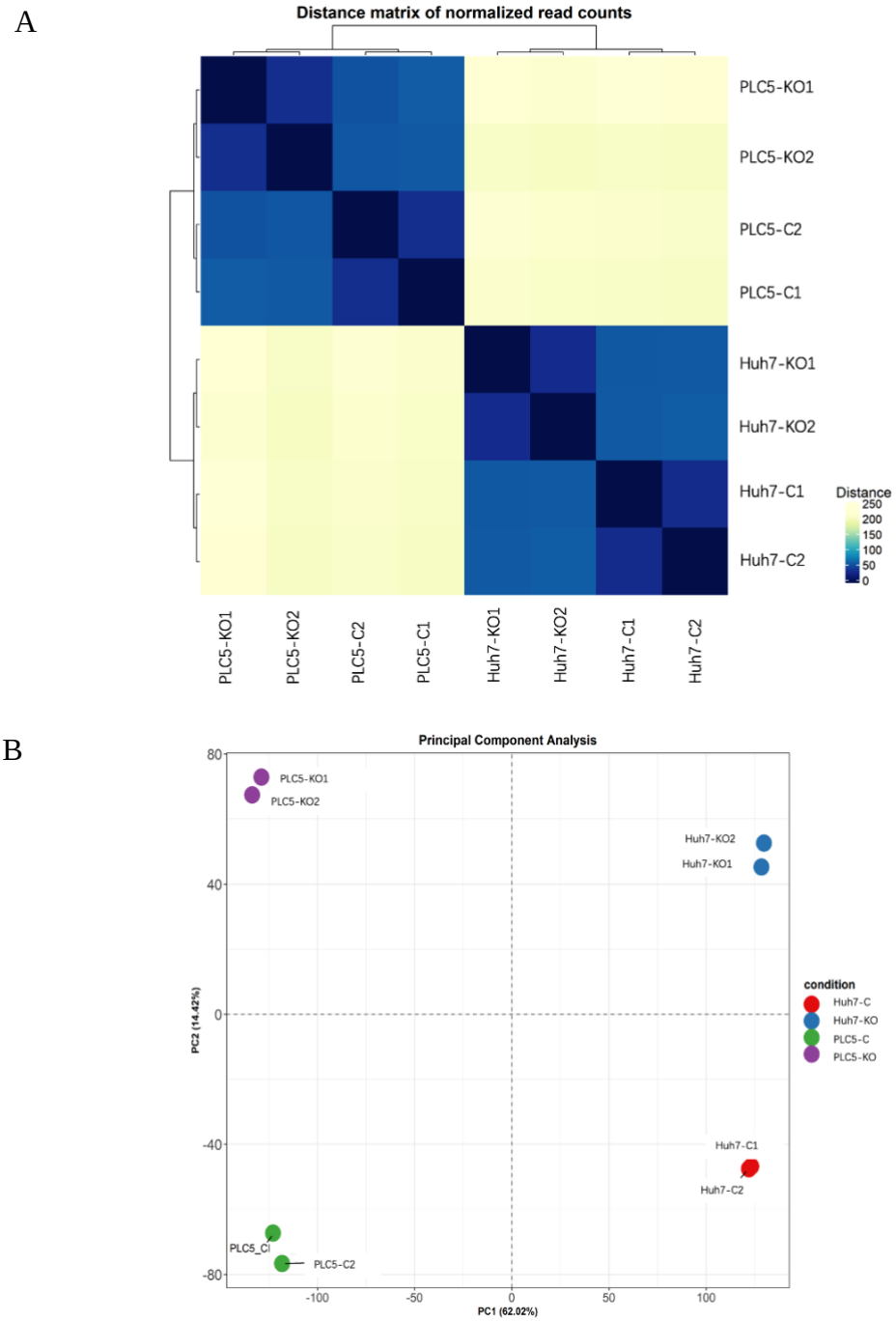

Figure 3.3–1. **Transcriptomic analysis on CTCF knockout cells**.

(A)Sample distance analysis and (B) principal component analysis of PLC5 and Huh7 CTCF knockout cells compared to the control cells.

A

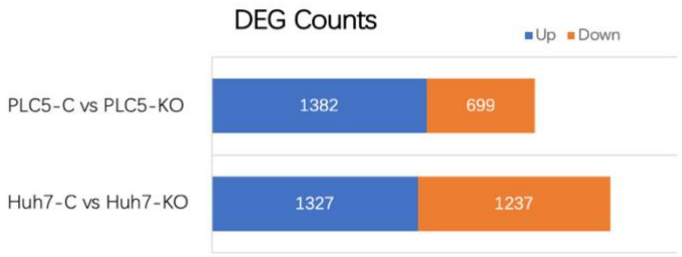

B

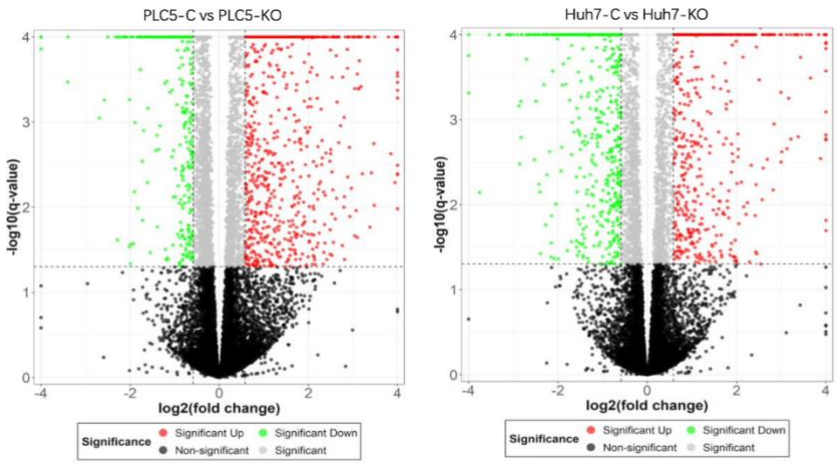

Figure 3.3–2. Differentially expressed genes (DEGs) were identified from transcriptomic analysis on CTCF knockout cells

(A) Summary of differentially expressed genes (DEGs) in CTCF knockout cells. (B). Volcano plots of PLC5-KO vs PLC5-C cells (left), and Huh7-KO vs Huh7-C cells (right). DEGs were consider significant (red: up; green: down) when fold change between CTCF knockout vs control is >1.5-folds.

3.3.2 Identification of commonly altered DEGs on CTCF knockout cells

Transcriptomic analysis revealed 313 up-regulated and 191 down-regulated DEGs were commonly altered in PLC5-KO and Huh7-KO cells (Figure 3.3–3 and Table 3.3-1). Analysis of these commonly regulated genes using KEGG analysis revealed metabolic pathways as one of the top significant enriched pathways (Figure 3.3–4A). Subsequent analysis further suggested that the enrichment of metabolic pathways is mainly attributed by the down-regulated DEGs (Figure 3.3–4B). g:GOSt functional enrichment analysis [240] of the down-regulated DEGs further revealed significant enrichment of Gene Ontology (GO) terms related to NAD binding, small molecule metabolic process, and organic acid metabolic process (Figure 3.3–5A). TRANSFAC analysis showed that 70% (134 out of the 191) of the down-regulated DEGs were highly enriched in CTCF-binding motifs (Figure 3.3–5A and Table 3.3-2). Importantly, ChIP-seq analysis comparing wild type and CTCF-knockout cells revealed genuine interaction between CTCF and these genes at the 5' flanking region or/and in the gene body (Figure 3.3–5B). Together, these data suggested that CTCF may regulate expression of genes potential related to NAD-binding and metabolic processes.

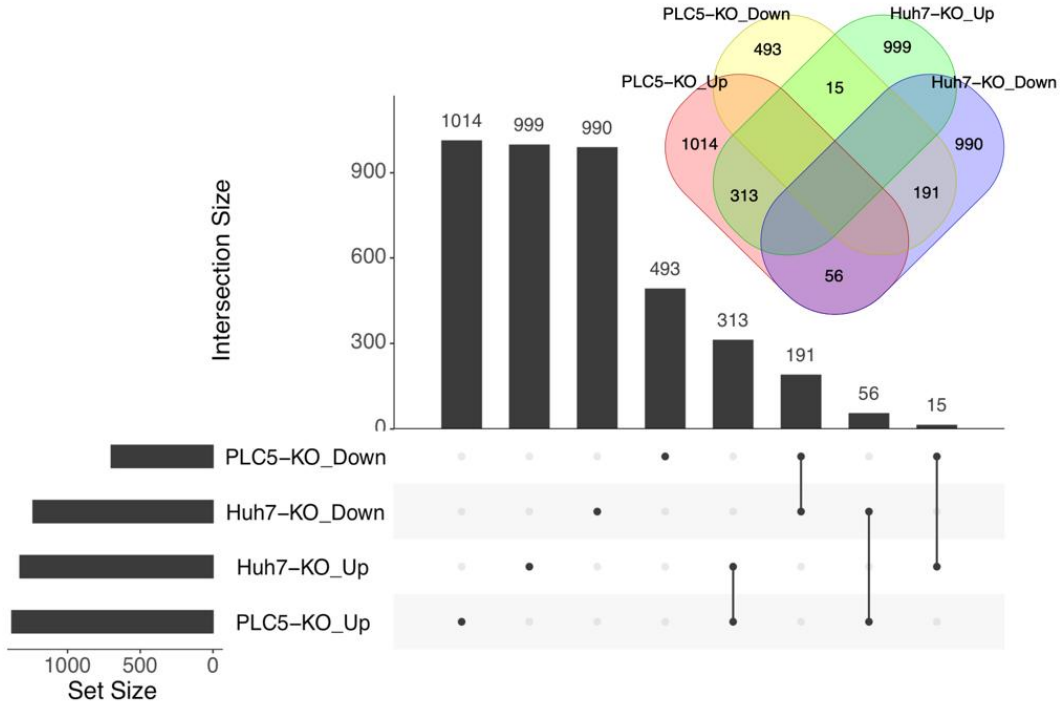

Figure 3.3–3. Upset plot showing DEG comparison (> 1.5-fold, q-value < 0.05) of PLC5-KO, PLC5-C, Huh7-KO, and Huh7-C cells.

313 up-regulated and 191 down-regulated differentially expressed genes DEGs were commonly altered in PLC5-KO and Huh7-KO cell lines.

A

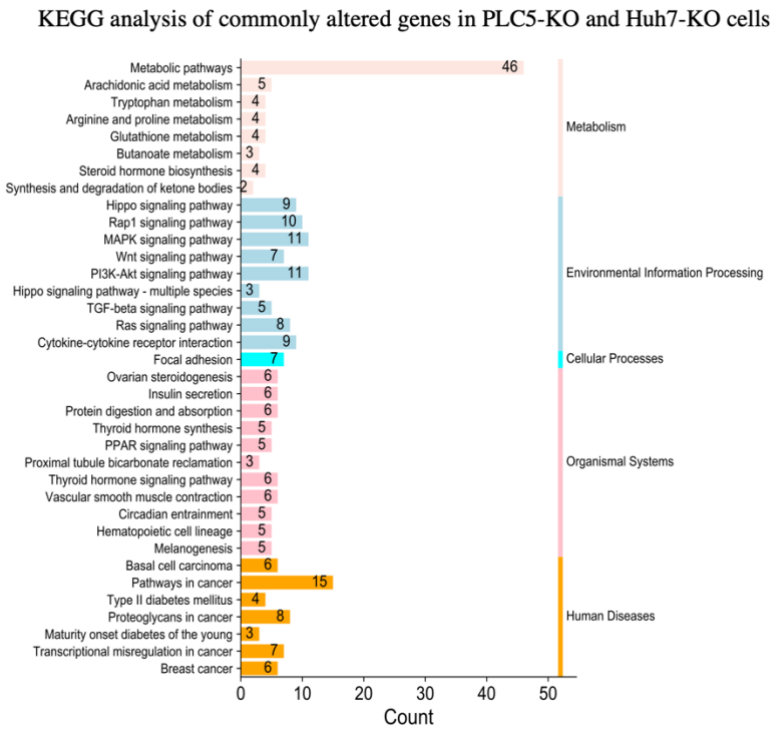

B

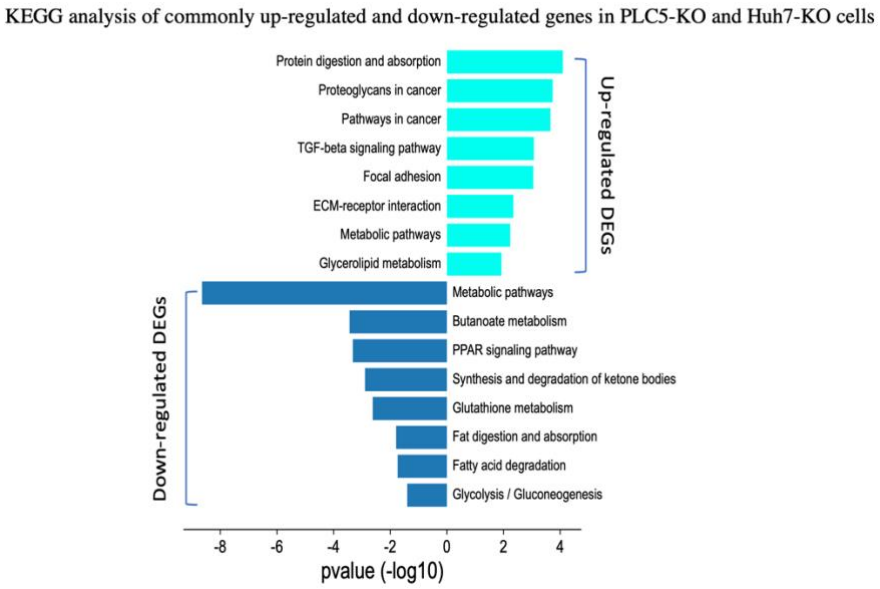

Figure 3.3–4. KEGG analysis of commonly altered DEGs in CTCF knockout cells.

(A)KEGG analysis of commonly altered DEGs in both PLC5-KO and Huh7-KO cells. (B) KEGG analysis by differentially analyzing up- and down-regulated genes in PLC5-KO and Huh7-KO cells.

A

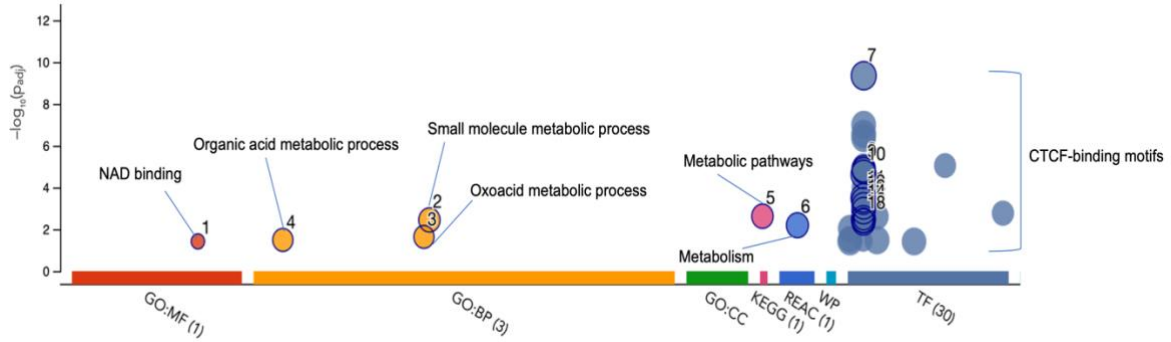

B

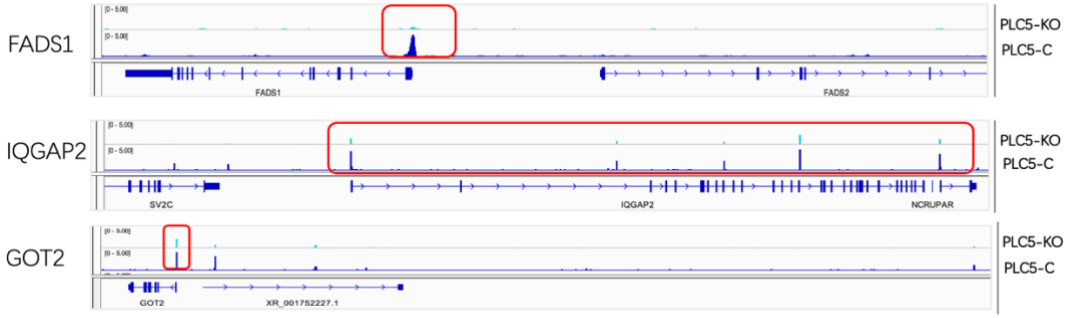

Figure 3.3–5. Functional enrichment analysis of commonly down-regulated DEGs on CTCF knockout cells.

(A). g:GOSt–functional enrichment analysis of DEGs commonly down-regulated in PLC5-KO and Huh7-KO cells. GO:MF, Gene Ontology: molecular function; BP, biological process; CC, cellular component; REAC, Reactome (REAC); WP, Wikipathways. TF: TRANSFAC. (B). Selected genes from down-regulated DEGs are confirmed by CHIP-seq analysis, indicating the loss of CTCF binding at the promoter region of these genes in the CTCF knockout cells.

Table 3.3-1. 313 up-regulated and 191 down-regulated DEGs were commonly altered in PLC5 and Huh7 knockout CTCF cell lines.

GENE_NAME	PLC5_C mean	PLC5_KO mean	Huh7_C mean	Huh7_KO mean	Log2FoldChange (PLC5-C vs PLC5-KO)	Log2FoldChange (Huh7-C vs Huh7-KO)	Group	Metabolic pathway gene
AC011511.4	467.8171	0.7107	295.9834	1.4085	-9.6161	-7.6877	Down	
AL390195.1	748.9595	45.2401	1508.3019	113.4277	-4.0734	-3.7245	Down	
SPEF2	392.4276	33.3856	104.8305	41.1130	-3.6119	-1.3485	Down	
NKD2	448.2686	42.2419	31.6853	7.9837	-3.3765	-2.0182	Down	
EPDR1	106.8434	18.0392	349.4871	169.8999	-2.5983	-1.0456	Down	
PRRT3-AS1	226.3419	36.4614	101.9438	18.0772	-2.5903	-2.4898	Down	
DEF8	2529.2926	420.8743	3687.2518	1219.8038	-2.5798	-1.5961	Down	
B4GALNT1	3636.4129	774.0953	1992.5948	324.0915	-2.2360	-2.6220	Down	*
AP001029.2	129.5142	30.6438	100.4580	33.6742	-2.2167	-1.5912	Down	
GTF2IRD2B	265.5371	60.6897	720.8268	369.7742	-2.1511	-0.9632	Down	
HBQ1	433.3067	100.5568	51.4351	16.1634	-2.1222	-1.6479	Down	
AL669918.1	298.3345	69.5743	29.2126	4.0929	-2.1112	-2.8565	Down	
AHSG	9829.3526	2341.2731	19884.2944	5040.9408	-2.0721	-1.9790	Down	
TPD52L1	168.6163	43.7263	956.2013	353.0277	-2.0069	-1.4393	Down	
TAMM41	926.7044	235.6976	821.2770	303.6121	-1.9668	-1.4388	Down	
ZBTB39	1732.0267	449.5196	1977.6006	882.4520	-1.9503	-1.1645	Down	
AGAP2-AS1	822.8925	212.4504	354.9651	82.3451	-1.9388	-2.1150	Down	
FXN	1468.7277	406.5662	1786.4649	737.5628	-1.8545	-1.2756	Down	
WIF1	126.2822	35.6239	245.6301	126.7486	-1.8220	-0.9562	Down	
C17orf113	91.5327	25.7149	93.4750	42.3948	-1.8141	-1.1344	Down	
TMPO-AS1	1019.2680	292.4008	446.7755	237.0159	-1.7937	-0.9164	Down	

AC011462.1	2260.9232	652.6123	3356.0755	1415.0786	-1.7850	-1.2451	Down	
SNHG26	898.9902	273.6906	167.0073	59.9319	-1.7168	-1.4813	Down	
AC080112.1	438.4121	135.4683	281.6756	102.8096	-1.7103	-1.4634	Down	
KRT15	520.9577	161.2644	57.6789	20.4931	-1.6866	-1.4818	Down	
BCYRN1	1940.4563	610.9077	372.1180	98.1992	-1.6722	-1.9142	Down	
TMC7	1563.5308	494.6049	1426.8585	657.1484	-1.6655	-1.1207	Down	
REX1BD	1667.4979	526.4264	1759.2107	558.2295	-1.6565	-1.6534	Down	
COMTD1	863.9304	287.5053	510.6545	141.3014	-1.5740	-1.8498	Down	
COLCA2	1029.0568	353.0674	161.6224	85.1121	-1.5517	-0.9292	Down	
FOXA3	1491.0588	514.7435	2661.6811	1392.6942	-1.5415	-0.9327	Down	
ADAP1	951.3868	328.4962	159.8774	39.3906	-1.5411	-2.0283	Down	
MUC12	654.4645	225.3257	88.1554	43.5380	-1.5349	-1.0299	Down	
APOL2	1082.0784	379.3844	1225.1024	726.6018	-1.5239	-0.7515	Down	
CC2D2A	714.7389	257.1735	1311.5297	466.2584	-1.4758	-1.4963	Down	
DENND4B	5373.4632	1945.6527	3722.3233	1425.5007	-1.4622	-1.3835	Down	
IFT46	487.4723	177.8201	429.5549	244.0211	-1.4604	-0.8135	Down	
HOMER3	341.8164	124.8140	1186.0241	294.5899	-1.4468	-2.0137	Down	
SLC2A2	2423.8859	912.7520	180.3611	86.6717	-1.4132	-1.0651	Down	
AC110285.7	151.6627	56.9104	202.5253	129.8943	-1.3807	-0.6373	Down	
PKN3	2804.4294	1074.8769	1921.8543	671.8866	-1.3772	-1.5181	Down	
PPA2	3693.4873	1425.8020	2788.5891	1155.7821	-1.3748	-1.2710	Down	
MRPS2	3858.3578	1488.5173	3896.4997	1539.4998	-1.3696	-1.3398	Down	
ZBED3-AS1	143.8000	56.6924	162.3236	84.3075	-1.3366	-0.9465	Down	
YDJC	3906.6428	1564.3279	2247.5928	815.5048	-1.3179	-1.4617	Down	

BOLA3	2843.1302	1152.2364	1644.6369	699.2841	-1.3081	-1.2329	Down	
CTCF	4941.7899	1994.2865	7606.2715	3597.0596	-1.3062	-1.0807	Down	
CIZ1	5004.5409	2069.5665	6527.9112	3283.1229	-1.2714	-0.9923	Down	
SYN3	191.8902	80.0057	197.5189	75.6446	-1.2624	-1.3845	Down	
AC092115.2	85.1468	35.2482	143.7556	79.0861	-1.2527	-0.8635	Down	
EOGT	1956.6817	825.8224	568.3043	201.3026	-1.2513	-1.5048	Down	
MYO18A	15351.1921	6458.3055	15640.0706	7681.2281	-1.2479	-1.0256	Down	
FIRRE	130.9325	54.8111	266.8628	145.5143	-1.2477	-0.8785	Down	
CEACAM6	1138.5398	483.9253	304.6405	111.2547	-1.2434	-1.4572	Down	
AAAS	5871.1593	2510.2356	3754.5123	1912.6188	-1.2228	-0.9732	Down	
PRSS12	1750.7250	754.7872	84.4133	31.1582	-1.2181	-1.4385	Down	
LRRC8C	702.2594	301.5499	970.0158	576.1267	-1.2163	-0.7510	Down	
ZG16	183.4366	78.1904	112.1159	39.3062	-1.2145	-1.5024	Down	
SLC27A2	1529.6221	662.0223	493.9783	138.5496	-1.2119	-1.8345	Down	
HSD3B7	3409.4712	1488.8488	616.1177	171.1065	-1.1969	-1.8508	Down	*
CDKN2AIPNL	3139.4497	1376.9987	1947.6331	1065.6608	-1.1908	-0.8688	Down	
DHX30	10089.3620	4460.1891	11108.5937	6526.0469	-1.1775	-0.7669	Down	
MAP3K15	1279.8060	566.7263	330.5122	152.2849	-1.1702	-1.1242	Down	
GTF2IRD2	117.3585	52.6266	401.6887	228.8025	-1.1611	-0.8102	Down	
INPP5E	961.9483	432.1345	1194.3262	630.2501	-1.1454	-0.9231	Down	*
LINC02015	1472.3114	671.4561	630.0012	137.0697	-1.1370	-2.1925	Down	
AL160162.1	122.1436	55.8363	63.3401	28.5112	-1.1291	-1.1371	Down	
ADCY7	232.3355	105.4090	520.3563	262.8790	-1.1247	-0.9865	Down	*
BOLA3-AS1	912.8541	420.0870	259.4641	152.4176	-1.1168	-0.7729	Down	

TONSL	5267.4912	2440.2014	3502.6879	1989.0634	-1.1086	-0.8175	Down	
NLRX1	1987.8965	937.3191	845.0759	268.5539	-1.0793	-1.6519	Down	
DMKN	183.0102	88.4887	1630.0195	656.7669	-1.0613	-1.3119	Down	
CAPN8	454.4122	219.1170	881.2901	552.3123	-1.0608	-0.6723	Down	
FAM171A2	867.9837	419.3697	359.8067	102.2666	-1.0574	-1.8209	Down	
AARS2	3477.4274	1676.8937	2730.5570	1751.1923	-1.0476	-0.6403	Down	
ZDHHC8P1	1498.0579	729.5823	518.7096	277.0804	-1.0422	-0.8991	Down	
C1orf115	2683.1570	1306.3386	5276.1149	2167.0005	-1.0359	-1.2827	Down	
DHRS4-AS1	371.4233	180.5225	432.5456	241.7865	-1.0356	-0.8355	Down	
ADRA2C	3093.3252	1521.1656	716.7678	228.8056	-1.0255	-1.6423	Down	
AC135048.4	1349.2263	660.4722	231.3038	114.3310	-1.0230	-1.0114	Down	
ERFE	503.4355	249.2452	94.5053	17.2372	-1.0063	-2.4305	Down	
GPX2	12489.9759	6245.7289	18788.6941	4668.9116	-0.9986	-2.0085	Down	*
TEX261	9702.6897	4869.2064	8120.9752	4922.9382	-0.9959	-0.7220	Down	
RP9	987.6177	495.1468	677.1470	293.1382	-0.9871	-1.2069	Down	
AADAT	918.7565	466.3775	1117.8075	407.7159	-0.9850	-1.4552	Down	*
SLC25A22	2178.3701	1111.3594	1226.9862	619.1404	-0.9687	-0.9889	Down	
COBLL1	3479.0933	1787.4801	8512.1193	4740.2487	-0.9580	-0.8437	Down	
AGMAT	9280.7428	4784.6687	8574.9561	4268.7267	-0.9568	-1.0060	Down	*
AKR1C3	22041.2702	11401.8766	3509.9230	1859.7670	-0.9509	-0.9157	Down	*
DBNDD1	1072.2197	554.1888	1731.3575	536.3820	-0.9469	-1.6920	Down	
NLE1	2820.9640	1463.8137	2583.1527	1352.1033	-0.9435	-0.9338	Down	
MZT2A	3260.3210	1693.3192	2598.5469	1391.4561	-0.9418	-0.9009	Down	
DNPH1	5388.8532	2802.9058	1050.3401	579.6097	-0.9404	-0.8548	Down	

GPRC5B	495.8064	257.6039	2907.5789	1690.1625	-0.9379	-0.7823	Down	
WDR70	1981.2954	1036.2832	3976.3797	2431.5758	-0.9316	-0.7090	Down	
AC027228.2	561.6268	295.6937	280.1293	164.0084	-0.9283	-0.7692	Down	
PDX1	298.4244	158.5486	1385.4666	647.0260	-0.9204	-1.1004	Down	
BIVM	1871.8705	994.6467	588.9650	77.8774	-0.9186	-2.9136	Down	
SLC35B2	2093.1232	1108.0166	777.0721	420.3310	-0.9183	-0.8884	Down	
SLCO4C1	568.0951	303.3014	2239.5172	1109.4535	-0.9136	-1.0123	Down	
IL17RB	2429.5935	1290.6156	4730.4714	2788.6657	-0.9106	-0.7614	Down	
C9orf116	167.2737	90.4030	61.0142	26.0095	-0.9034	-1.2354	Down	
NDUFAF4	1751.9457	937.2618	2187.4859	1326.3737	-0.9008	-0.7201	Down	
IQGAP2	19948.8223	10696.0984	13733.8989	6289.3457	-0.8992	-1.1264	Down	
TDRD3	781.8966	424.0013	646.0205	412.4686	-0.8829	-0.6442	Down	
S100A14	10317.0344	5610.6038	140.3131	49.9768	-0.8796	-1.4932	Down	
DACT2	2228.7964	1213.7596	687.8620	391.4288	-0.8756	-0.8160	Down	
NOX4	1381.8303	755.4713	151.3120	51.8348	-0.8734	-1.5354	Down	
OIT3	328.7059	180.3783	348.2387	217.4695	-0.8629	-0.6820	Down	
ARHGEF16	1983.0393	1099.1883	1820.3387	867.1978	-0.8515	-1.0685	Down	
NSMCE4A	5379.8203	2983.6761	2168.7804	705.4250	-0.8496	-1.6215	Down	
GOT2	13349.0425	7406.1098	10823.1584	5743.1524	-0.8493	-0.9143	Down	*
GGT7	1636.7892	910.9956	1350.7816	890.3347	-0.8492	-0.6028	Down	*
FAM155B	1265.4782	706.2880	17.7821	2.1475	-0.8414	-3.1316	Down	
SOWAHA	415.4238	232.1822	369.7035	135.3325	-0.8412	-1.4482	Down	
C3orf33	869.6948	486.9723	389.0962	215.7034	-0.8401	-0.8509	Down	
AC073073.2	301.1993	168.2934	194.8588	126.6537	-0.8388	-0.6278	Down	

PNMA6A	653.4465	363.6450	289.9933	181.8835	-0.8359	-0.6701	Down	
GPR3	412.6415	234.1890	280.5744	172.2258	-0.8201	-0.6992	Down	
ZNF777	1765.5895	1000.9815	1652.0103	530.3014	-0.8173	-1.6388	Down	
RAD51D	1633.2527	925.7049	1144.7708	715.1125	-0.8156	-0.6787	Down	
EXOSC6	3058.6360	1738.0909	3906.8655	2136.8844	-0.8139	-0.8698	Down	
TMEM74B	176.0270	100.3909	142.3022	62.5562	-0.8105	-1.1948	Down	
AL160269.1	658.1504	377.8506	1425.9103	950.8884	-0.8094	-0.5869	Down	
FXYD3	1632.0244	944.3046	205.6645	31.9085	-0.7960	-2.6754	Down	
SMIM8	735.9350	424.5432	540.1660	329.6097	-0.7956	-0.7123	Down	
QDPR	3887.6883	2251.7554	6406.6831	2409.5995	-0.7904	-1.4097	Down	*
MBL2	235.5983	136.8100	669.8140	162.6631	-0.7802	-2.0389	Down	
PCK1	2650.6135	1545.7984	52.1445	15.0958	-0.7783	-1.8107	Down	*
TAP2	4159.3439	2421.3250	1024.1048	569.3328	-0.7777	-0.8482	Down	
HPGD	1123.5648	661.5783	4058.9445	1512.1156	-0.7686	-1.4237	Down	
GRK2	6450.8096	3790.5550	16030.6113	9779.2170	-0.7672	-0.7128	Down	
IRF6	456.0118	266.7213	61.7221	24.8228	-0.7670	-1.3288	Down	
ALG5	1840.2275	1085.5789	1596.6905	999.9278	-0.7652	-0.6763	Down	*
EEF1A2	747.0845	442.7883	322.0670	39.2052	-0.7584	-3.0229	Down	
GAS8	1115.5961	660.4451	1519.1217	928.2896	-0.7555	-0.7117	Down	
HDDC3	1168.7178	696.3838	499.6436	213.2302	-0.7539	-1.2270	Down	*
FAM131C	198.1696	117.8263	28.5834	1.6106	-0.7516	-4.2360	Down	
RHOU	7720.7721	4589.8034	8570.0072	3136.3263	-0.7499	-1.4494	Down	
ALB	82792.2279	49287.8776	467742.9205	199514.0339	-0.7484	-1.2292	Down	
R3HCC1	1550.0286	928.1399	2027.4829	1305.1034	-0.7452	-0.6349	Down	

CBX2	2580.0772	1542.5610	4297.8462	1999.9466	-0.7412	-1.1042	Down	
RNPEPL1	4601.8999	2754.2831	2424.7435	831.1896	-0.7404	-1.5456	Down	
BDH2	967.6779	586.4027	1933.5145	961.5514	-0.7311	-1.0070	Down	*
PIGO	8469.1804	5106.7530	3352.1481	1570.3058	-0.7292	-1.0928	Down	*
ADH1C	1007.6077	611.0752	459.6096	72.2771	-0.7288	-2.6654	Down	*
RUFY2	1256.2458	756.6971	777.1716	484.5078	-0.7280	-0.6813	Down	
SNHG11	669.6102	406.7417	492.3886	288.9755	-0.7238	-0.7713	Down	
SPSB2	2089.4261	1261.8606	533.3924	347.4860	-0.7223	-0.6163	Down	
RINT1	3827.4994	2338.8733	3777.1263	2391.5431	-0.7127	-0.6591	Down	
CEBPA	9618.7100	5889.2482	19359.9659	12875.7176	-0.7076	-0.5882	Down	
PAIP1	6601.1101	4041.9469	11529.5863	7431.1607	-0.7075	-0.6339	Down	
SAPCD2	8987.1243	5521.2041	9293.1143	6161.1948	-0.7025	-0.5929	Down	
FADS1	26294.9112	16312.3205	20890.8127	7583.2390	-0.6893	-1.4616	Down	
ACD	2016.9728	1253.0201	1955.7469	1258.0023	-0.6851	-0.6343	Down	
FBXO4	709.0814	444.0665	824.2845	519.4198	-0.6809	-0.6658	Down	
CHDH	7243.7284	4519.5201	5435.7787	2828.9957	-0.6793	-0.9410	Down	*
NAT8	3218.5407	2011.6182	468.2245	295.7654	-0.6787	-0.6633	Down	*
FAM122A	1140.2927	710.5619	1651.1201	1072.3070	-0.6770	-0.6232	Down	
OAS1	3015.3716	1892.0531	123.9789	59.0252	-0.6753	-1.0737	Down	
SULT1B1	1368.0818	859.4828	489.1321	126.1045	-0.6749	-1.9504	Down	
CLUH	16429.4790	10290.0912	12323.2771	8036.5153	-0.6741	-0.6171	Down	
METTL5	4649.1354	2911.7683	2616.5269	1576.3470	-0.6738	-0.7305	Down	
DBH-AS1	559.4070	349.9711	294.5705	185.8059	-0.6685	-0.6618	Down	
MPZL2	3999.6360	2524.5777	3341.9346	1900.4113	-0.6651	-0.8137	Down	

METTL7B	5518.4309	3489.9205	1047.2687	547.8342	-0.6630	-0.9336	Down	
MTMR6	5458.3375	3445.8288	1225.4060	766.0562	-0.6628	-0.6795	Down	*
TMEM189-UBE2V1	1984.9668	1256.7138	2916.8340	1214.2738	-0.6617	-1.2644	Down	
RUSC1	3136.3475	1979.7703	2477.6964	1500.8582	-0.6604	-0.7223	Down	
ITPK1	4762.9313	3010.1559	1783.2774	1185.0569	-0.6590	-0.5893	Down	*
AL161772.1	544.4978	344.3295	151.5935	54.9767	-0.6502	-1.4737	Down	
APOA2	7707.6527	4915.0389	15670.1401	6969.7004	-0.6493	-1.1681	Down	
HMGCS2	682.1603	437.0700	721.8640	210.8584	-0.6490	-1.7787	Down	*
MINDY1	918.1373	585.6989	462.1957	280.8794	-0.6482	-0.7196	Down	
PLA2G12B	1422.2872	914.5946	1230.7036	664.6867	-0.6397	-0.8889	Down	*
THEM6	4973.9553	3188.6441	189.8348	106.2207	-0.6395	-0.8354	Down	
DHODH	1625.2423	1046.1992	1133.1830	756.1522	-0.6322	-0.5852	Down	*
MAGEA8	6442.8877	4160.7431	115.8092	62.9178	-0.6309	-0.8858	Down	
NSMF	5596.5101	3617.0064	3375.8114	1369.1784	-0.6306	-1.3017	Down	
SEMA3D	398.7035	256.8330	3898.2007	2029.7191	-0.6243	-0.9409	Down	
ZNF746	1862.5707	1213.3861	2133.3851	1060.2999	-0.6232	-1.0109	Down	
NR2C1	2504.7578	1625.5276	2653.2630	1577.7844	-0.6202	-0.7505	Down	
NFKBIZ	1890.7902	1233.2937	14268.1047	8802.2767	-0.6192	-0.6969	Down	
CA2	13555.6728	8855.4432	5730.7233	2582.1880	-0.6148	-1.1488	Down	*
HADH	3128.4599	2049.9697	2140.9724	1347.3853	-0.6134	-0.6668	Down	*
RNF144A	1052.6580	689.6461	939.9173	566.4558	-0.6114	-0.7293	Down	
SPATA20	1391.1870	913.3829	3919.5925	2129.3049	-0.6074	-0.8790	Down	
SLC39A5	723.0886	477.7545	2903.9083	1382.3638	-0.6019	-1.0699	Down	
STARD10	5066.4894	3343.6701	7951.5054	4196.7695	-0.6000	-0.9209	Down	

TMEM82	406.1599	268.7705	250.6525	162.4610	-0.5906	-0.6194	Down	
SAMD1	3004.6200	1999.1560	2007.5893	1283.4604	-0.5890	-0.6462	Down	
UCP2	3494.9434	5277.0390	3074.0561	5688.4767	0.5950	0.8884	Up	
GPATCH2L	2207.9366	3349.8536	1681.8998	2756.9009	0.6002	0.7147	Up	
AC244197.3	1265.8239	1924.8607	485.2924	1195.2790	0.6025	1.3060	Up	
UPP1	1686.1447	2556.7766	680.1405	1514.7127	0.6026	1.1523	Up	*
TFEB	232.6831	358.0418	76.8802	176.4089	0.6143	1.2031	Up	
INKA2	496.6473	758.8727	704.8558	1215.8132	0.6159	0.7888	Up	
TM2D3	2521.9096	3861.9083	1204.8503	1897.8553	0.6164	0.6542	Up	
EML6	556.0602	859.3576	2032.0481	3277.7328	0.6237	0.6893	Up	
MATN3	834.5616	1288.1067	8023.8990	15538.8562	0.6273	0.9534	Up	
PIAS3	4522.3850	6989.5827	1072.4139	1800.3644	0.6293	0.7473	Up	
SLC25A45	678.8460	1049.2780	184.4475	278.6614	0.6324	0.5993	Up	
FGFR1	2879.7501	4459.7430	3202.4179	5041.6863	0.6332	0.6551	Up	
CSF1	441.4444	682.6967	3125.1482	7545.8035	0.6345	1.2733	Up	
EIF5A2	6442.2304	10028.3779	1453.2832	3240.8386	0.6374	1.1555	Up	
KLHL5	15116.9886	23548.4356	7535.6401	11358.5531	0.6393	0.5913	Up	
SMIM31	302.4452	471.8417	54.7557	172.3383	0.6459	1.6488	Up	
CAV1	1185.8876	1862.2596	2176.6251	3825.6162	0.6488	0.8120	Up	
GCNT4	913.4774	1430.7418	1398.8027	2897.8687	0.6503	1.0509	Up	*
ADCY10	903.5770	1426.9226	198.2218	396.8257	0.6582	0.9994	Up	*
TLN2	2885.4222	4579.1761	5311.1515	9517.7574	0.6684	0.8412	Up	
MIR4435-2HG	1575.5707	2511.2534	2547.5687	4070.1300	0.6743	0.6765	Up	
PRKCH	1271.6585	2033.0407	138.9124	396.3483	0.6786	1.5357	Up	

RAB6B	1040.9287	1669.4815	734.5798	1121.9402	0.6787	0.6133	Up	
SHISA4	194.5529	313.6739	14.2005	41.7946	0.6844	1.5445	Up	
GADD45B	4101.3486	6587.6088	1912.2408	3794.1685	0.6844	0.9867	Up	
ZBED9	1312.3318	2110.4291	719.7493	1105.3274	0.6861	0.6212	Up	
TMEM216	453.1652	732.1457	694.6198	1043.1889	0.6877	0.5894	Up	
C11orf1	535.6139	863.8783	323.9889	489.5770	0.6880	0.5950	Up	
LGALS8	4268.3465	6877.6510	4237.5673	8434.5711	0.6900	0.9939	Up	
ETFDH	2755.4389	4470.7211	1396.5665	2514.5413	0.6964	0.8484	Up	
LCA5	161.0087	262.6594	239.1186	419.5876	0.6999	0.8108	Up	
SYDE2	1502.2688	2442.3721	867.6456	1797.6413	0.7018	1.0508	Up	
FAM84B	421.5818	684.4807	118.3825	246.2539	0.7040	1.0597	Up	
STAG1	5108.3181	8350.1182	4657.2956	11050.3956	0.7077	1.2476	Up	
MT-TM	332.9770	546.0594	136.1803	259.5988	0.7110	0.9281	Up	
NPFFR2	301.3165	495.0389	135.3943	476.3724	0.7155	1.8181	Up	
CPN1	2756.6716	4531.9676	1118.9179	1702.5245	0.7161	0.6041	Up	
PLCD1	583.8941	962.6548	829.1366	1344.5929	0.7229	0.6993	Up	*
REEP1	509.6065	840.3696	578.0222	1035.5350	0.7235	0.8394	Up	
UNC5B	697.4338	1152.7425	2666.2643	5172.8978	0.7260	0.9547	Up	
RCN1	11343.0314	18862.5587	387.8065	718.5202	0.7337	0.8885	Up	
GDPD1	991.2508	1655.2577	313.4951	506.0807	0.7355	0.6947	Up	
TGFB2	190.0157	317.2290	3132.1511	6345.5470	0.7379	1.0179	Up	
SNAP25	1663.7924	2790.5197	171.7880	313.3096	0.7478	0.8705	Up	
NUAK1	3319.0353	5596.2069	4926.2651	7679.1024	0.7526	0.6396	Up	
ERO1B	2511.4382	4240.2325	575.8577	1151.9177	0.7559	0.9977	Up	

PELI1	2656.4734	4506.7992	3233.3736	5563.7452	0.7632	0.7840	Up	
SOCS2	609.7041	1031.7236	80.0144	168.7769	0.7645	1.0841	Up	
KCNMB4	212.5276	364.6792	374.3027	712.6207	0.7702	0.9324	Up	
MMP11	230.7798	394.9966	614.2231	1203.9824	0.7704	0.9723	Up	
CSRP2	1540.7571	2629.9389	3136.0683	7689.8540	0.7730	1.2943	Up	
TSPAN13	12011.3009	20542.6461	11412.0907	18375.3072	0.7740	0.6873	Up	
PRPF40B	973.6890	1662.8620	188.4243	485.8013	0.7764	1.3690	Up	
COL5A2	604.4432	1042.6042	66577.7274	104062.6419	0.7849	0.6442	Up	
DKK3	3596.7382	6212.0384	1109.5651	3260.0166	0.7871	1.5551	Up	
EFNA3	678.2701	1176.2939	19.2118	161.0647	0.7932	3.0779	Up	
NCALD	204.3384	353.8033	847.7872	1607.3800	0.7937	0.9215	Up	
IGF1R	1269.5848	2202.1747	6942.3009	10911.1051	0.7952	0.6523	Up	
OVGP1	218.0867	380.1550	350.0449	531.5201	0.7982	0.6013	Up	
CPEB3	279.8916	487.8918	152.7937	244.5604	0.8012	0.6800	Up	
TUBD1	631.3402	1101.2834	621.1664	1143.3331	0.8050	0.8817	Up	
C1QL1	395.2331	690.6561	14.7384	57.5222	0.8087	1.9360	Up	
IGFBPL1	856.8058	1499.7142	63.3816	157.3638	0.8088	1.3080	Up	
NPAS1	592.4345	1039.4520	125.6418	731.2058	0.8117	2.5416	Up	
DLX2	580.4514	1018.9723	36.5312	88.8457	0.8123	1.2836	Up	
ARMCX1	1228.8461	2161.6972	480.7655	758.8747	0.8146	0.6618	Up	
AL109918.1	352.1972	624.7574	2846.3492	4859.1852	0.8224	0.7729	Up	
PIK3IP1	458.1070	810.5989	228.9874	423.5297	0.8232	0.8922	Up	
SRD5A3	2660.5136	4711.4727	1347.7033	2044.4254	0.8238	0.6015	Up	
ZFAND4	451.8205	803.0263	260.6278	757.3980	0.8268	1.5337	Up	

USP42	2186.6775	3877.0623	1322.9312	2048.9031	0.8273	0.6297	Up	
JDP2	698.2597	1243.8282	387.3918	892.5311	0.8293	1.2090	Up	
PHOSPHO1	250.3459	444.0024	0.0000	10.1522	0.8311	5.7387	Up	*
HLTF	5826.3474	10383.9885	4112.1261	6725.0718	0.8335	0.7102	Up	
FSCN1	2483.8341	4450.5410	2304.6148	4387.2424	0.8415	0.9282	Up	
SNAPC1	662.9727	1189.7694	781.5618	1617.2184	0.8440	1.0505	Up	
U91328.1	318.4315	575.3293	138.0112	385.6461	0.8523	1.4779	Up	
ZNF334	153.5350	277.3212	7.2683	35.7823	0.8534	2.2806	Up	
IFIT1	188.0739	343.7399	117.1998	274.9537	0.8637	1.2341	Up	
SELENOM	2156.4506	3929.3631	2828.9670	5542.3129	0.8649	0.9704	Up	
TPBG	3252.0413	5932.3848	764.9160	1931.1236	0.8678	1.3349	Up	
C2CD4A	415.4219	765.4655	136.9590	631.8995	0.8844	2.1990	Up	
KIAA0319	172.5953	319.3688	126.0708	422.3283	0.8863	1.7371	Up	
FAM129A	1712.7149	3168.3773	181.9969	364.7202	0.8869	1.0014	Up	
TMEM178B	4172.1627	7762.2040	65.9785	152.7779	0.8957	1.2200	Up	
GLIPR2	167.5139	314.9585	243.2019	449.1501	0.9019	0.8789	Up	
PDGFRL	580.9337	1091.2662	264.1727	522.4197	0.9055	0.9791	Up	
WTIP	546.6088	1025.9467	390.3578	769.4479	0.9077	0.9784	Up	
MMP24	164.3501	308.0795	685.0195	1296.0412	0.9100	0.9196	Up	
DTWD2	932.0084	1763.4668	1014.5329	1867.3286	0.9164	0.8816	Up	
SLC9A7	1781.3123	3367.9712	1837.0285	2903.2295	0.9185	0.6604	Up	
TMOD2	329.5273	623.1633	124.6234	372.2794	0.9219	1.5871	Up	
SPATA6L	190.6944	365.1321	87.0180	148.2859	0.9335	0.7773	Up	
PRRX2	190.1956	366.7316	0.0000	12.7462	0.9392	6.0637	Up	

AL121899.1	87.0911	166.3711	17.3243	96.6958	0.9425	2.4749	Up	
ISM2	159.1934	309.2012	0.0000	19.6878	0.9523	6.6945	Up	
FAM174B	813.2022	1578.0193	584.0846	899.8952	0.9547	0.6208	Up	
P4HA1	8260.9118	16021.1368	4041.1817	7569.6713	0.9549	0.9045	Up	*
NR4A3	4992.3669	9764.9573	37.1434	122.8955	0.9677	1.7113	Up	
ARHGEF17	175.1908	344.0709	3909.3188	5871.9222	0.9686	0.5862	Up	
AP001282.1	56.2377	109.7990	27.3141	67.0094	0.9712	1.2815	Up	
TCF7L1	381.8875	752.7007	440.5802	741.6120	0.9775	0.7499	Up	
CRABP2	80.3620	159.1960	82.8573	526.7329	0.9837	2.6686	Up	
PLPPR1	75.5466	152.3755	157.4760	296.3330	0.9995	0.9098	Up	
TMEM158	231.7003	464.8685	119.8863	319.2124	1.0001	1.4088	Up	
RIN1	361.8588	722.0317	437.8455	679.3200	1.0009	0.6373	Up	
AC126175.1	243.3753	493.5091	43.2653	102.6331	1.0157	1.2351	Up	
TNS2	318.3282	646.6981	149.1310	292.0823	1.0175	0.9739	Up	
LOX	2996.5305	6087.2233	10131.2054	16491.0073	1.0211	0.7031	Up	
AC027097.1	263.0206	536.7391	98.3039	432.6268	1.0245	2.1503	Up	
AQP7	124.5764	253.0010	40.9717	96.5192	1.0267	1.1685	Up	
AGPAT2	3730.2961	7625.3205	4297.9100	7727.5125	1.0306	0.8460	Up	*
DNM3	68.5290	138.8170	43.3179	292.9668	1.0317	2.7565	Up	
PPM1J	107.5365	219.4133	17.9278	44.1828	1.0353	1.3027	Up	
ITGA1	8262.9148	16943.7656	5193.7512	10228.9555	1.0357	0.9773	Up	
HAP1	135.7875	277.4555	41.3900	194.4106	1.0369	2.2121	Up	
REEP2	223.1539	463.8278	134.4224	227.3093	1.0466	0.7642	Up	
HINT3	2376.7529	4923.5051	2618.6632	8896.2087	1.0507	1.7640	Up	

ANKRD1	669.7487	1384.4900	8733.6249	19621.6587	1.0510	1.1672	Up	
CYP1B1	146.0098	303.5974	101.9256	173.1698	1.0539	0.7614	Up	
TLL2	122.3823	255.8528	105.7770	640.1160	1.0649	2.5904	Up	
ELOVL4	234.7526	494.5076	661.3233	1403.7603	1.0667	1.0841	Up	*
ALDOC	3041.6952	6422.0192	342.7315	677.9297	1.0784	0.9871	Up	*
TMEM170B	4529.2882	9585.7093	1081.1909	2590.2013	1.0810	1.2597	Up	
CTHRC1	360.0681	766.3718	389.9634	716.2215	1.0874	0.8746	Up	
ZNF532	1128.3505	2394.4012	947.2145	1712.0224	1.0908	0.8557	Up	
EFHD1	199.1968	423.9428	474.6278	1609.3932	1.0961	1.7603	Up	
SPARC	125.9971	269.1478	1774.6319	4814.6016	1.0963	1.4398	Up	
CABYR	1262.2861	2699.0684	314.0241	632.0883	1.0974	1.0104	Up	
MOXD1	1856.2863	3984.4154	1179.8914	2416.6567	1.1009	1.0353	Up	
BMP2	492.7917	1057.2560	20030.3441	32015.2937	1.1010	0.6764	Up	
FCGBP	255.3448	546.7766	293.5858	1361.6738	1.1045	2.2173	Up	
SOCS2-AS1	74.1324	160.3106	3.3098	31.9842	1.1117	3.2230	Up	
NDUFA6-DT	371.0841	812.1955	91.3041	448.0700	1.1354	2.3241	Up	
SMARCD3	150.3897	333.0703	1985.0904	3066.0158	1.1403	0.6268	Up	
SCUBE3	74.1205	162.6908	279.3634	551.2835	1.1423	0.9778	Up	
CCDC7	217.8558	481.2753	11.7169	95.3707	1.1485	2.9859	Up	
MIR497HG	735.5989	1635.8560	776.0989	1438.0487	1.1517	0.8866	Up	
TTC9	204.2837	456.2475	64.2734	134.4986	1.1522	1.0752	Up	
C17orf49	923.8144	2060.8658	1076.6665	1965.4439	1.1592	0.8679	Up	
LTBP1	1701.0630	3832.2970	2458.4232	4276.2369	1.1702	0.7976	Up	
OXTR	149.9940	342.9390	286.4919	612.2862	1.1871	1.0948	Up	

PPM1N	145.9479	336.7301	30.8473	79.0235	1.1959	1.3393	Up	
SKP1	6618.3037	15177.4769	8955.4035	23200.7532	1.1977	1.3734	Up	
MAP1A	115.9027	265.1341	1724.4050	3782.7303	1.2019	1.1341	Up	
SH3YL1	133.0377	304.7381	136.4635	317.0509	1.2022	1.2212	Up	
RASSF6	321.5435	736.5757	320.0412	699.3975	1.2032	1.1295	Up	
DHRS2	500.5045	1164.7436	11.8204	108.0294	1.2144	3.1442	Up	
AC145098.2	67.1740	155.9124	104.7011	163.0101	1.2170	0.6363	Up	
HEG1	2581.7602	6025.8029	16057.6041	29664.3459	1.2221	0.8855	Up	
MYEF2	297.1275	703.9982	218.6970	419.5693	1.2353	0.9391	Up	
AL772337.3	58.6084	138.7079	0.0000	9.9608	1.2380	5.7135	Up	
NPTX2	1545.4346	3675.3519	453.4075	1123.1285	1.2482	1.3091	Up	
GPX8	863.6201	2060.3560	1098.8732	2373.1721	1.2527	1.1104	Up	*
WWTR1	2590.2914	6189.6820	3155.2452	5621.7385	1.2565	0.8332	Up	
INA	2268.4606	5472.1194	66.7225	316.9444	1.2708	2.2550	Up	
TMEM108	33.9321	82.0706	11.5605	52.4533	1.2844	2.1672	Up	
LIPH	6170.6310	15101.3788	614.7971	1202.6231	1.2914	0.9712	Up	*
WIPI1	2766.4451	6785.8919	1503.9509	2486.0517	1.2940	0.7250	Up	
DNAJB13	35.8085	89.4691	2.3529	30.1456	1.3084	3.4703	Up	
SLC7A8	757.9280	1882.8892	602.6696	920.0854	1.3124	0.6095	Up	
GMNC	72.0787	180.8743	73.8510	242.6208	1.3166	1.7279	Up	
PXN-AS1	533.2319	1332.3081	259.3454	1269.2540	1.3190	2.2892	Up	
FAM184A	1358.2919	3412.2230	1075.6387	2405.8549	1.3277	1.1612	Up	
TFPI2	64.1557	160.7023	736.0426	3576.8227	1.3308	2.2797	Up	
CD55	890.7995	2241.3872	514.9911	844.7420	1.3324	0.7140	Up	

TMIE	66.7957	170.4262	27.4259	101.0824	1.3407	1.8997	Up	
SUGCT	182.8892	466.5327	324.8705	575.8255	1.3501	0.8278	Up	
DGCR6	1169.5718	2980.4376	676.7401	1047.0997	1.3539	0.6278	Up	
ISM1	40.4885	103.1913	345.7540	600.0453	1.3564	0.7938	Up	
SUSD2	30.9434	80.3225	977.2558	4498.8707	1.3790	2.2032	Up	
AHRR	78.2957	204.9501	0.7930	21.6210	1.3847	4.5715	Up	*
CNBD2	86.2688	225.8550	33.1899	393.2441	1.3858	3.5765	Up	
MT-TV	1238.4082	3255.0502	103.1565	516.1467	1.3923	2.3196	Up	
FZD4	2259.5044	5974.0967	7735.6389	13601.2386	1.4049	0.8138	Up	
PRODH	472.0267	1262.4812	359.3375	556.7442	1.4137	0.6284	Up	*
MYOM1	667.5994	1802.4163	244.5139	484.2235	1.4303	0.9907	Up	
THEMIS2	50.0112	136.8764	139.9522	238.0212	1.4332	0.7565	Up	
DACT3	54.9478	149.8803	17.8669	83.0703	1.4441	2.2188	Up	
AFAP1L1	390.2856	1066.9057	1360.6482	2395.1244	1.4442	0.8176	Up	
DNAH7	81.7863	222.3534	6.2072	44.1468	1.4589	2.8554	Up	
KLHDC7A	235.5983	650.0476	15.8253	54.0234	1.4591	1.7762	Up	
SNCA	180.6129	497.8776	395.4976	648.1295	1.4649	0.7098	Up	
FOLR1	32.4828	90.2114	104.4620	169.2335	1.4660	0.6988	Up	
APLN	30.2947	84.0857	11.6602	39.1103	1.4741	1.7334	Up	
AC027097.2	53.2380	147.7926	65.0785	358.0335	1.4779	2.4480	Up	
CLDN16	312.9154	873.5371	280.5394	846.8365	1.4841	1.5896	Up	
BMP4	738.6213	2069.1787	938.6168	2585.8971	1.4873	1.4633	Up	
ULBP1	102.7427	289.4227	40.3129	141.8005	1.4878	1.8139	Up	
CYBRD1	34.8338	98.9695	38.1548	138.1118	1.4984	1.8501	Up	

CLUL1	78.7264	223.9546	43.5722	603.0313	1.5018	3.7830	Up	
LINC02331	41.9716	118.3679	117.9279	246.5872	1.5021	1.0731	Up	
ZG16B	86.5197	246.5769	24.3430	68.4878	1.5122	1.4925	Up	
GFPT2	364.7471	1050.0288	26.9932	63.1941	1.5242	1.2377	Up	*
TENM1	171.3535	493.9612	347.3678	533.6615	1.5353	0.6169	Up	
BHLHE41	160.2760	468.2138	186.2313	442.3284	1.5441	1.2425	Up	
PLA2G4C	161.8073	474.6408	153.4805	313.7375	1.5543	1.0276	Up	*
LIFR	165.4619	488.3668	11625.4225	19047.2995	1.5562	0.7118	Up	
IGFBP2	43.2364	127.1822	2851.4477	5271.5792	1.5616	0.8873	Up	
AL627171.2	73.1364	220.6113	22.9587	136.9597	1.5914	2.5747	Up	
C5AR1	351.1392	1057.0560	12.9531	40.0074	1.5956	1.6400	Up	
CLIP1-AS1	81.4326	248.9069	82.2615	160.0920	1.6014	0.9651	Up	
LOXL2	139.9839	429.8675	1756.1971	4109.9258	1.6091	1.2267	Up	
BEST3	22.9461	69.6816	106.1087	252.5671	1.6110	1.2457	Up	
TMEM61	52.7110	165.8246	0.0000	8.6533	1.6349	5.5083	Up	
FZD8	25.3862	78.2733	323.2578	570.4855	1.6395	0.8177	Up	
VGF	125.7769	390.4098	16.3707	61.1632	1.6407	1.9057	Up	
RPS6KA5	96.9172	301.9997	43.9196	114.0860	1.6427	1.3630	Up	
METTL25	363.3597	1136.7019	469.0377	1121.1137	1.6442	1.2593	Up	
EXD1	18.1946	56.8884	3.6343	23.7623	1.6450	2.7348	Up	
CDC42EP3	29.3385	93.6343	37.8072	119.1374	1.6596	1.6383	Up	
IL11	74.6698	240.8796	22.8627	58.9941	1.6797	1.3650	Up	
CDKN1C	15.4647	49.8241	65.5087	142.0838	1.6874	1.1162	Up	
ABCG1	173.1397	567.8299	53.0838	129.1250	1.7069	1.2873	Up	

TRIM46	30.3923	99.0030	6.0313	34.0617	1.7116	2.5226	Up	
CYGB	40.7817	133.0805	98.9928	223.9730	1.7124	1.1768	Up	
STAT4	42.4290	141.1977	268.1109	512.6232	1.7156	0.9295	Up	
SHE	142.4888	469.7230	383.2309	737.3048	1.7221	0.9397	Up	
MED12L	32.8924	102.5625	308.7454	679.5404	1.7233	1.1407	Up	
GCOM1	30.7710	104.1360	274.9428	627.0205	1.7312	1.1805	Up	
GPC4	139.4308	468.0007	311.8383	3241.2120	1.7408	3.3722	Up	
AC008429.1	163.5581	544.3144	35.9226	178.2936	1.7413	2.3129	Up	
AC254562.1	16.3979	56.6111	3.7876	35.5542	1.7641	3.1578	Up	
KIF5C	5732.0484	19633.0427	2271.0311	5472.1303	1.7754	1.2678	Up	
FAM13C	40.8593	141.5570	125.2507	248.8721	1.7782	0.9866	Up	
LGALS1	838.8084	2894.3685	105.8226	172.8321	1.7847	0.7057	Up	
AL713922.2	15.2880	52.6397	10.9964	31.9982	1.7920	1.5520	Up	
OLFML2A	219.8397	774.0994	351.1439	1121.3486	1.8063	1.6780	Up	
LINC02475	49.4749	171.3085	325.8547	630.6666	1.8068	0.9528	Up	
TRIM67	47.8894	166.6601	174.8781	451.9855	1.8136	1.3596	Up	
ITIH5	2081.2422	7324.1613	7.4951	95.5149	1.8137	3.6493	Up	
SLC7A10	16.1204	57.7008	901.4101	1832.7188	1.8379	1.0265	Up	
COL1A1	121.8236	439.3162	816.7847	4848.5176	1.8383	2.5664	Up	
HPSE	282.6444	1017.2232	157.0452	946.5781	1.8464	2.5920	Up	*
SYT12	36.2250	131.2107	82.5881	189.5485	1.8677	1.1882	Up	
EFNB3	93.6588	344.3685	56.8586	177.0138	1.8688	1.6525	Up	
CALCRL	78.2860	288.0977	49.8514	126.9732	1.8695	1.3153	Up	
ATL1	214.3676	780.5302	93.4251	251.4867	1.8718	1.4223	Up	

RAPGEF3	79.2910	288.6923	56.1058	120.1314	1.8724	1.0971	Up	
ATP8B3	320.4127	1170.4570	72.0273	171.5868	1.8782	1.2355	Up	
IL1RAP	1634.8068	6085.5458	7298.5795	15113.1963	1.8995	1.0500	Up	
ALG1L	22.3338	85.5917	205.0049	567.5361	1.9256	1.4697	Up	
ZNF582	93.4172	352.3145	111.2442	268.9159	1.9299	1.2717	Up	
LINC00632	45.2677	177.2698	274.9162	1141.1343	1.9422	2.0586	Up	
AL109615.3	51.9741	199.5718	37.1434	74.5951	1.9424	0.9929	Up	
FDXACB1	693.0050	2693.5900	248.0100	1296.0106	1.9618	2.3865	Up	
ATP1B2	192.0499	799.1556	77.6277	244.8694	2.0496	1.6561	Up	
AC131011.1	41.5984	171.8924	7.4148	34.2467	2.0530	2.2268	Up	
ANXA1	9172.1024	38475.7307	10881.6908	63709.9123	2.0687	2.5491	Up	
TMCC2	188.0740	788.7525	12.2311	97.5488	2.0734	2.9877	Up	
TIGD3	126.6477	534.3159	89.6198	187.5870	2.0753	1.0625	Up	
LIN28A	13.9886	60.0833	6.4538	31.1265	2.0781	2.2418	Up	
MDGA1	15.7492	66.7755	25.4942	83.9496	2.0786	1.7401	Up	
CADM1	25.1634	106.3080	4293.0241	7819.2845	2.0892	0.8644	Up	
HTRA3	15.6736	69.3405	2294.3344	4317.6781	2.1029	0.9110	Up	
SMIM32	17.5116	74.5930	74.7099	352.5803	2.1135	2.2310	Up	
MCF2L2	10.6884	48.8083	5.5184	35.6276	2.1692	2.7025	Up	
ITGB3	10.9307	50.7175	51.2797	166.9583	2.1749	1.6981	Up	
AL138828.1	8.4494	38.0910	16.7477	50.5609	2.2098	1.5729	Up	
LINC00853	26.6798	126.1448	3.2041	42.4581	2.2144	3.6320	Up	
ZNF560	38.9155	179.9197	0.0000	15.7276	2.2329	6.3763	Up	
CYP26B1	12.2281	58.2049	2238.4378	4866.4186	2.2372	1.1221	Up	*

TAC3	7.7030	36.5905	292.8560	530.5027	2.2670	0.8624	Up	
WEE2-AS1	26.0321	130.4994	91.9857	200.2297	2.3154	1.1204	Up	
ATP6V1G2	18.8489	94.2511	12.0867	91.4291	2.3445	2.8939	Up	*
LIPG	34.8303	179.3613	1834.4680	4058.8840	2.3532	1.1441	Up	*
TMEFF2	9.2957	48.9926	16.0703	41.3884	2.3664	1.3604	Up	
COL4A4	45.6783	232.3107	19.4069	221.6949	2.3678	3.5105	Up	
AP001528.2	11.5813	60.8769	45.8512	127.8223	2.3969	1.4740	Up	
FSTL1	124.6038	656.9284	5213.8707	17878.4006	2.4109	1.7768	Up	
OLFML1	13.2846	71.4672	9.9887	168.1924	2.4184	4.0754	Up	
AL024508.2	12.0444	65.6013	20.3224	64.8997	2.4428	1.6686	Up	
COL12A1	24.9128	136.4503	5302.9457	20207.1410	2.4519	1.9298	Up	
MUC6	48.0856	263.5826	124.8174	213.7173	2.4661	0.7763	Up	
CRLF1	48.6349	280.0585	35.9873	114.8301	2.5055	1.6864	Up	
SCIN	35.7600	213.6132	118.4895	222.4717	2.5586	0.9107	Up	
EIF4E3	12.5075	74.4239	170.5081	575.0846	2.5692	1.7576	Up	
C6orf223	29.2248	172.6109	3.2523	20.3260	2.5716	2.6519	Up	
ZEB2	6.0222	36.7525	63.0507	136.4356	2.6150	1.1119	Up	
HCN4	5.6510	35.3734	1239.8784	1879.3107	2.6193	0.5993	Up	
ROPN1L	35.4790	220.6110	18.8343	110.7195	2.6236	2.5983	Up	
CACNA1G	294.0173	1824.1062	253.0711	1236.7037	2.6342	2.2899	Up	
TEX14	19.4540	123.3053	24.7392	59.2972	2.6393	1.2660	Up	
P3H2	1668.0623	10419.5768	2586.7721	13310.2381	2.6446	2.3618	Up	
GNAO1	9.8887	61.4903	16.8065	78.9530	2.6617	2.2015	Up	
PARM1	410.8394	2869.9711	5454.0450	8591.1492	2.8075	0.6554	Up	

ADAMTS3	20.1008	148.9340	745.1983	2525.2575	2.8525	1.7636	Up	
PCOTH	23.5300	178.0332	39.4886	129.0604	2.8869	1.7241	Up	
FIBIN	4.1698	29.9367	9.6579	90.1584	2.8953	3.1713	Up	
TLE4	18.0697	134.1058	1626.1673	2640.2149	2.9152	0.6993	Up	
BEND6	120.8788	935.7556	275.7500	775.5405	2.9489	1.5008	Up	
SNAP91	7.6574	61.6162	0.0000	9.1208	2.9597	5.5914	Up	
SLC38A4	17.3917	133.7492	810.7687	3078.6766	2.9600	1.9256	Up	
ZNF185	451.4592	3896.4383	56.6413	1362.8441	3.1040	4.5914	Up	
NEURL1B	86.6872	812.0396	107.1440	205.7726	3.1177	0.9505	Up	
OLFML3	12.0818	112.3205	2748.7386	7733.3506	3.2123	1.4910	Up	
NGFR	13.1543	124.8991	4.1651	55.0083	3.2228	3.7360	Up	
ENPP3	38.5677	364.8493	51.8815	371.8880	3.2332	2.8580	Up	*
MRPS30-DT	4.1523	41.5243	22.8504	160.5710	3.2695	2.7713	Up	
CRISPLD2	12.5323	125.0557	489.3190	985.8613	3.3062	1.0102	Up	
NID2	12.4118	143.8746	641.2684	1121.3087	3.4818	0.8065	Up	
AC005523.1	6.2997	72.4593	5.9158	48.7679	3.4964	3.0854	Up	
NEK5	3.8836	45.8809	16.3345	53.7041	3.5016	1.7132	Up	
SCN4B	13.5401	158.6256	26.7305	62.0510	3.5809	1.1956	Up	
AC004974.1	2.3155	36.6224	0.0000	9.1208	3.8918	5.5914	Up	
EGFLAM	2.2105	42.0151	861.4360	1392.0093	4.0843	0.6921	Up	
P3H2-AS1	3.2436	67.9448	0.0000	37.7589	4.5259	7.6395	Up	
SYCE3	22.6132	645.6930	2.7928	89.2115	4.8875	5.0808	Up	
PLXDC1	5.0941	191.7087	5.7900	65.4743	5.2054	3.5213	Up	
GLIPR1L2	1.7660	82.8434	8.4698	91.9250	5.2754	3.4374	Up	

BRINP2	0.0000	33.2414	69.5035	125.2706	7.3708	0.8450	Up	
KRT4	0.0000	43.6090	0.9155	122.2576	7.7510	6.9024	Up	
DNAAF4-CCPG1	0.0000	173.8830	0.0000	542.6506	22.4392	11.4802	Up	

Table 3.3-2. 134 out of the 191 down-regulated DEGs which were highly enriched in CTCF-binding motifs (*).

CTCF binding site	GENE_NAME	PLC5_C mean	PLC5_KO mean	Huh7_C mean	Huh7_KO mean	Log2FoldChange (PLC5-KO vs PLC5-C)	Log2FoldChange (Huh7-KO vs Huh7-C)
	ALB	82792.22786	49287.87759	467742.9205	199514.0339	-0.74839535	-1.229219831
*	FADS1	26294.91116	16312.32045	20890.8127	7583.238971	-0.689310119	-1.461635289
*	AKR1C3	22041.27022	11401.87658	3509.922997	1859.76699	-0.950871872	-0.915730044
*	IQGAP2	19948.82228	10696.09844	13733.89888	6289.345673	-0.899174757	-1.12636248
*	CLUH	16429.479	10290.09115	12323.27708	8036.51531	-0.6740847	-0.617079087
*	MYO18A	15351.19211	6458.305492	15640.07058	7681.228077	-1.24787285	-1.025632496
*	CA2	13555.67277	8855.443203	5730.723332	2582.188027	-0.614791873	-1.148752696
	GOT2	13349.04254	7406.109781	10823.15839	5743.152369	-0.849349264	-0.914279347
	GPX2	12489.97594	6245.728918	18788.69405	4668.911606	-0.998617298	-2.008505767
*	S100A14	10317.03437	5610.603807	140.3131047	49.97679261	-0.879589356	-1.493188628
*	DHX30	10089.36203	4460.189117	11108.59374	6526.046935	-1.177469363	-0.766929987
*	AHSG	9829.352645	2341.273138	19884.29439	5040.940776	-2.07210098	-1.97896663
*	TEX261	9702.689688	4869.206438	8120.975203	4922.938164	-0.995944717	-0.722014622
*	CEBPA	9618.709998	5889.248195	19359.96586	12875.71764	-0.707637131	-0.588227605
	AGMAT	9280.742802	4784.668659	8574.956052	4268.726654	-0.9567722	-1.005966438
*	SAPCD2	8987.124324	5521.204075	9293.114279	6161.194847	-0.702474768	-0.59290303
*	PIGO	8469.180355	5106.752954	3352.148105	1570.305834	-0.729174059	-1.092751704
*	RHOU	7720.772135	4589.803432	8570.007223	3136.32634	-0.749880921	-1.44935681
	APOA2	7707.65272	4915.038877	15670.14012	6969.700356	-0.649250081	-1.16813442
	CHDH	7243.728376	4519.52007	5435.778671	2828.995667	-0.679315649	-0.941022727
*	PAIP1	6601.110136	4041.946941	11529.58632	7431.1607	-0.707512331	-0.633946828
*	GRK2	6450.809571	3790.555045	16030.61133	9779.216958	-0.767180193	-0.712776367
*	MAGEA8	6442.887661	4160.743075	115.8092412	62.91781864	-0.630929157	-0.885762803
*	AAAS	5871.159293	2510.235622	3754.512289	1912.618781	-1.222766188	-0.973208015

*	NSMF	5596.510107	3617.006376	3375.811444	1369.1784	-0.630563119	-1.301740429
*	METTL7B	5518.430871	3489.920514	1047.268692	547.8342253	-0.662985746	-0.933605702
*	MTMR6	5458.337526	3445.828794	1225.405958	766.0561884	-0.662757674	-0.679484434
*	DNPH1	5388.853162	2802.905836	1050.340077	579.6097149	-0.940385383	-0.854793001
*	NSMCE4A	5379.820348	2983.676082	2168.780391	705.4249913	-0.849561624	-1.621464053
*	DENND4B	5373.463191	1945.652722	3722.323275	1425.500722	-1.462189626	-1.383468516
*	TONSL	5267.49118	2440.201384	3502.687863	1989.063401	-1.10856337	-0.817525812
*	STARD10	5066.489388	3343.670112	7951.50539	4196.76946	-0.600019536	-0.920908578
	CIZ1	5004.540937	2069.566476	6527.911151	3283.122902	-1.271436635	-0.992323826
*	THEM6	4973.955262	3188.64405	189.8348109	106.2207397	-0.639454486	-0.835407865
*	CTCF	4941.789942	1994.286533	7606.271502	3597.05957	-1.306244174	-1.080651394
*	ITPK1	4762.931344	3010.155903	1783.277431	1185.056852	-0.659044372	-0.589335056
*	METTL5	4649.135405	2911.768298	2616.526888	1576.34699	-0.673825636	-0.730518345
*	RNPEPL1	4601.899853	2754.283064	2424.74348	831.1896124	-0.740390655	-1.545556874
*	TAP2	4159.343905	2421.324957	1024.104786	569.3328168	-0.777666637	-0.848185465
*	MPZL2	3999.636018	2524.577654	3341.93459	1900.411287	-0.66508619	-0.81369539
*	YDJC	3906.642758	1564.327864	2247.59279	815.5047731	-1.317861929	-1.461653272
*	QDPR	3887.688266	2251.755409	6406.683125	2409.599544	-0.790382695	-1.409716083
*	MRPS2	3858.357793	1488.517273	3896.499725	1539.499775	-1.369612358	-1.339830817
*	RINT1	3827.499374	2338.87328	3777.126276	2391.543081	-0.712720579	-0.659054476
*	PPA2	3693.487311	1425.802025	2788.589113	1155.782095	-1.374782664	-1.270975232
*	B4GALNT1	3636.412933	774.095283	1992.594764	324.0915284	-2.236047559	-2.622018319
*	COBLL1	3479.093308	1787.480079	8512.119284	4740.24872	-0.958033265	-0.843704287
*	AARS2	3477.427376	1676.893706	2730.557036	1751.192334	-1.047578313	-0.640348067
*	HSD3B7	3409.471212	1488.848822	616.1177259	171.1065002	-1.19692821	-1.850839776
*	MZT2A	3260.320998	1693.319206	2598.546892	1391.456071	-0.941760074	-0.900867233
*	NAT8	3218.540711	2011.618236	468.2244641	295.7653908	-0.678741235	-0.66327766
*	CDKN2AIPNL	3139.449701	1376.998657	1947.633054	1065.660763	-1.190782713	-0.868824269
*	RUSC1	3136.3475	1979.770321	2477.696362	1500.858175	-0.66043211	-0.72234437

*	HADH	3128.459864	2049.969738	2140.972439	1347.385308	-0.613425185	-0.666813855
*	ADRA2C	3093.325168	1521.165576	716.7678281	228.8056181	-1.025466969	-1.642344375
*	EXOSC6	3058.635988	1738.09093	3906.865501	2136.884401	-0.813862868	-0.869792155
	OAS1	3015.371636	1892.053116	123.9789057	59.02521617	-0.675251612	-1.073699349
*	SAMD1	3004.620048	1999.155966	2007.589276	1283.460375	-0.589044423	-0.646200997
*	BOLA3	2843.130198	1152.236396	1644.636859	699.2841019	-1.308116211	-1.232906946
*	NLE1	2820.963952	1463.813749	2583.152687	1352.10331	-0.943499433	-0.933784861
*	PKN3	2804.429421	1074.876906	1921.854288	671.8865696	-1.377165558	-1.518127023
*	C1orf115	2683.157041	1306.338584	5276.11492	2167.00047	-1.03593701	-1.282686816
*	PCK1	2650.613529	1545.798408	52.14448591	15.09579887	-0.778292362	-1.81070792
*	CBX2	2580.077202	1542.560991	4297.846185	1999.946643	-0.741170443	-1.104171373
*	DEF8	2529.292633	420.8742994	3687.251826	1219.803815	-2.579781762	-1.596088675
*	NR2C1	2504.757752	1625.527616	2653.262999	1577.784364	-0.620182681	-0.75054881
	IL17RB	2429.593525	1290.615605	4730.471403	2788.66569	-0.910644358	-0.761449314
	SLC2A2	2423.885921	912.7519732	180.3610555	86.67172988	-1.413194087	-1.065092429
	AC011462.1	2260.92323	652.61232	3356.075508	1415.078597	-1.785027447	-1.245139918
*	DACT2	2228.796428	1213.759606	687.8619959	391.4288213	-0.87563486	-0.815972624
*	SLC25A22	2178.370138	1111.359444	1226.986193	619.140399	-0.96871026	-0.988912099
*	SLC35B2	2093.123171	1108.016627	777.0721226	420.3309606	-0.918254235	-0.888354944
*	SPSB2	2089.426143	1261.860626	533.3924155	347.4860395	-0.722259465	-0.616317587
	ACD	2016.972822	1253.020118	1955.746851	1258.00234	-0.685138216	-0.634295223
*	NLRX1	1987.896482	937.3191031	845.075864	268.553928	-1.079269223	-1.651857812
	TMEM189-UBE2V1	1984.966751	1256.713817	2916.833992	1214.273824	-0.661678544	-1.264434806
*	ARHGEF16	1983.039338	1099.188274	1820.338707	867.19776	-0.851544489	-1.068522907
	WDR70	1981.295382	1036.28316	3976.379665	2431.575823	-0.931636737	-0.708967192
*	EOGT	1956.681737	825.8223887	568.3043102	201.3026211	-1.251312547	-1.504805536
	BCYRN1	1940.456295	610.9076617	372.1179801	98.19924725	-1.672183625	-1.914226299
*	NFKBIZ	1890.790173	1233.293722	14268.10468	8802.276726	-0.61920797	-0.696925142

*	BIVM	1871.870492	994.6467119	588.9649791	77.87743447	-0.918635855	-2.913599653
*	ZNF746	1862.570657	1213.386057	2133.385069	1060.299947	-0.623247549	-1.010920042
*	ALG5	1840.227494	1085.578851	1596.690458	999.9278338	-0.765201446	-0.676336662
*	ZNF777	1765.589527	1000.981483	1652.010274	530.3014469	-0.81728211	-1.638771676
*	NDUFAF4	1751.945689	937.2618241	2187.485873	1326.373683	-0.900848778	-0.720107043
*	PRSS12	1750.725011	754.7871804	84.41334527	31.15817898	-1.218075632	-1.438498059
*	ZBTB39	1732.026733	449.5195513	1977.600633	882.452046	-1.950347597	-1.164543596
*	REX1BD	1667.497868	526.4264122	1759.210691	558.2295343	-1.656504443	-1.653415688
*	GGT7	1636.789246	910.9955788	1350.781595	890.3347273	-0.849182714	-0.602751933
*	RAD51D	1633.252709	925.7048888	1144.770758	715.1125151	-0.81561452	-0.678746762
*	FXYD3	1632.024396	944.3045601	205.6645141	31.90848997	-0.796013271	-2.675353457
*	DHODH	1625.242292	1046.199197	1133.182986	756.1521999	-0.632247697	-0.585168546
*	TMC7	1563.53082	494.6048571	1426.858492	657.1484177	-1.665452147	-1.120692718
*	R3HCC1	1550.028558	928.1398568	2027.482919	1305.103415	-0.745239841	-0.634948125
*	SLC27A2	1529.622135	662.0223111	493.9782537	138.5495965	-1.211890814	-1.834521033
	ZDHHC8P1	1498.057879	729.582305	518.7096395	277.0804322	-1.042235067	-0.899141507
*	FOXA3	1491.058776	514.7435247	2661.681057	1392.694152	-1.541526315	-0.93268937
	LINC02015	1472.311399	671.4560835	630.0011606	137.0696551	-1.137029439	-2.192530781
	FXN	1468.72766	406.5662393	1786.464864	737.5628211	-1.854523699	-1.275639974
	PLA2G12B	1422.28718	914.5945722	1230.703592	664.686724	-0.639687693	-0.888930582
*	SPATA20	1391.187044	913.3829343	3919.592542	2129.304916	-0.607425917	-0.879043314
	NOX4	1381.830315	755.4712792	151.3119733	51.83481472	-0.873402319	-1.535361177
	SULT1B1	1368.081845	859.4828426	489.1320784	126.1045315	-0.674892286	-1.950382836
	AC135048.4	1349.226276	660.472176	231.3037997	114.331033	-1.022957145	-1.011392545
*	MAP3K15	1279.805963	566.7263026	330.5121784	152.28487	-1.170239171	-1.124225813
*	FAM155B	1265.478196	706.2879728	17.7820759	2.147502335	-0.841383947	-3.131597402
*	RUFY2	1256.245793	756.6971431	777.1716248	484.5077949	-0.728036901	-0.681290234
*	HDDC3	1168.717793	696.3838426	499.6435638	213.230241	-0.753900855	-1.227005196
	FAM122A	1140.292738	710.5619024	1651.120148	1072.306987	-0.677003362	-0.623184317

	CEACAM6	1138.539757	483.9253179	304.6405062	111.2547137	-1.243430222	-1.457221445
	HPGD	1123.564817	661.5783459	4058.944522	1512.115644	-0.768553993	-1.423738714
*	GAS8	1115.596136	660.445079	1519.121744	928.2895621	-0.755533157	-0.711651897
*	APOL2	1082.078407	379.384396	1225.102393	726.6018228	-1.523916326	-0.751496159
*	DBNDD1	1072.21966	554.1888273	1731.357474	536.3820257	-0.946906888	-1.691966379
*	RNF144A	1052.658019	689.6461448	939.9173405	566.4558355	-0.611425728	-0.729321953
*	COLCA2	1029.056807	353.0674419	161.6224191	85.11209472	-1.551655343	-0.92915346
	TMPO-AS1	1019.267979	292.4007576	446.7755151	237.0158951	-1.79373128	-0.916419108
*	ADH1C	1007.607707	611.0751707	459.6095765	72.27713598	-0.72876348	-2.665430535
*	RP9	987.61766	495.1467875	677.1469646	293.1381723	-0.987056022	-1.206928061
*	BDH2	967.6779311	586.4027109	1933.514485	961.5513842	-0.731149487	-1.006994699
*	INPP5E	961.9483354	432.1345497	1194.326177	630.2501321	-1.145364031	-0.9230916
*	ADAP1	951.3867573	328.4962284	159.877442	39.39064203	-1.541069919	-2.028267701
*	TAMM41	926.7043807	235.697595	821.2770481	303.6121222	-1.966848085	-1.438836617
*	AADAT	918.7565465	466.377481	1117.80745	407.7159277	-0.985034713	-1.455151856
	MINDY1	918.1373373	585.6989496	462.1956635	280.8793936	-0.648169841	-0.719573038
*	BOLA3-AS1	912.8540936	420.0869688	259.4641031	152.4175581	-1.116820259	-0.772901521
	SNHG26	898.9902279	273.6906137	167.0072725	59.93186624	-1.716751316	-1.481270182
*	C3orf33	869.694842	486.972323	389.0962415	215.7034308	-0.840076038	-0.850949478
*	FAM171A2	867.9837336	419.3697471	359.8066585	102.26664	-1.057391931	-1.820939805
*	COMTD1	863.9303617	287.5053239	510.6545097	141.3013772	-1.574020356	-1.849757816
	AGAP2-AS1	822.8925453	212.4504054	354.9650675	82.34508395	-1.938830387	-2.115018901
*	TDRD3	781.8966478	424.0012765	646.0204759	412.4685613	-0.882887954	-0.644191429
	AL390195.1	748.959537	45.2401323	1508.301943	113.4277343	-4.073429019	-3.724529461
*	EEF1A2	747.0844763	442.7883394	322.0670449	39.20518966	-0.758436368	-3.022908293
*	SMIM8	735.9350289	424.5432199	540.1659652	329.6096912	-0.795556409	-0.712253458
*	SLC39A5	723.0885972	477.7544695	2903.908332	1382.363812	-0.601867559	-1.069913398
	CC2D2A	714.7388871	257.173507	1311.529654	466.2583542	-1.475830778	-1.496268157
*	FBXO4	709.0813881	444.0665477	824.2845291	519.4198453	-0.680858877	-0.665839338

*	LRRC8C	702.2594394	301.5499458	970.0157867	576.126745	-1.216284953	-0.751041991
	HMGCS2	682.1603303	437.0700295	721.864012	210.8584198	-0.648959082	-1.778691393
	SNHG11	669.6102052	406.741714	492.3886077	288.9754959	-0.723805671	-0.771297109
	AL160269.1	658.1504344	377.8505648	1425.910334	950.8883753	-0.809397538	-0.586902752
	MUC12	654.4645209	225.325731	88.1553836	43.53795867	-1.534886427	-1.029927524
*	PNMA6A	653.4464567	363.6449675	289.9932661	181.8834586	-0.835894265	-0.670093801
*	SLCO4C1	568.0951331	303.3014401	2239.51719	1109.453475	-0.913604126	-1.012286719
	AC027228.2	561.6268439	295.6936643	280.1293495	164.008358	-0.928318994	-0.769177013
	DBH-AS1	559.4069865	349.9711157	294.5705286	185.8059171	-0.668494745	-0.661753315
	AL161772.1	544.4978176	344.329529	151.5935496	54.97667532	-0.650233273	-1.473677746
	KRT15	520.9576541	161.2643843	57.67892258	20.49311386	-1.686550445	-1.48184917
*	ERFE	503.4354511	249.245217	94.50528354	17.23717814	-1.006293325	-2.430516701
*	GPRC5B	495.80635	257.6039491	2907.578877	1690.162462	-0.937880077	-0.782264544
*	IFT46	487.4723041	177.8201077	429.5548584	244.0210648	-1.460386698	-0.813499305
	AC011511.4	467.8170962	0.710688212	295.98338	1.408533023	-9.616129123	-7.687676451
*	IRF6	456.0117678	266.7213232	61.72211324	24.82284191	-0.766998002	-1.328806554
	CAPN8	454.4122491	219.1170357	881.2901335	552.3123293	-1.060818791	-0.672271073
*	NKD2	448.2686172	42.2418932	31.68530045	7.983728157	-3.376491815	-2.018168704
	AC080112.1	438.4120878	135.4683167	281.6756482	102.8096387	-1.710266432	-1.463430093
*	HBQ1	433.3066594	100.5567564	51.43509437	16.16342697	-2.122154689	-1.647859172
*	SOWAHA	415.4238319	232.1821664	369.7035162	135.3324633	-0.841175129	-1.448220732
*	GPR3	412.6414563	234.1890076	280.5744125	172.2258212	-0.820136524	-0.699204356
*	TMEM82	406.1599479	268.7704501	250.652452	162.4610138	-0.590648714	-0.619371671
	SEMA3D	398.7034884	256.8330043	3898.200693	2029.719089	-0.624298711	-0.940886751
*	SPEF2	392.4275842	33.38555474	104.8304604	41.11299205	-3.611859702	-1.348520726
	DHRS4-AS1	371.4233003	180.5224972	432.5455847	241.7864959	-1.035630022	-0.835519788
*	HOMER3	341.8163983	124.8140423	1186.024126	294.5898745	-1.446842787	-2.013664581
	OIT3	328.7058705	180.3783311	348.2386655	217.4695325	-0.862940189	-0.681979468
	AC073073.2	301.1992545	168.2933648	194.8588193	126.6536532	-0.838793388	-0.627841743

*	PDX1	298.4244328	158.5486243	1385.466602	647.0259633	-0.920411108	-1.100365697
	AL669918.1	298.3344566	69.57430728	29.21256896	4.092910942	-2.111234365	-2.856549749
*	GTF2IRD2B	265.5370612	60.68969894	720.8268137	369.7742027	-2.151108089	-0.963238563
	MBL2	235.5982652	136.8100221	669.8140471	162.6631075	-0.780185676	-2.038940587
*	ADCY7	232.335523	105.4090137	520.3562684	262.8790494	-1.124663533	-0.986534009
	PRRT3-AS1	226.3419351	36.46142694	101.9437559	18.07719431	-2.590269386	-2.489815045
*	FAM131C	198.1696055	117.8263348	28.58340572	1.610626751	-0.751574856	-4.236016797
*	SYN3	191.8902263	80.0057277	197.5189098	75.64460686	-1.262445114	-1.384459214
	ZG16	183.4366118	78.19040377	112.1159225	39.30623653	-1.214540694	-1.502431135
*	DMKN	183.0101975	88.48870513	1630.019451	656.7669149	-1.061316474	-1.311904414
*	TMEM74B	176.0270154	100.3908807	142.3022115	62.55621602	-0.810500127	-1.194813583
*	TPD52L1	168.616342	43.72629247	956.2013082	353.0276626	-2.006869044	-1.439330625
*	C9orf116	167.2736749	90.40296781	61.0141694	26.00947676	-0.903364365	-1.235377321
	AC110285.7	151.6626794	56.91040961	202.5253133	129.8943018	-1.38073645	-0.637310368
	ZBED3-AS1	143.7999756	56.69239489	162.3235766	84.30747016	-1.33655261	-0.946450712
	FIRRE	130.9325007	54.81109977	266.8628497	145.5143293	-1.247685025	-0.87847157
	AP001029.2	129.51417	30.64384469	100.4580203	33.67419432	-2.216714864	-1.591246115
*	WIF1	126.2821678	35.62388194	245.6301265	126.748577	-1.821998923	-0.95619394
	AL160162.1	122.1435723	55.83626675	63.34007715	28.51120031	-1.129090151	-1.137059835
*	GTF2IRD2	117.3585155	52.62659627	401.6886853	228.8024894	-1.16107793	-0.810248668
*	EPDR1	106.8434115	18.0391723	349.4871001	169.8998963	-2.598322421	-1.045577556
*	C17orf113	91.53268831	25.71489919	93.47497875	42.3948019	-1.814070299	-1.134429658
	AC092115.2	85.1468214	35.24821173	143.7556186	79.08606611	-1.252710838	-0.86353989

3.4 Role of CTCF in the regulation of energy metabolism

Pathway analysis above suggested that CTCF may play a role in the regulation of cellular energy metabolism. To further explore the biological implications of these observations, we determined glycolytic flux and mitochondrial respiration, the two major energy production pathways in the cells, using the Seahorse instrument.

3.4.1 CTCF plays a role in regulating mitochondrial respiration

Measurement of mitochondrial respiration under steady-state conditions showed the basal oxygen consumption rate (OCR) in CTCF knockout and control PLC5 cells was not differed significantly. However, the maximal respiration rate and spare respiratory capacity were reduced by ~43% and ~39% respectively in the both CTCF knockout cells, comparing to the control cells (Figure 3.4–1and Figure 3.4–2). PLC5-KO cells also exhibited a ~28% reduction in ATP production, although the difference did not reach statistical significance (Figure 3.4–1). Huh7-KO cells showed a similar drop in the maximal respiration rate (~30%) and spare respiratory capacity (~33%) (Figure 3.4–2). In addition, Huh7-KO cells exhibited a significant reduction in basal respiration of OCR (28%) and ATP production (~33%) (Figure 3.4–2). Using an independent bioluminescence-based assay, it is confirmed that there is a significant reduction in ATP levels in both cell lines (Figure 3.4–3). Together, these data suggested that CTCF plays a role in oxidative phosphorylation (OXPHOS) and energy production. Insignificant proton leak was observed in both CTCF knockout cell lines (Figure 3.4–1 and Figure

3.4–2), suggesting that the observed reduction in OXPHOS is not due to lost in mitochondrial activity. Together, these data suggested that CTCF plays a role in regulating mitochondrial respiration.

A

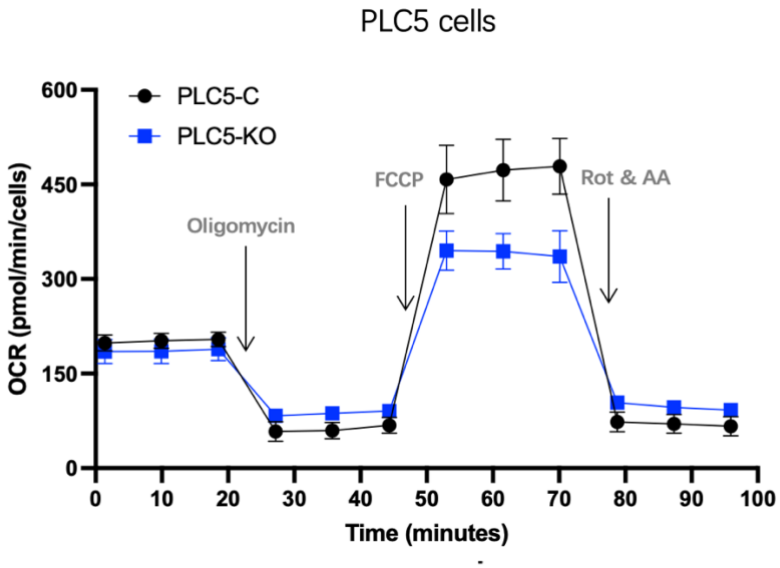

B

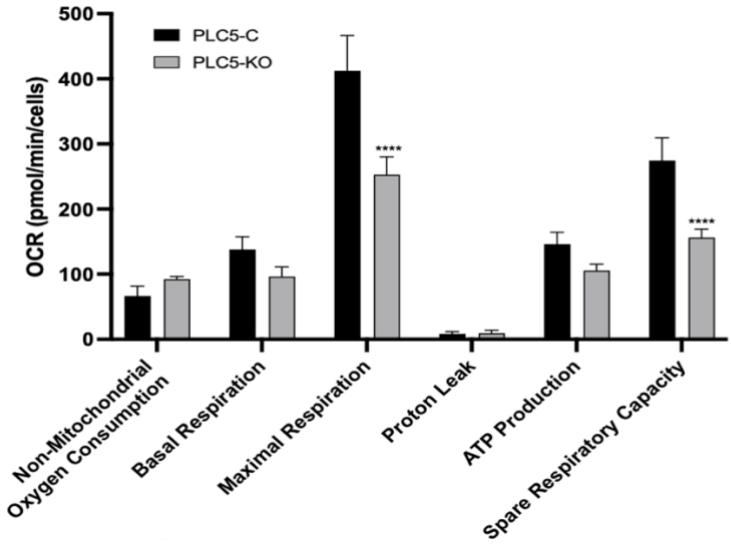

Figure 3.4–1 Reduced mitochondrial respiration activity in PLC5-KO cells.
(A) Oxygen consumption rate (OCR) measurements of PLC5-C and PLC5-KO cells. FCCP: carbonyl cyanide-4 (trifluoromethoxy) phenylhydrazone (FCCP); Rot: rotenone AA: antimycin. (B) Analytics of the OCR results from (A). ****, $p<0.0001$ by student's t test.

A

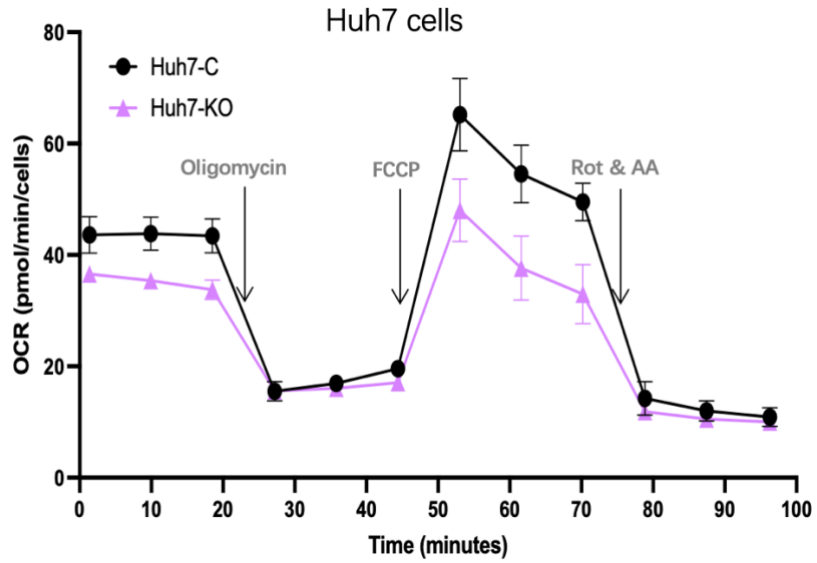

B

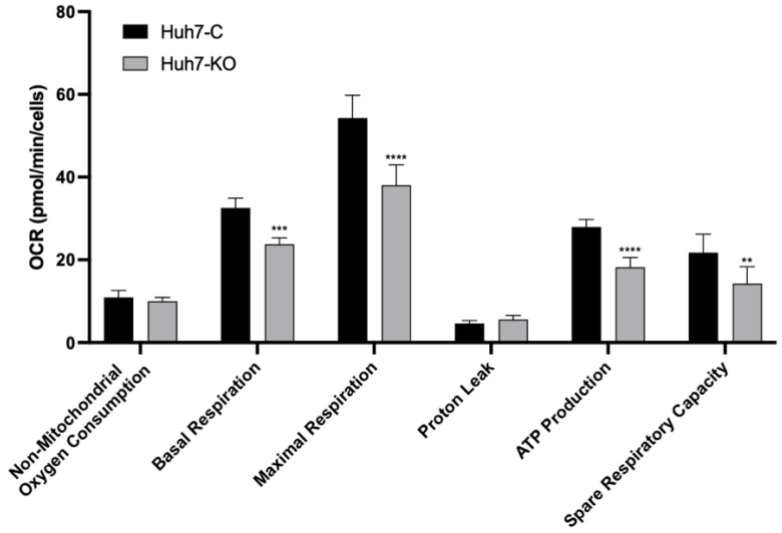

Figure 3.4–2 Reduced mitochondrial respiration activity in Huh7-KO cells.

(A) Oxygen consumption rate (OCR) measurements of Huh7-C and Huh7-KO cells. FCCP: carbonyl cyanide-4 (trifluoromethoxy) phenylhydrazone (FCCP); Rot: rotenone AA: antimycin. (B) Analytics of the OCR results from (A). ****, $p<0.0001$ ***, $p<0.001$, **, $p<0.01$ by student's t test.

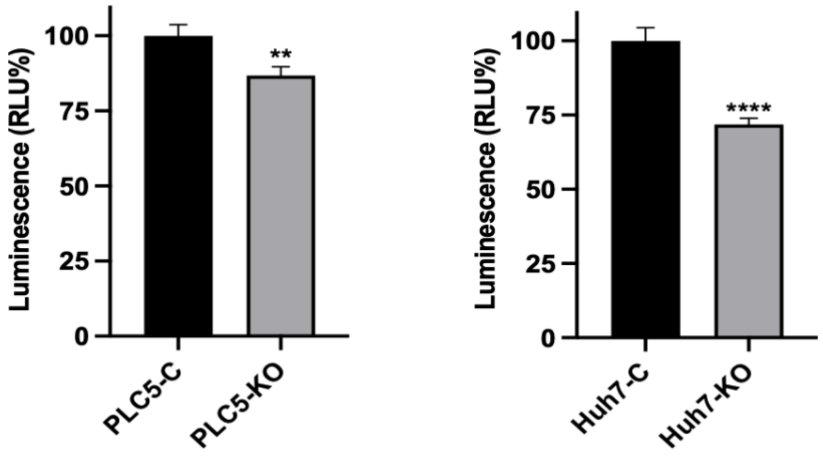

Figure 3.4–3. ATP levels in control and CTCF knockout cells.

Intracellular ATP level was measured in a bioluminescence assay using the CellTiter-Glo Luminescent Cell Viability Assay kit. Left: PLC5-C vs PLC5-KO cells; right: Huh7-C vs Huh7-KO cells. ****, $p<0.0001$, **, $p<0.01$ by student's t test.

3.4.2 CTCF is essential for in regulating glycolytic ability in HCC cells.

To determine how glycolytic activity was affected, we measured extracellular acidification rate (ECAR) in these cells. We found that the rate of glycolysis, maximum glycolytic capacity, and glycolytic reserve, were significantly reduced under basal condition in PLC5-KO cells, compares to PLC5-C cells (Figure 3.4–4). On the other hand, there was also a significant reduction in the rate of glycolysis and glycolytic activity in Huh7-KO cells, although the reduction was less prominent (Figure 3.4–5). Concordantly, CTCF knockout resulted in a significant reduction in glucose uptake (~50% and ~70% reduction in PLC5-KO and Huh7-KO cells respectively) (Figure 3.4–6A) and lactate production (~50% in both PLC5-KO and Huh7-KO cells) respectively (Figure 3.4–6B). Together, these data suggested that CTCF is essential for HCC glycolysis and energy production.

A

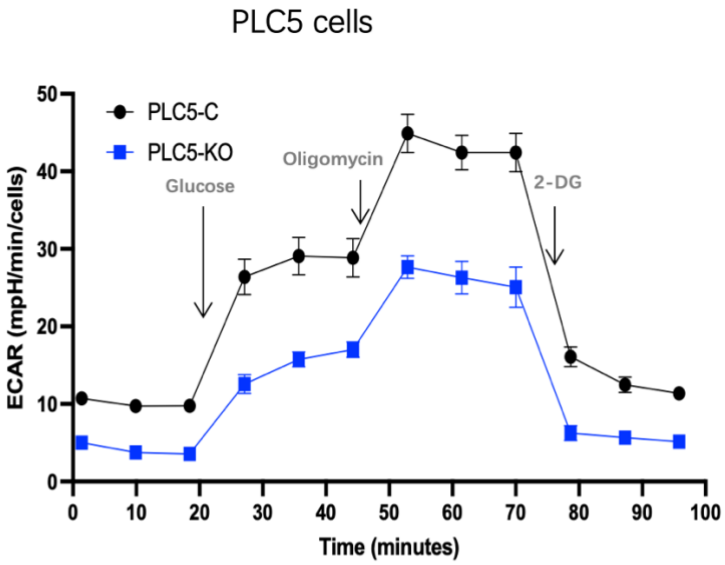

B

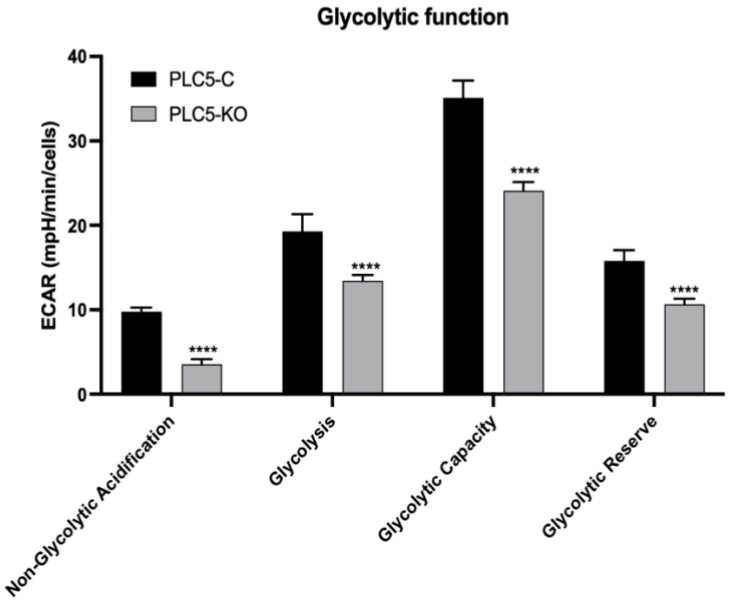

Figure 3.4–4 Reduced glycolytic activity in PLC5-KO cells.

(A)Extracellular acidification rate (ECAR) measurements of PLC5-C and PLC5-KO cells. 2-DG: 2-deoxyglucose. (B) Analytics of the OCR results from (A). ****, $p<0.0001$ by student's t test.

A

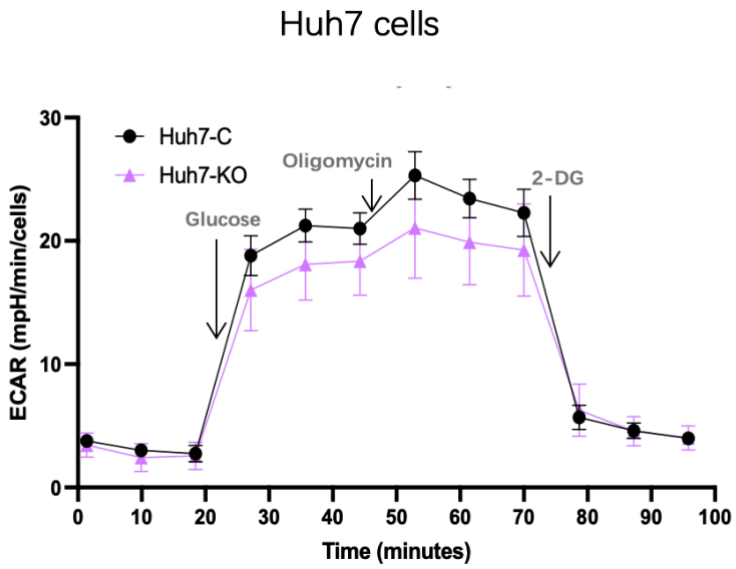

B

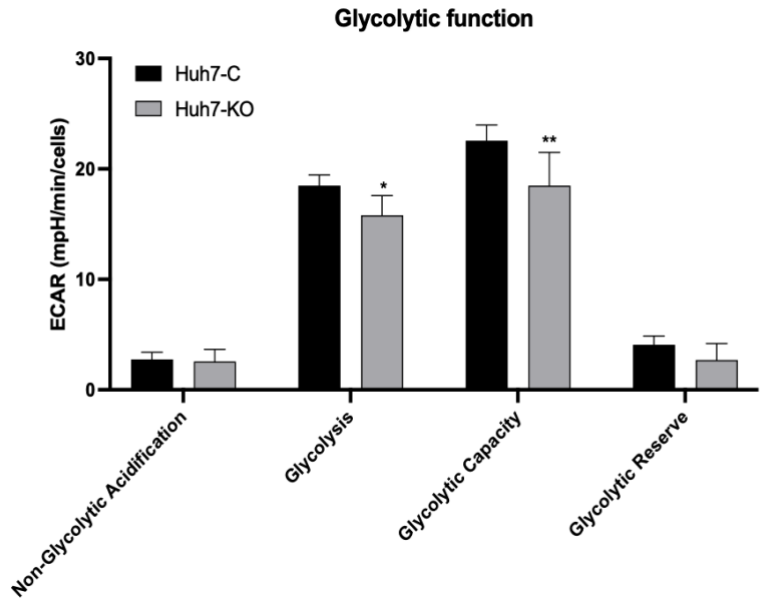

Figure 3.4–5 Reduced glycolytic activity in Huh7-KO cells.

(A)Extracellular acidification rate (ECAR) measurements of Huh7-C and PLC5-KO cells. 2-DG: 2-deoxyglucose. (B) Analytics of the OCR results from (A). ****, $p<0.0001$ by student's t test.

A

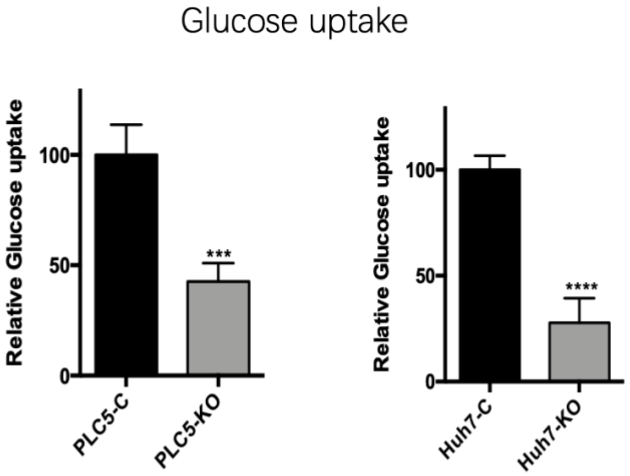

B

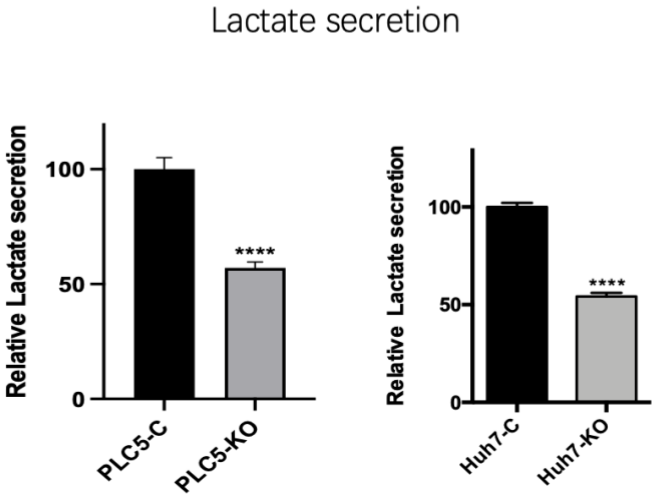

Figure 3.4–6 Glucose uptake and lactate production in CTCF knockout cells.
(A). Glucose uptake was determined by using the Glucose Uptake-Glo Assay kit. Glucose update was significantly reduced in PLC5-KO and Huh7-KO cells repsecitvely. ****, $p<0.0001$; ***, $p<0.001$ by student's t test. (B). Extracellular lactate levels was determined by Lactate-Glo Assay kit. Lactate production was significantly reduced in PLC5-KO and Huh7-KO cells repsectively. ****, $p<0.0001$; ***, $p<0.001$ by student's t test.

3.4.3 CTCF may play a role in maintaining NAD+/NADH ratio.

The findings above suggested that cellular energy homeostasis was compromised in the absence of CTCF. The profound reduction in glucose uptake in CTCF knockout cells suggested that CTCF may play a role in controlling the flux through glycolysis, which is the preceding steps for ATP production through aerobic glycolysis and oxidative phosphorylation. Among others, glycolytic flux is tightly regulated by the availability of NAD^+, a cofactor the regulation of GADPH activity [241]. Accordingly, we found that NAD^+/NADH ratio in both PLC5 and Huh7 cells was significantly reduced in the absence of CTCF, suggesting that CTCF may play a role in maintaining NAD^+/NADH ratio that is necessary for glycolytic flux and sustains energy production (Figure 3.4–7).

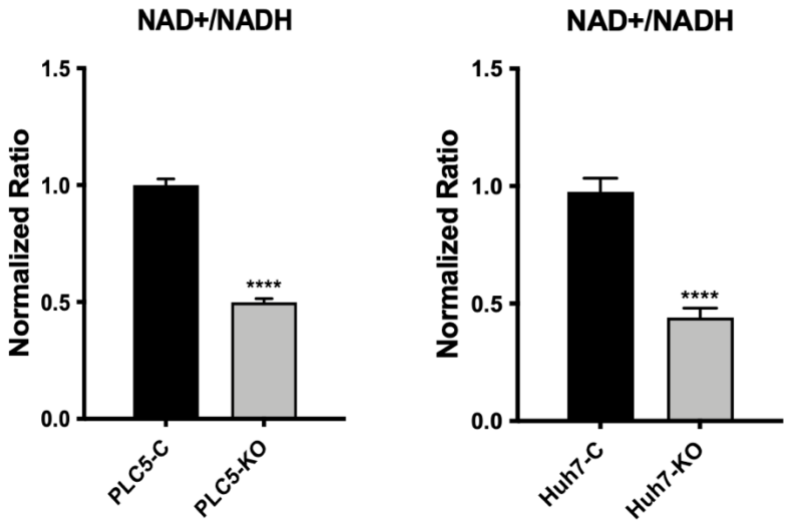

Figure 3.4–7 Reduced NAD$^+$/ NADH ratio in CTCF knockout cells.

The NAD+/NADH ratio of CTCF knockout cells was determined by the NAD+/NADH-Glo assay kit. Significant reduction in NAD+/NADH ratio was observed in PLC5-KO cells (Left), and Huh7-KO cells (Right), in compared to their respective control cells. ****, $p<0.0001$ by student's t test.

3.5 Identification of CTCF-regulated genes responsible for energy metabolism in HCC cells.

To gain more insights into the role of CTCF in HCC, the top 50 down-regulated genes on CTCF knockout HCC cells were further analyzed among them(Figure 3.5–1A), we found that IQ Motif Containing GTPase Activating Protein 2(IQGAP2), Glutamic-Oxaloacetic Transaminase 2 (GOT2), Fatty acid desaturase 1(FADS1) genes are implicated in the maintaining of NAD+/NADH ratio [242]–[244]. The expression of IQGAP2, GOT2, and FADS1 was reduced by 0.46, 0.45 and 0.38 folds in PLC5-KO, and by 0.52, 0.47 and 0.64 folds in Huh7-KO cells respectively (Figure 3.5–1B). In addition, several DEGs of interest were found to be altered after CTCF knockout in HCC cells (Figure 3.5–1C).We determined the role of each of IQGAP2, GOT2, and FADS1 gene in the regulation of NAD+/NADH homeostasis of HCC cells using shRNAs. Gene knockdown analysis showed that depletion of FADS1 or IQGAP2, but not GOT2, significantly reduced cellular NAD+/NADH ratio (Figure 3.5–2).

To further examine if FADS1 and IQGAP2 are essential for energy homeostasis in HCC cells, we measure rate of oxidative phosphorylation and glycolysis in these cells respectively. Concordantly, knockdown of FADS1 and IQGAP2 significantly reduced glycolytic functions, and oxidative phosphorylation activity in PLC5 cells (Figure 3.5–3, Figure 3.5–4). We further determined if and how FADS1 and IQGAP2 deficiency may affect cell growth and metastasis. Knockdown of FADS1 and IQGAP2 also

significantly reduced cell growth (Figure 3.5–5), cell mobility and invasiveness (Figure 3.5–6) of PLC5 cells, similar to CTCF knockout. These data suggested that FADS1 and IQGAP2 as putative CTCF-regulated genes are responsible for the regulating energy homeostasis.

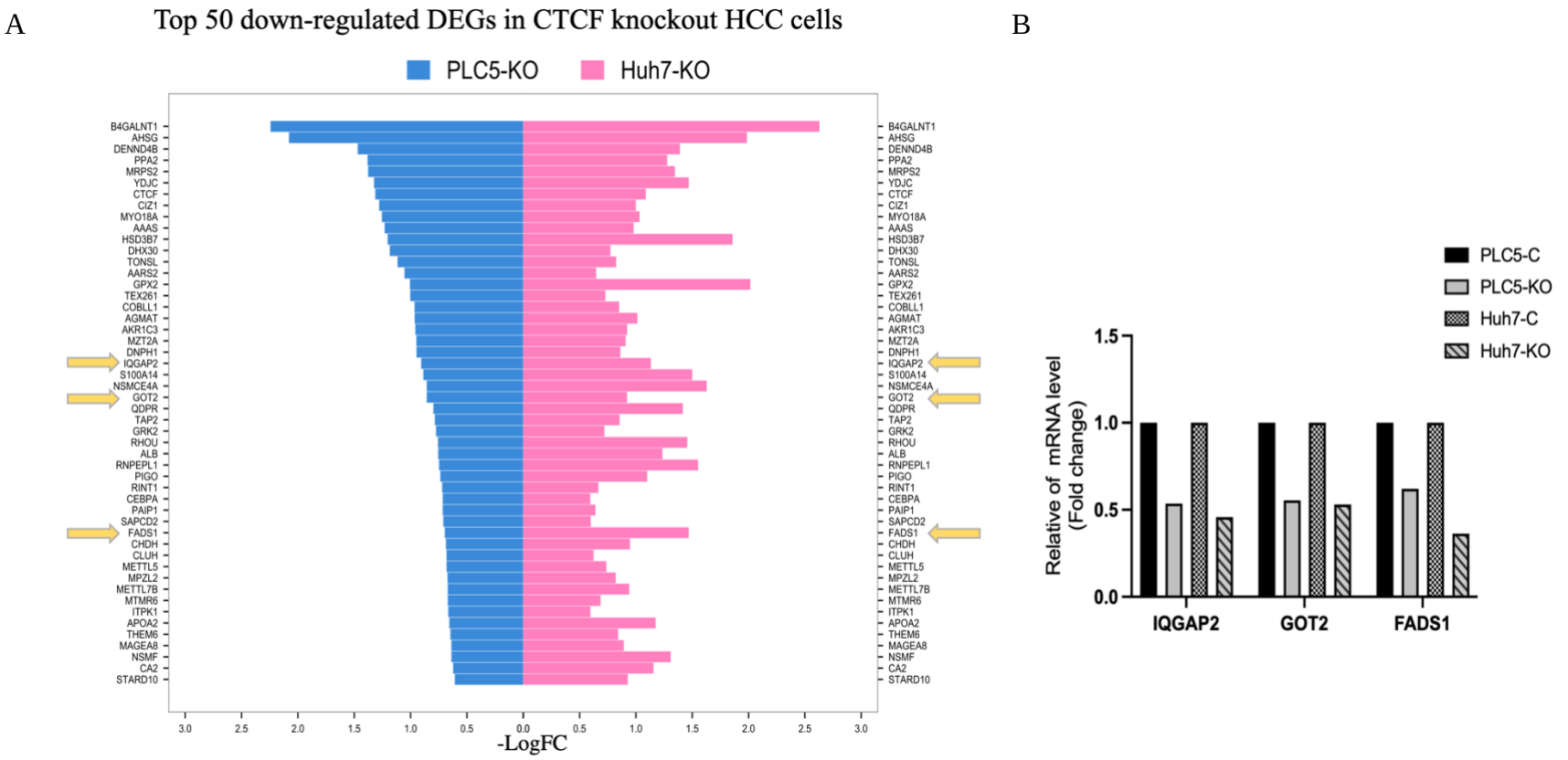

Figure 3.5–1. Commonly regulated DEGs in CTCF knockout HCC cells.

(A)Top 50 commonly down-regulated DEGs in CTCF knockout HCC cells. Genes were list in the order of reducing level of downregulation in PLC5-KO cells. X axis: -Log (Fold change). (B)The expression of IQGAP2, GOT2, and FADS1 folds changes in PLC5 and Huh7 cells. (C) The expression of several DEGs folds changes in PLC5 and Huh7 cells.

C

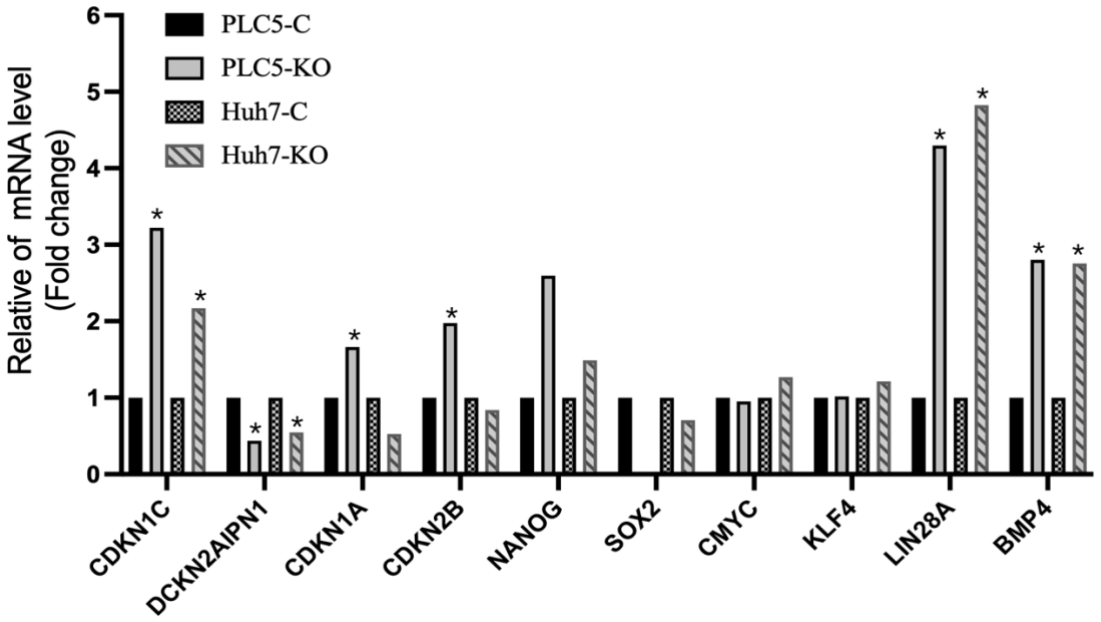
PLC5-C
PLC5-KO
Huh7-C
Huh7-KO
Relative of mRNA level
(Fold change)
0
1
2
3
4
5
6
CDKN1C
DCKN2AIPN1
CDKN1A
CDKN2B
NANOG
SOX2
CMYC
KLF4
LIN28A
BMP4

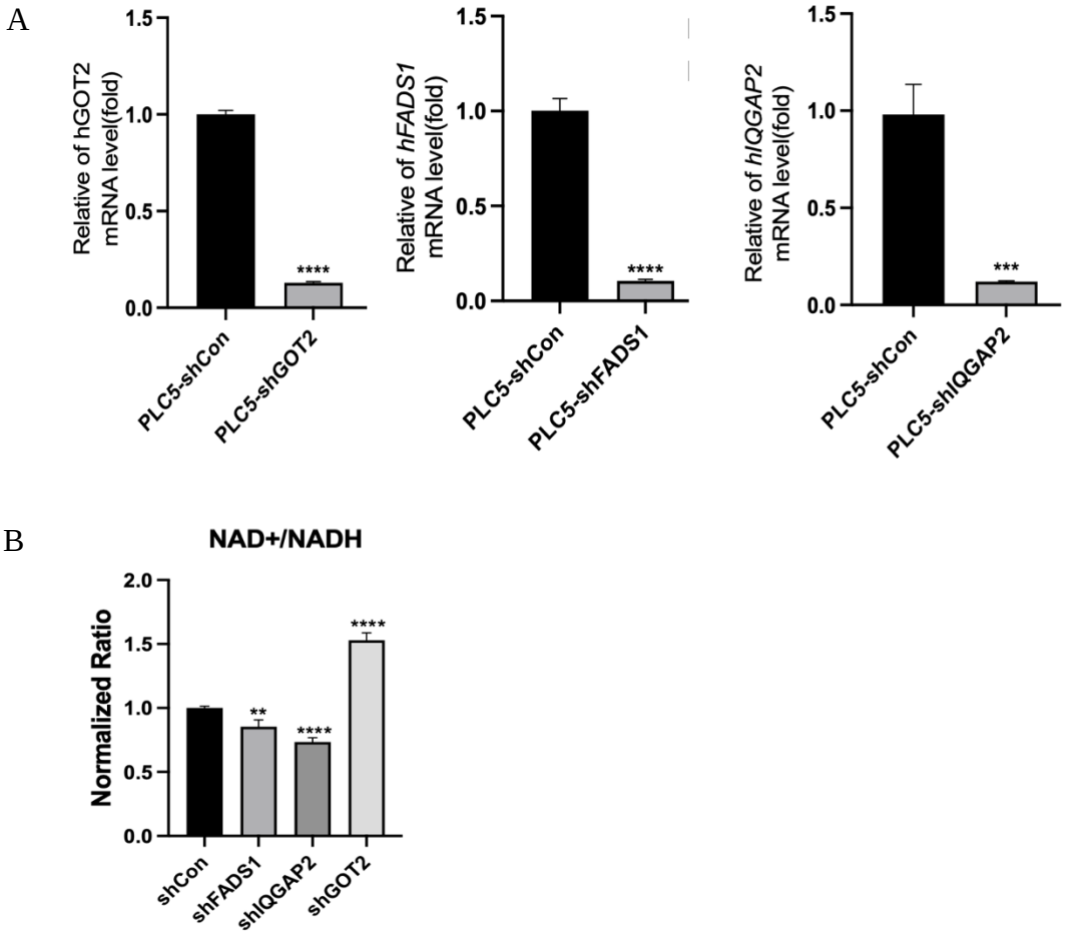

Figure 3.5–2 Effect of GOT2, FADS1, and IQGAP2 knockdown on cellular NAD+/NADH ratio.

(A) RT-qPCR analysis of genes expression of GOT2, FADS1 and IQGAP2 in response to shRNA knockdown. (B) Cellular NAD+/NADH ratio in response to gene knockdown of FADS1, IQGAP2 and GOT2 respectively. ****, $p<0.0001$; ***,$p<0.001$; **, $p<0.01$ by student's t test.

A

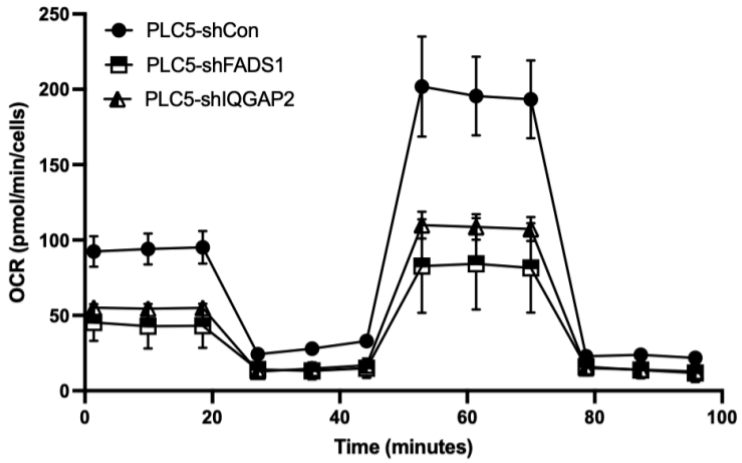

B

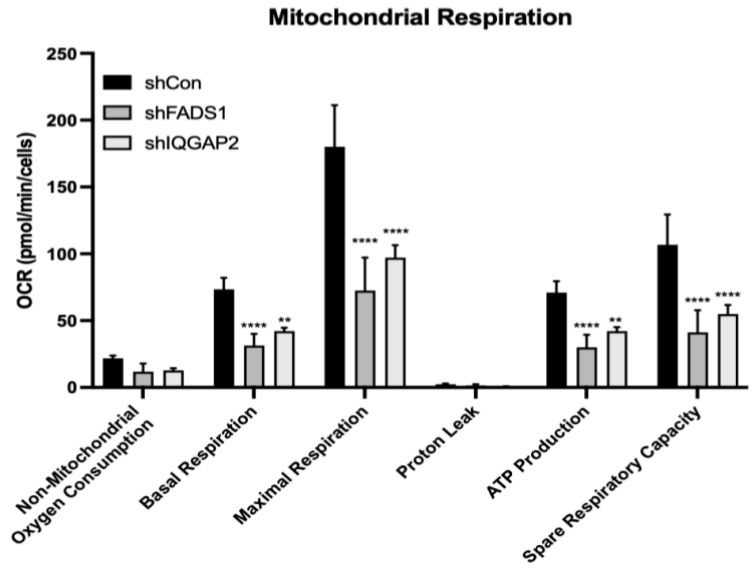

Figure 3.5–3 shRNA knockdown of FADS1 or IQGAP2 in PLC5 cells reduced oxidative phosphorylation.

Oxygen consumption rate (OCR) in PLC5 cells transfected with control shRNA (PLC5-shCon), FADS1 shRNA (PLC5-shFADS1) and IQGAP2 shRNA (PLC5-shIQGAP2) respectively. FCCP: carbonyl cyanide-4 (trifluoromethoxy) phenylhydrazone; Rot: rotenone; AA: antimycin. (B) Analytics of the OCR results from (A). ****, $p<0.0001$; ***, $p<0.001$; **, $p<0.01$ by student's t test.

A

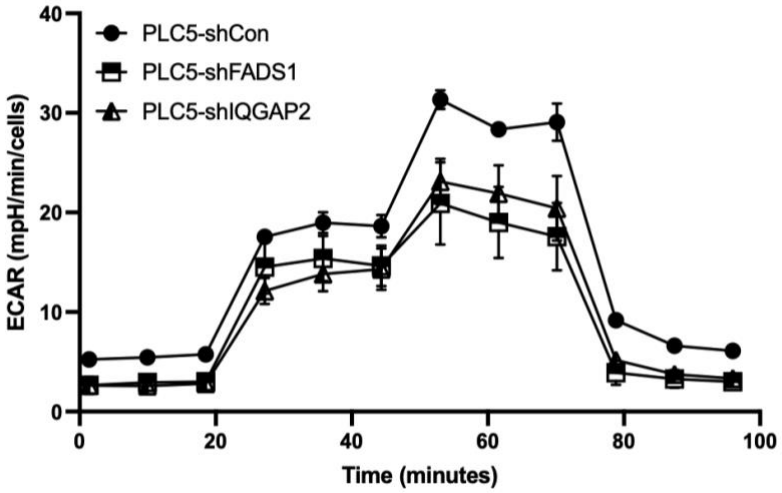

B

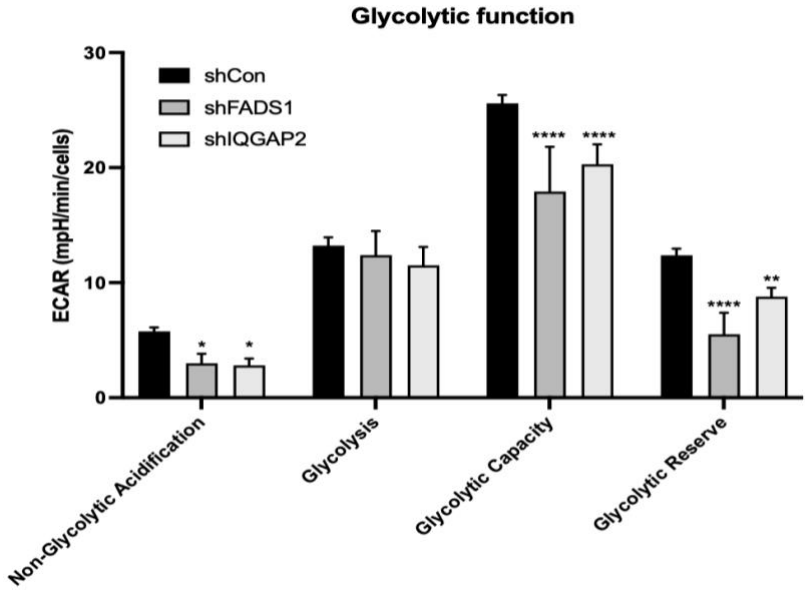

Figure 3.5–4 Knockdown of FADS1 or IQGAP2 in PLC5 cells reduced rate of glycolysis.

Extracellular acidification rate (ECAR) in PLC5 cells transfected with control shRNA (PLC5-shCon), FADS1 shRNA (PLC5-shFADS1) and IQGAP2 shRNA (PLC5-shIQGAP2) respectively. B) Analytics of the ECAR results from (A). ****, $p<0.0001$; ***, $p<0.001$; **, $p<0.01$ by student's t test.

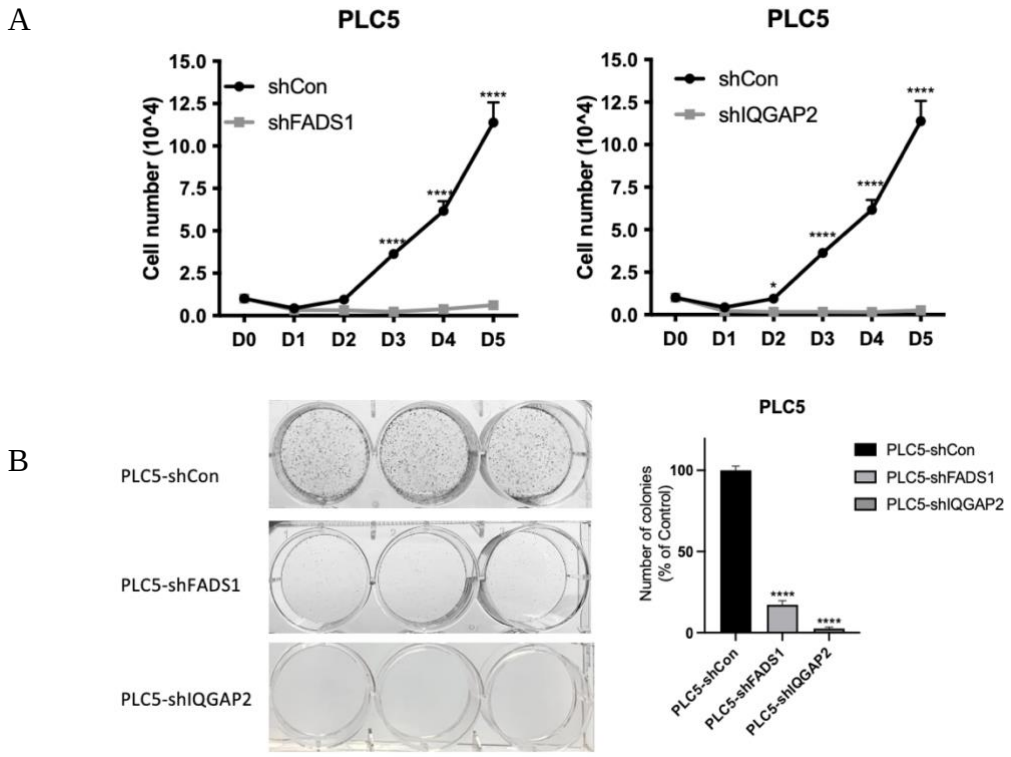

Figure 3.5–5 Gene knockdown of FADS1 and IQGAP2 inhibited cell growth on PLC5 cells.

(A) Cell proliferation PLC5 cells transfected with FADS1 shRNA (PLC5-shFADS1) (Left) or IQGAP2 shRNA (PLC5-shIQGAP2) (Right) in compare with cells transfected with Control shRNA (PLC5-shcon). 10,000 cells were counted daily after trypsinization followed by trypan blue staining. ****, $p<0.0001$; ***, $p<0.001$; *, $P<0.05$ by student's t test. (B) Colony formation assay was conducted by culturing cells for 7 days in the presence of 5 μg/mL puromycin. Colonies were stained using 0.25% crystal violet.

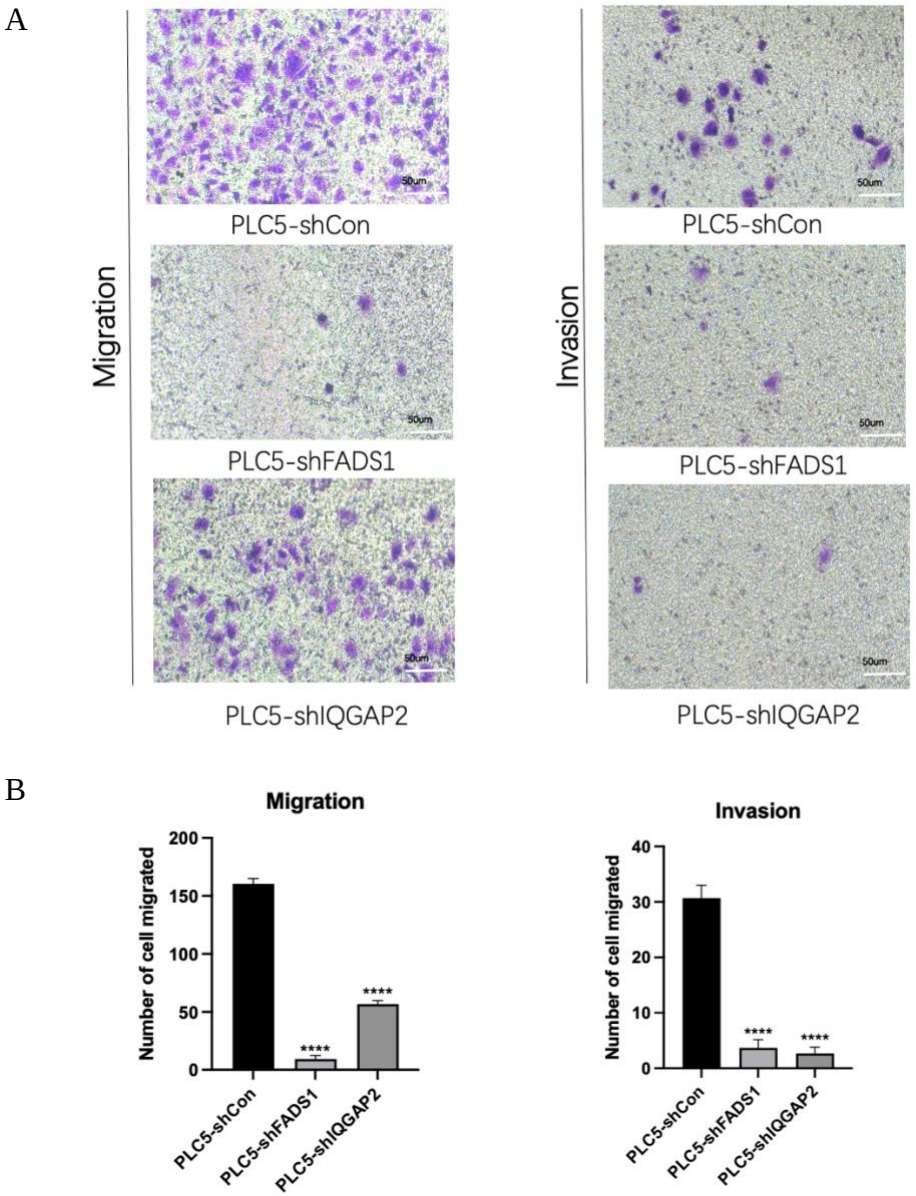

Figure 3.5–6 Gene knockdown of FADS1 and IQGAP2 inhibited mobility and invasiveness of PLC5 cells.

PLC5 cells transfected with Control shRNA (PLC5-shCon), FADS1 shRNA (PLC5-shFADS1), IQGAP2 shRNA (PLC5-shIQGAP2) were seeded in transwell (migration), or transwell coated with Matrigel (invasion) for 16 hours. (A) Left, representative pictures of cell migration in different treatments. Right, representative pictures of cell invasion in different treatments. (B) Quantification of cells migrated (Left) or invaded (Right) through the transwell. Each condition was done in triplicate. In each experiment, three randomly chosen fields were counted. Bars represent mean ± SD; ****, $p < 0.0001$; ***< 0.001.

Chapter Four: Discussion

An earlier publication from Dr. Ko's laboratory has established the clinical relationship between CTCF overexpression and the prognosis of HCC patients [219]. The work has also established a role of CTCF in HCC cells growth and metastasis *in vivo*[219]. Therefore, the goal of my study is to extend on the earlier study to further delineate the underlying molecular mechanisms how CTCF orchestrates the two most important phenotypes, namely, tumor growth and metastasis, in HCC. The earlier study relied primarily on the shRNA-mediated gene knockdown technology to interrogate the role of CTCF in the HCC model system. However, due to the recent concerns over the nonspecific effects of shRNA in cell growth and off-target activities may lead to undesired toxicity[245]–[248]. I have decided to continue the investigation by establishing CTCF-null cell models using the CRISPIR/Cas9 gene knockout technology[222], [249]. This experimental approach has been proven successful and effective in knockout of most CTCF expression in the two HCC cell lines we tested. To ensure the specificity of knockout, I examined the on-targeted and top 10 off-targeted (Table 3.2-1) effect of CTCF sgRNA used, and I found that that most of the indels are identified in the CTCF loci while minimal indels are found in the potential off-target loci (Figure 3.2–2, Figure 3.2–3). Overall, these data suggest that CTCF sgRNA and Cas9 carried out specific editing in PLC5 and Huh7 cells in this study. The residual expression of CTCF observed in the knockout cells (Figure 3.2–1)are most probably

due to the present of drug resistant cells. In agreement with the shRNA knockdown cell models, the CTCF CRISPR/Cas9 gene knock out cell models mostly recapitulated the cell growth and metastatic phenotypes of CTCF-depleted cells generated by shRNA-mediated knockdown (Figure 3.2–5, Figure 3.2–10).

Nevertheless, a major difference in the findings between this and the previous study lies in the observations in the mechanisms of CTCF-driven metastasis. In the earlier study, shRNA-mediated knockdown of CTCF resulted in a the rearrangement of actin organization and repression of FOXM1 expression[219]. However, in the current study, gene knockout of CTCF in the same HCC cells neither resulted in the arrangement of actin organization, nor repression in FoxM1 expression. The reasons underlying such discrepancy is not clear, but it might be due to the non-specific effect of the shRNAs. Different from the previous study that aimed to characterize the cellular phenotypes when CTCF has been depleted, in the current study I focused on the use of a systematic approach by whole genome transcriptomic analysis to elucidate the CTCF-regulated gene networks in HCC. This allowed me to correlate the observed cellular phenotypes with altered gene expressions.

HCC cell growth inhibition in response to CTCF knockdown is associated from cell cycle arrest in these cells (Figure 3.2–8). Transcriptome analysis (Figure 3.5–1C) revealed that several important cyclin-dependent kinases (CDKs) inhibitors were

altered in CTCF knockout cells. In both PLC5 and Huh7 cells, there were up regulation in the expression of cyclin dependent kinase inhibitor 1C (CDKN1C/$p57^{KIP2}$) and down regulation in CDKN2A interacting protein N-terminal like (CDKN2AIPNL). The CDKN1C gene, which encodes p57(KIP2), is an inhibitor of a couple of G1 cell cycle protein/CDK complexes and serves as a negative regulator of cell proliferation[250], [251]. Increased expression of CDKN1C/p57 has been associated with cellular senescence in HCC cells[252]. Besides, cyclin dependent kinase inhibitor 1A(CDKN1A/p21) and cyclin dependent kinase inhibitor 2B (CDKN2B/ $p15^{INK4B}$) were both up-regulated in CTCF knockout of PLC5 cells. CDKN1A/p21 functions as a regulator of cell cycle progression during the G1 phase. CDKN1A/P21 protein expression mediates a p53-dependent cell cycle G1 phase arrest in response to diverse stress stimuli[253], [254]. Additionally, in the presence of TGF-beta treatment, CDKN2B/$p15^{INK4B}$ may function as an effector of cell cycle arrest[255]. Another study also showed that the dominant role of CDKN2B/$p15^{INK4B}$ can inhibit cell cycle and knockdown of CDKN2B/$p15^{INK4B}$ significantly decreased glycolysis in bladder cancer cells[256]. Overall, CTCF knockout induced the upregulation of certain CDKs, which may lead to the cell cycle and cellular senescence observed in the HCC cells.

Another observation from this study is related to CTCF-dependent spheroid formation in HCC cells (Figure 3.2–6). Recent study [257] suggested that the knockdown of CTCF in human embryonic stem cells (hESCs) reduces the expression of genes

associated with pluripotency maintenance. These included NANOG, SOX2, cMYC, KLF4 and LIN28. However, our transcriptomic data (Figure 3.5–1C) suggested that CTCF does not regulate NANOG, SOX2, cMYC, KLF4 expression. Nevertheless, LIN28A was up-regulated in both HCC cell lines. In addition, bone morphogenetic protein 4 (BMP4) was significantly upregulated in the absence of CTCF from PLC5-KO and Huh7-KO cells (Figure 3.5–1C), which is associated with a loss of cell pluripotency[257] and the induction of liver cancer stem cells (CSCs) differentiation [258]. A possible explanation for my findings might be that CTCF regulate BMP4 expression to play a role in stem cell properties in HCC cells.

CTCF is a highly conserved nuclear factor. It has been known to play multiple functional roles in transcriptional regulation, insulator activity, imprinting and X chromosome inactivation[158]–[162]. The best characterized functions of CTCF are its involvement in the formation of topologically associating domains (TADs)[259][260], responsible for defining chromosomal boundaries. However, recently evidence suggested that the interaction between CTCF and its binding sites can be transient [261], suggesting that the action of CTCF on chromatin/gene regulations can be regulated temporally according to cell status or stimulations. Accordingly, differential CTCF occupancies has been observed in triple-negative breast tumor cells, comparing to normal breast cells, resulting in a dramatic change in tumor local 3D architectures[262]. On other hand, as demonstrated in prostate cancer model, alternations in CTCF-DNA

interaction may result in a change enhancer-promoter loops, resulting in the change in expression of oncogenes[263]. Therefore, it is possible that CTCF-DNA contacts might be formed or disassembled during HCC tumorigenesis and determined the phenotypes of the HCC cells. It will be important to characterize and compare the 3D architectures of HCC cells and primary hepatocytes, which can be accomplished by Hi-C analysis. This will further reveal the correlation between physical changes in genomic structure and gene alternations mediated by CTCF in HCC.

It is worth-noting that CTCF may play a tumor-specific role. CTCF may act as a tumor suppressor in cancers. Recent study established that ectopic expression of CTCF inhibits cell colony formation in many cell types, including Hela, HEK 293, K562 and PC3 cells [264]. Besides, ectopic expression of CTCF inhibits cell growth by inhibiting DNA replication and cell divisions [264]. However, it is observed that overexpression CTCF protein can partially protect breast cancer cells from apoptosis[265]. In addition, in breast cancer, another evidence indicated that depletion of CTCF inhibited MCF-7 cells growth and proliferation, arrested cell cycle and increased apoptosis [266]. Together, these data suggest that CTCF may play an important role in regulating cancer cell growth, acting as an oncogenic or suppressive role in different cancer cells.

CTCF acts an essential genome weaver that interacts with thousands of binding sites in the genome, and is responsible for the formation of topologically associating domains

(TADs) of the genome. Therefore, as expected, thousands of DEGs were recorded in each of the HCC cell lines (Figure 3.3–2) upon the knockout of CTCF, suggesting that many cellular pathways may be disrupted. To identify the central processes regulated by CTCF in HCC, I focused on analyzing those DEGs that were commonly altered in both HCC cell lines. Importantly, this approach successfully identified metatbolic pathway as the potentially important pathway regulated by CTCF (Figure 3.3–4), suggesting that cellular energy status may be altered when CTCF has been knocked down. To further investigate such possibility, I compared and analyzed the rate of oxidatative phosphorylation and glycolysis between control and CTCF knockout cells. Importantly, these two major energy production pathways were significantly compromised (Figure 3.4–1,Figure 3.4–2, Figure 3.4–4, Figure 3.4–5), confirming the role of CTCF in energy-related process in HCC cells. Furthermore, my finding suggested that altered NAD^+/NADH homeostasis (Figure 3.4–7) could be a potential cause for the observed energy deficit.

In comparison to normal cells, cancer cells require more energy for metabolism and counteract aerobic glycolysis by (1) enhancing glucose uptake, (2) converting most pyruvate to lactate, and (3) boosting fatty acid oxidation to provide acetyl CoA[241]. In this study, CTCF knockout cells significantly inhibited glycolysis, which is the main energy metabolism in cancers[267]. In HCC, glycolysis plays an important role in energy metabolism[115], [267], [268]. HCC cells utilize glucose to generate energy via

aerobic glycolysis to produce lactate [268]. Aerobic glycolysis has found to contribute to cell proliferation, metastasis, as well as drug resistance in HCCs [268]. Recent study found that forkhead box O6 (FOXO6), which is highly expressed in HCCs [269], plays an important role in glycolysis and drug resistance, by inhibiting the PI3K/Akt signaling pathway[269]. In our study, the substantial reduction in glucose uptake (Figure 3.4–6) in CTCF knockout cells suggested that CTCF may contribute to control fluxes through glycolysis, which is a preliminary step in the production of ATP through aerobic glycolysis and oxidative phosphorylation. Among others, Glycolytic flux is strictly regulated by the presence of NAD^+, which is a cofactor in the regulation of GADPH activity[241]. The reduced NAD^+/NADH ratio found in CTCF knockout cells (Figure 3.4–7) suggesting that CTCF may play a role in maintaining the NAD^+/NADH ratio, which is necessary for glycolytic flux. Hence, it could conceivably be hypothesized that CTCF may be involved in energy metabolism and NAD^+/NADH homeostasis, regulating proliferation and metastasis in HCC cells (Figure 4–1).

Several genes in the GO and KEGG term metabolism, including the Ras GTPase-activating-like protein (IQGAP2), Glutamate oxaloacetate transaminase 2 (GOT2) and, Fatty Acid Desaturase 1(FADS1) genes, are implicated in the regulation of cellular NAD^+/NADH ratio. These genes were downregulated in both CTCF knockout HCC cells (Figure 3.5–1B). FADS1 encodes for the δ-5 desaturase (D5D), which is involved in the synthesis of highly unsaturated fatty acids (HUFAs), using linoleic acid (LA) and

alpha-linolenic acid (ALA) as precursors. Recent study suggested that HUFA synthesis may act as a possible route for the NAD^+ cycle of glycolysis[243]. Inhibiting either aerobic respiration or lactate production would lead to an increase in NADH levels and a parallel decrease in the NAD^+/NADH ratio. Interestingly, they found that inhibition of aerobic respiration can cause an increase in lipid HUFA levels, which is associated with an increased level of FADS1 activity. FADS1can catalyze lipid desaturation to HUFAs using NAD^+ as cofactor, and therefore, contributed by glycolytic NAD^+ recycling. Furthermore, overexpression of FADS1 induced an increase of the cytosolic NAD+/ NADH ratio, whereas knockdown of FADS1 diminished the NAD+/ NADH ratio[243]. Evidence suggested that FADS1 is involved in intracellular NAD^+/NADH homeostasis for the glycolytic NAD^+ cycle[243]. On the other hand, IQGAP2 is an enzyme that is encoded by the human IQGAP2 gene. IQGAP2 protein predominantly found in the liver. IQGAP2 is considered as a potential target in HCC[270]. Disruption of Iqgap2 in mice is associated with apoptosis in HCC [271]. Besides, lack of Iqgap2 in mice exhibits an inhibition of hepatic long-chain fatty acid (LCFA) uptake and prevents the accumulation of hepatic triglycerides[272]. In addition, depletion of Iqgap2 also enhances the sensitivity of insulin[272]. This evidence suggested that IQGAP2 may be involved in fatty acid uptake and glucose homeostasis. One more evidence suggested that IQGAP2-deficient mice exhibits metabolic inflexibility, which leading to the impaire TCA cycle and an increase supply of acetyl CoA for de novo lipogenesis[242]. These results suggested that IQGAP2 may regulate metabolic

homeostasis in HCC cells. In addition, GOT2 is required for the malate-aspartate shuttle between the mitochondria and the cytoplasm[244], which is essential for cytosolic NADH transfer to mitochondria, regulating glycolysis and promoting tumor cell growth. Acetylation of GOT2 at residues K159, K185 and K404 (3K) facilitates the net transfer of cytosolic NADH to mitochondria, modifying the mitochondrial NAD^+/NADH redox state to support ATP production[244].

To determine whether FADS1, IQGAP2 and GOT2 are involved in regulating NAD+/NADH homeostasis in HCC cells, I used the shRNA-mediated manner to deprive the expression of these genes. The result showed that depletion of the FADS1 or IQGAP2 genes, but not the GOT2 gene, reduced the cellular NAD^+/NADH ratio ( ), and suppressed both oxidative phosphorylation and glycolytic activity (Fig xx). These data suggest that FADS1 and IQGAP2 are important regulators of NAD^+/NADH homeostasis in HCC cells. Furthermore, these genes are potential mediators of CTCF in the regulation of energy homeostasis in HCC cells. Consistent with energy depletion phenotypes, knockdown of FADS1 and IQGAP2 also markedly reduced cell growth, cell mobility and invasiveness HCC cells, similar to CTCF knockout cells (Figure 3.5–5 and Figure 3.5–6). These data suggested that FADS1 and IQGAP2 as putative CTCF-regulated genes are responsible for the regulating energy homeostasis, which may be involved in regulation of cell growth and metastasis.

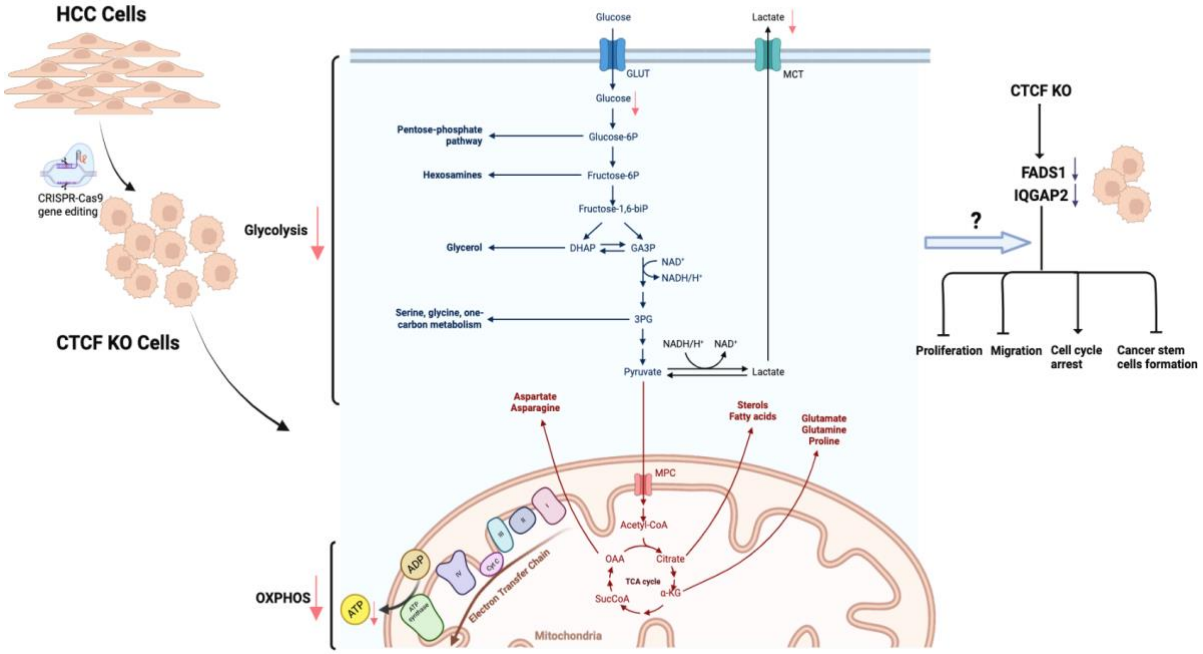

Figure 4–1 Schematic diagram showing the potential functional role of CTCF in regulating energy metabolisms in HCC cells. Figure generated using BioRender (https://biorender.com/).

Chapter Five: Summary and Future Plan

My study has provided significant insights into the pathogenesis of HCC at least in two major respects. Firstly, we provided experimental evidence that CTCF plays a critical role in HCC growth and metastasis, and revealed that it is a potential therapeutic target for the control of HCC growth and metastasis. Secondly, we made pivotal discovery that CTCF plays a novel functional role in the regulation of NAD^+/NADH homeostasis, glycolytic flux, and oxidative phosphorylation for energy production. We have further identified FADS1 and IQGAP2 as putative mediators of CTCF. Nevertheless, the definitive role of FADS1 and IQGPAP2 has not been established in this work. A more definitive understanding on the role of the two proteins in CTCF-regulatory process can be achieved by ectopic expression of each of the genes in a CTCF-null background, and determine if the expressed gene could rescue the reduction in NAD^+/NADH, glycolytic flux, oxidative phosphorylation, cell growth and metastatic phenotypes in the CTCF-knockout HCC cells. On the other hand, as a change in CTCF expression and 3D genome architecture has been found in tumors[262][273], it would be very important to determine if overexpression of CTCF leads to change in 3D genome architecture in HCC cells. Conformational analysis such as Hi-C analysis will be very useful for the further understanding of this aspect of alternations. On the other hand, my current work has demonstrated the function of CTCF in HCC pathogenesis. Accordingly, it will be important to explore the development of potential inhibitor of CTCF, which include

small molecule inhibitor, DNA decoy, and miRNA, etc, for restraining the activity of CTCF. These potential inhibitors can be tested in the cell and animal models established in Dr. Ko's lab. Our findings suggested that targeting CTCF may be a potential therapeutic strategy for HCC.

References

[1] H. Sung *et al.*, “Global Cancer Statistics 2020: GLOBOCAN Estimates of Incidence and Mortality Worldwide for 36 Cancers in 185 Countries,” *CA. Cancer J. Clin.*, vol. 71, no. 3, pp. 209–249, 2021.

[2] R. L. Siegel, K. D. Miller, H. E. Fuchs, and A. Jemal, “Cancer statistics, 2022,” *CA. Cancer J. Clin.*, vol. 72, no. 1, pp. 7–33, 2022.

[3] H.-J. Chen, M.-H. Hu, F.-G. Xu, H.-J. Xu, J.-J. She, and H.-P. Xia, “Understanding the inflammation-cancer transformation in the development of primary liver cancer,” *Hepatoma Res.*, vol. 4, no. 7, p. 29, 2018.

[4] A. Forner, M. Reig, and J. Bruix, “Hepatocellular carcinoma,” *Lancet*, vol. 391, no. 10127, pp. 1301–1314, 2018.

[5] C. Fitzmaurice *et al.*, “Global, regional, and national cancer incidence, mortality, years of life lost, years lived with disability, and disability-adjusted life-years for 32 cancer groups, 1990 to 2015: A Systematic Analysis for the Global Burden of Disease Study Global Burden ,” *JAMA Oncol.*, vol. 3, no. 4, pp. 524–548, 2017.

[6] J. S. Park, “Liver Lesions,” *Mt. Sinai Expert Guid. Hepatol.*, pp. 317–324, 2014.

[7] J. M. Llovet, R. Montal, D. Sia, and R. S. Finn, “Molecular therapies and precision medicine for hepatocellular carcinoma,” *Nat. Rev. Clin. Oncol.*, vol. 15, no. 10, pp. 599–616, 2018.

[8] F. X. Bosch, J. Ribes, M. Díaz, and R. Cléries, “Primary liver cancer: Worldwide incidence and trends,” *Gastroenterology*, vol. 127, no. 5, pp. S5–S16, 2004.

[9] S. F. Altekruse, K. A. Mcglynn, and M. E. Reichman, “Hepatocellular Carcinoma Incidence , Mortality , and Survival Trends in the United States From 1975 to 2005,” vol. 27, no. 9, pp. 1485–1491, 2009.

[10] H. B. El-Serag and A. C. Mason, “Rising incidence of hepatocellular carcinoma in the United States.,” *N. Engl. J. Med.*, vol. 340, no. 10, pp. 745–50, 1999.

[11] C. L. Lai, V. Ratziu, M. F. Yuen, and T. Poynard, “Viral hepatitis B,” *Lancet*, vol. 362, pp. 2089–2094, 2003.

[12] D. M. Parkin, F. Bray, J. Ferlay, and P. Pisani, “Global cancer statistics, 2002,” *CA Cancer J Clin*, vol. 55, pp. 74–108, 2005.

[13] R. Cotran, V. Kumar, S. Robbins, A. K. Abbas, J. C. Aster, and J. C. Aster, *Robbins and Cotran pathologic basis of disease*. 2015.

[14] Q. Zhang and G. Cao, “Genotypes, mutations, and viral load of hepatitis B virus and the risk of hepatocellular carcinoma,” *Hepatitis Monthly*, vol. 11, no. 2. pp. 86–91, 2011.

[15] W. H. Gerlich, “Medical Virology of Hepatitis B: how it began and where we are now,” *Virol. J.*, vol. 10, no. 1, p. 239, 2013.

[16] O. O. Ogunwobi *et al.*, “Mechanisms of hepatocellular carcinoma progression,” *World J. Gastroenterol.*, vol. 25, no. 19, pp. 2279–2293, 2019.

[17] M. Liu, L. Jiang, and X. Y. Guan, “The genetic and epigenetic alterations in human hepatocellular carcinoma: A recent update,” *Protein Cell*, vol. 5, no. 9, pp. 673–691, 2014.

[18] X. Y. Guan *et al.*, “Recurrent chromosome alterations in hepatocellular carcinoma detected by comparative hybridization,” *Genes Chromosom. Cancer*, vol. 29, no. 2, pp. 110–116, 2000.

[19] Y. Wang, M. C. Wu, J. S. T. Sham, W. Zhang, W. Q. Wu, and X. Y. Guan, “Prognostic significance of c-myc and AIB1 amplification in hepatocellular carcinoma: A broad survey using high-throughput tissue microarray,” *Cancer*, vol. 95, no. 11, pp. 2346–2352, 2002.

[20] N. F. Ma *et al.*, “Isolation and characterization of a novel oncogene, amplified in liver cancer 1, within a commonly amplified region at 1q21 in hepatocellular carcinoma,” *Hepatology*, vol. 47, no. 2, pp. 503–510, 2008.

[21] N. Iwata *et al.*, “Frequent hypermethylation of CpG islands and loss of expression of the 14-3-3 σ gene in human hepatocellular carcinoma,” *Oncogene*, vol. 19, no. 46, pp. 5298–5302, 2000.

[22] S. Nakayama, A. Sasaki, H. Mese, R. E. Alcalde, T. Tsuji, and T. Matsumura, “The E-cadherin gene is silenced by CpG methylation in human oral squamous cell carcinomas,” *Int. J. Cancer*, vol. 93, no. 5, pp. 667–673, 2001.

[23] A. Fujimoto *et al.*, “Whole-genome sequencing of liver cancers identifies etiological influences on mutation patterns and

recurrent mutations in chromatin regulators," *Nat. Genet.*, vol. 44, no. 7, pp. 760–764, 2012.

[24] C. Guichard *et al.*, "Integrated analysis of somatic mutations and focal copy-number changes identifies key genes and pathways in hepatocellular carcinoma," *Nat. Genet.*, vol. 44, no. 6, pp. 694–698, 2012.

[25] H. Yoshikawa *et al.*, "SOCS-1, a negative regulator of the JAK/STAT pathway, is silenced by methylation in human hepatocellular carcinoma and shows growth-suppression activity," *Nat. Genet.*, vol. 28, no. 1, pp. 29–35, 2001.

[26] T. Kouzarides, "Chromatin Modifications and Their Function," *Cell*, vol. 128, no. 4, pp. 693–705, 2007.

[27] X. Zheng *et al.*, "Histone acetyltransferase PCAF Up-regulated cell apoptosis in hepatocellular carcinoma via acetylating histone H4 and inactivating AKT signaling," *Mol. Cancer*, vol. 12, no. 1, pp. 1–11, 2013.

[28] M. Guttman and J. L. Rinn, "Modular regulatory principles of large non-coding RNAs," *Nature*, vol. 482, no. 7385, pp. 339–346, 2012.

[29] T. R. Mercer, M. E. Dinger, and J. S. Mattick, "Long non-coding RNAs: Insights into functions," *Nat. Rev. Genet.*, vol. 10, no. 3, pp. 155–159, 2009.

[30] F. Yang *et al.*, "Long noncoding RNA high expression in hepatocellular carcinoma facilitates tumor growth through enhancer of zeste homolog 2 in humans," *Hepatology*, vol. 54, no. 5, pp. 1679–1689, 2011.

[31] H. B. El-Serag and K. L. Rudolph, "Hepatocellular Carcinoma: Epidemiology and Molecular Carcinogenesis," *Gastroenterology*, vol. 132, no. 7, pp. 2557–2576, 2007.

[32] S. Kumar, C. J. Chan, and L. M. Coussens, "Inflammation and Cancer," *Encycl. Immunobiol.*, vol. 4, no. December, pp. 406–415, 2016.

[33] Y. Guo, Q. Zhao, L. Cao, and B. Zhao, "Hepatoprotective effect of Gan Kang Yuan against chronic liver injury induced by alcohol," *J. Ethnopharmacol.*, vol. 208, pp. 1–7, 2017.

[34] Z. C. Liu *et al.*, "Epidermal growth factor and tumor necrosis factor α cooperatively promote the motility of hepatocellular carcinoma cell lines via synergistic induction of fibronectin by NF-κB/p65," *Biochim. Biophys. Acta - Gen. Subj.*, vol. 1861, no. 11, pp. 2568–2582, 2017.

[35] Q. Zhang *et al.*, "Fatty acid oxidation contributes to IL-1β secretion in M2 macrophages and promotes macrophage-mediated

tumor cell migration," *Mol. Immunol.*, vol. 94, no. December 2017, pp. 27–35, 2018.

[36] H. Nakagawa *et al.*, "Serum IL-6 levels and the risk for hepatocarcinogenesis in chronic hepatitis C patients: An analysis based on gender differences," *Int. J. Cancer*, vol. 125, no. 10, pp. 2264–2269, 2009.

[37] J. Bayo *et al.*, "IL-8, GRO and MCP-1 produced by hepatocellular carcinoma microenvironment determine the migratory capacity of human bone marrow-derived mesenchymal stromal cells without affecting tumor aggressiveness," *Oncotarget*, vol. 8, no. 46, pp. 80235–80248, 2017.

[38] W. Guo *et al.*, *ICAM-1-related noncoding RNA in cancer stem cells maintains ICAM-1 expression in hepatocellular carcinoma*, vol. 22, no. 8. 2016.

[39] J. C. R. Wadkin *et al.*, "CD151 supports VCAM-1-mediated lymphocyte adhesion to liver endothelium and is upregulated in chronic liver disease and hepatocellular carcinoma," *Am. J. Physiol. - Gastrointest. Liver Physiol.*, vol. 313, no. 2, pp. G138–G149, 2017.

[40] Y. Y. Shao *et al.*, "High plasma interleukin-6 levels associated with poor prognosis of patients with advanced hepatocellular carcinoma," *Jpn. J. Clin. Oncol.*, vol. 47, no. 10, pp. 949–953, 2017.

[41] Q. He *et al.*, *IL-1β-Induced Elevation of Solute Carrier Family 7 Member 11 Promotes Hepatocellular Carcinoma Metastasis Through Up-regulating Programmed Death Ligand 1 and Colony-Stimulating Factor 1*, vol. 74, no. 6. 2021.

[42] B. Delire, P. Henriet, P. Lemoine, I. A. Leclercq, and P. Stärkel, "Chronic liver injury promotes hepatocarcinoma cell seeding and growth, associated with infiltration by macrophages," *Cancer Sci.*, vol. 109, no. 7, pp. 2141–2152, 2018.

[43] V. Hernandez-Gea, S. Toffanin, S. L. Friedman, and J. M. Llovet, "Role of the microenvironment in the pathogenesis and treatment of hepatocellular carcinoma," *Gastroenterology*, vol. 144, no. 3, pp. 512–527, 2013.

[44] S. Affo, L. X. Yu, and R. F. Schwabe, "The Role of Cancer-Associated Fibroblasts and Fibrosisin Liver Cancer," *Annu. Rev. Pathol. Mech. Dis.*, vol. 12, no. November 2016, pp. 153–186, 2017.

[45] Y. Lu, N. Lin, Z. Chen, and R. Xu, "Hypoxia-induced secretion of platelet-derived growth factor-BB by hepatocellular

carcinoma cells increases activated hepatic stellate cell proliferation, migration and expression of vascular endothelial growth factor-A," *Mol. Med. Rep.*, vol. 11, no. 1, pp. 691–697, 2015.

[46] H. L. Lee *et al.*, "Inflammatory cytokines and change of Th1/Th2 balance as prognostic indicators for hepatocellular carcinoma in patients treated with transarterial chemoembolization," *Sci. Rep.*, vol. 9, no. 1, pp. 4–11, 2019.

[47] T. Ding *et al.*, "High tumor-infiltrating macrophage density predicts poor prognosis in patients with primary hepatocellular carcinoma after resection," *Hum. Pathol.*, vol. 40, no. 3, pp. 381–389, 2009.

[48] N. Wang *et al.*, "Cancer stem cells in hepatocellular carcinoma: an overview and promising therapeutic strategies," *Ther. Adv. Med. Oncol.*, vol. 10, pp. 1–25, 2018.

[49] E. N. Proctor and D. M. Simeone, "Pancreatic cancer stem cells," *Adv. Cancer Stem Cell Biol.*, vol. 414, no. November, pp. 197–209, 2013.

[50] C. Hu *et al.*, "Analysis of ABCG2 expression and side population identifies intrinsic drug efflux in the HCC cell line MHCC-97L and its modulation by Akt signaling," *Carcinogenesis*, vol. 29, no. 12, pp. 2289–2297, 2008.

[51] Q. Lin *et al.*, "ZHX2 restricts hepatocellular carcinoma by suppressing stem cell-like traits through KDM2A-mediated H3K36 demethylation," *EBioMedicine*, vol. 53, 2020.

[52] N. B. Vu *et al.*, "Doxorubicin and 5-fluorouracil resistant hepatic cancer cells demonstrate stem-like properties," *Cytotechnology*, vol. 65, no. 4, pp. 491–503, 2013.

[53] T. B. Toh, J. J. Lim, L. Hooi, M. B. M. A. Rashid, and E. K. H. Chow, "Targeting Jak/Stat pathway as a therapeutic strategy against SP/CD44+ tumorigenic cells in Akt/β-catenin-driven hepatocellular carcinoma," *J. Hepatol.*, vol. 72, no. 1, pp. 104–118, 2020.

[54] J. U. Marquardt *et al.*, "Human hepatic cancer stem cells are characterized by common stemness traits and diverse oncogenic pathways," *Hepatology*, vol. 54, no. 3, pp. 1031–1042, 2011.

[55] T. Yamashita *et al.*, "EpCAM-Positive Hepatocellular Carcinoma Cells Are Tumor-Initiating Cells With Stem/Progenitor Cell Features," *Gastroenterology*, vol. 136, no. 3, pp. 1012-1024.e4, 2009.

[56] S. Ma *et al.*, “Identification and Characterization of Tumorigenic Liver Cancer Stem/Progenitor Cells,” *Gastroenterology*, vol. 132, no. 7, pp. 2542–2556, 2007.
[57] T. Kin *et al.*, “Article Self-Renewal and Tumor Initiation through STAT3-Mediated NANOG Regulation,” *Stem Cell*, vol. 9, no. 1, pp. 50–63, 2011.
[58] H. M. Kim *et al.*, “Increased CD13 expression reduces reactive oxygen species, promoting survival of liver cancer stem cells via an epithelial-mesenchymal transition-like phenomenon,” *Ann. Surg. Oncol.*, vol. 19, no. SUPPL. 3, 2012.
[59] Z. Zhu *et al.*, “Cancer stem/progenitor cells are highly enriched in CD133 +CD44+ population in hepatocellular carcinoma,” *Int. J. Cancer*, vol. 126, no. 9, pp. 2067–2078, 2010.
[60] K. Mima *et al.*, “CD44s regulates the TGF-β-mediated mesenchymal phenotype and is associated with poor prognosis in patients with hepatocellular carcinoma,” *Cancer Res.*, vol. 72, no. 13, pp. 3414–3423, 2012.
[61] Z. F. Yang *et al.*, “Significance of CD90+ Cancer Stem Cells in Human Liver Cancer,” *Cancer Cell*, vol. 13, no. 2, pp. 153–166, 2008.
[62] H. Clevers, “Wnt/β-Catenin Signaling in Development and Disease,” *Cell*, vol. 127, no. 3. pp. 469–480, Nov-2006.
[63] B. T. MacDonald, K. Tamai, and X. He, “Wnt/β-Catenin Signaling: Components, Mechanisms, and Diseases,” *Dev. Cell*, vol. 17, no. 1, pp. 9–26, 2009.
[64] P. Laurent-Puig and J. Zucman-Rossi, “Genetics of hepatocellular tumors,” *Oncogene*, vol. 25, no. 27, pp. 3778–3786, 2006.
[65] C. Niehrs, “The complex world of WNT receptor signalling,” *Nat. Rev. Mol. Cell Biol.*, vol. 13, no. 12, pp. 767–779, 2012.
[66] D. Levanon *et al.*, “Transcriptional repression by AML1 and LEF-1 is mediated by the TLE/Groucho corepressors,” *Proc. Natl. Acad. Sci. U. S. A.*, vol. 95, no. 20, pp. 11590–11595, 1998.
[67] S. Patel, A. Alam, R. Pant, and S. Chattopadhyay, “Wnt Signaling and Its Significance Within the Tumor Microenvironment: Novel Therapeutic Insights,” *Front. Immunol.*, vol. 10, no. December, 2019.
[68] L. Chen, Q. Zhou, J. Liu, and W. Zhang, “CTNNB1 Alternation Is a Potential Biomarker for Immunotherapy Prognosis in Patients

With Hepatocellular Carcinoma," *Frontiers in Immunology*, vol. 12. 2021.

[69] A. De La Coste *et al.*, "Somatic mutations of the β-catenin gene are frequent in mouse and human hepatocellular carcinomas," *Proc. Natl. Acad. Sci. U. S. A.*, vol. 95, no. 15, pp. 8847–8851, 1998.

[70] Y. Miyoshi *et al.*, "Activation of the β-catenin gene in primary hepatocellular carcinomas by somatic alterations involving exon 3," *Cancer Res.*, vol. 58, no. 12, pp. 2524–2527, 1998.

[71] S. Abitbol *et al.*, "AXIN deficiency in human and mouse hepatocytes induces hepatocellular carcinoma in the absence of β-catenin activation," *J. Hepatol.*, vol. 68, no. 6, pp. 1203–1213, 2018.

[72] K. C. Ban, H. Singh, R. Krishnan, and H. F. Seow, "GSK-3β phosphorylation and alteration of β-catenin in hepatocellular carcinoma," *Cancer Lett.*, vol. 199, no. 2, pp. 201–208, 2003.

[73] Y. Wei, J. T. Van Nhieu, S. Prigent, P. Srivatanakul, P. Tiollais, and M. A. Buendia, "Altered expression of E-cadherin in hepatocellular carcinoma: Correlations with genetic alterations, β-catenin expression, and clinical features," *Hepatology*, vol. 36, no. 3, pp. 692–701, 2002.

[74] S. xian Yuan *et al.*, "Long noncoding RNA DANCR increases stemness features of hepatocellular carcinoma by derepression of CTNNB1," *Hepatology*, vol. 63, no. 2, pp. 499–511, 2016.

[75] B. Liang *et al.*, "TBX3 functions as a tumor suppressor downstream of activated CTNNB1 mutants during hepatocarcinogenesis," *J. Hepatol.*, vol. 75, no. 1, pp. 120–131, 2021.

[76] A. de La Coste *et al.*, "Somatic mutations of the beta-catenin gene are frequent in mouse and human hepatocellular carcinomas.," *Proc. Natl. Acad. Sci. U. S. A.*, vol. 95, no. 15, pp. 8847–51, 1998.

[77] F. Kawai-Kitahata *et al.*, "Comprehensive analyses of mutations and hepatitis B virus integration in hepatocellular carcinoma with clinicopathological features," *J. Gastroenterol.*, vol. 51, no. 5, pp. 473–486, 2016.

[78] S. Lee, M. J. Lee, J. Zhang, G. R. Yu, and D. G. Kim, "C-terminal-truncated HBV X promotes hepato-oncogenesis through inhibition of tumor-suppressive β-catenin/BAMBI signaling," *Exp. Mol. Med.*, vol. 48, no. 12, pp. e275-10, 2016.

[79] H. Huang *et al.*, “β-Catenin mutations are frequent in human hepatocellular carcinomas associated with hepatitis C virus infection,” *Am. J. Pathol.*, vol. 155, no. 6, pp. 1795–1801, 1999.

[80] Y. Yin, F. Li, S. Li, J. Cai, J. Shi, and Y. Jiang, “TLR4 Influences Hepatitis B Virus Related Hepatocellular Carcinoma by Regulating the Wnt/β-Catenin Pathway,” *Cell. Physiol. Biochem.*, vol. 42, no. 2, pp. 469–479, 2017.

[81] S. Wang *et al.*, “Nonalcoholic fatty liver disease induced by noncanonical Wnt and its rescue by Wnt3a,” *FASEB J.*, vol. 29, no. 8, pp. 3436–3445, 2015.

[82] J. M. Kyriakis and J. Avruch, “Mammalian MAPK signal transduction pathways activated by stress and inflammation: A 10-year update,” *Physiol. Rev.*, vol. 92, no. 2, pp. 689–737, 2012.

[83] U. Degirmenci, M. Wang, and J. Hu, “Targeting Aberrant RAS/RAF/MEK/ERK Signaling for Cancer Therapy,” *Cells*, vol. 9, no. 1, pp. 1–34, 2020.

[84] L. Li, G. D. Zhao, Z. Shi, L. L. Qi, L. Y. Zhou, and Z. X. Fu, “The Ras/Raf/MEK/ERK signaling pathway and its role in the occurrence and development of HCC (Review),” *Oncology Letters*, vol. 12, no. 5. pp. 3045–3050, 2016.

[85] Y. Keshet and R. Seger, *The MAP kinase signaling cascades: a system of hundreds of components regulates a diverse array of physiological functions.*, vol. 661. 2010.

[86] M. Karin and L. Chang, “Mammalian MAP kinase signaling cascades.,” *Nature*, vol. 410, no. 6824, pp. 37–40, 2001.

[87] J. M. Kyriakis and J. Avruch, “Mammalian mitogen-activated protein kinase signal transduction pathways activated by stress and inflammation,” *Physiol. Rev.*, vol. 81, no. 2, pp. 807–869, 2001.

[88] G. L. Johnson and R. Lapadat, “Mitogen-activated protein kinase pathways mediated by ERK, JNK, and p38 protein kinases,” *Science (80-.).*, vol. 298, no. 5600, pp. 1911–1912, 2002.

[89] Z. Xia, M. Dickens, J. Raingeaud, R. J. Davis, and M. E. Greenberg, “Opposing effects of ERK and JNK-p38 MAP kinases on apoptosis,” *Science (80-.).*, vol. 270, no. 5240, pp. 1326–1331, 1995.

[90] L. Chang and M. Karin, “Mammalian MAP kinase signalling cascades,” *Nature*, vol. 410, no. 6824, pp. 37–40, 2001.

[91] M. Höpfner, D. Schuppan, and H. Scherübl, “Growth factor receptors and related signalling pathways .pdf,” *World J. Gastroenterol.*, vol. 14, no. 1, pp. 1–14, 2008.
[92] M. A. Avila, C. Berasain, B. Sangro, and J. Prieto, “New therapies for hepatocellular carcinoma,” *Oncogene*, vol. 25, no. 27, pp. 3866–3884, 2006.
[93] S. G. Hymowitz and S. Malek, “Targeting the MAPK Pathway in RAS Mutant Cancers,” *Cold Spring Harb. Perspect. Med.*, vol. 8, no. 11, pp. 1–16, 2018.
[94] Z. Zhang, X. Zhou, H. Shen, and D. Wang, “Phosphorylated ERK is a potential predictor of sensitivity to sorafenib when treating hepatocellular carcinoma: Evidence from an in vitro study,” *BMC Med.*, vol. 7, pp. 1–12, 2009.
[95] J. Downward, “Targeting RAS signalling pathways in cancer therapy,” *Nat. Rev. Cancer*, vol. 3, no. 1, pp. 11–22, 2003.
[96] J. Downward, “Targeting RAS signalling pathways in cancer therapy,” *Nat. Rev. Cancer*, vol. 3, no. 1, pp. 11–22, 2003.
[97] Y. H. Hwang *et al.*, “Over-expression of c-raf-1 proto-oncogene in liver cirrhosis and hepatocellular carcinoma,” *Hepatol. Res.*, vol. 29, no. 2, pp. 113–121, 2004.
[98] P. J. Roberts and C. J. Der, “Targeting the Raf-MEK-ERK mitogen-activated protein kinase cascade for the treatment of cancer,” *Oncogene*, vol. 26, no. 22, pp. 3291–3310, 2007.
[99] R. Zhang *et al.*, “The collagen triple helix repeat containing 1 facilitates hepatitis B virus-associated hepatocellular carcinoma progression by regulating multiple cellular factors and signal cascades,” *Mol. Carcinog.*, vol. 54, no. 12, pp. 1554–1566, 2015.
[100] H. Nagata *et al.*, “Inhibition of c-Jun NH2-terminal kinase switches Smad3 signaling from oncogenesis to tumor-suppression in rat hepatocellular carcinoma,” *Hepatology*, vol. 49, no. 6, pp. 1944–1953, 2009.
[101] H. Y. Wu, X. Q. Tang, H. Liu, X. F. Mao, and Y. X. Wang, “Both classic Gs-cAMP/PKA/CREB and alternative Gs-cAMP/PKA/p38β/CREB signal pathways mediate exenatide-stimulated expression of M2 microglial markers,” *J. Neuroimmunol.*, vol. 316, no. December, pp. 17–22, 2018.
[102] A. G. Bader, S. Kang, L. Zhao, and P. K. Vogt, “Oncogenic PI3K deregulates transcription and translation,” *Nat. Rev. Cancer*, vol. 5, no. 12, pp. 921–929, 2005.

[103] I. Vivanco and C. L. Sawyers, “The phosphatidylinositol 3-kinase-AKT pathway in humancancer,” *Nat. Rev. Cancer*, vol. 2, no. 7, pp. 489–501, 2002.
[104] Q. Zhou, V. W. Y. Lui, and W. Yeo, “Targeting the PI3K/Akt/mTOR pathway in hepatocellular carcinoma,” *Futur. Oncol.*, vol. 7, no. 10, pp. 1149–1167, 2011.
[105] J. A. Engelman, “Targeting PI3K signalling in cancer: Opportunities, challenges and limitations,” *Nat. Rev. Cancer*, vol. 9, no. 8, pp. 550–562, 2009.
[106] J. S. Chen *et al.*, “Involvement of PI3K/PTEN/AKT/mTOR pathway in invasion and metastasis in hepatocellular carcinoma: Association with MMP-9,” *Hepatol. Res.*, vol. 39, no. 2, pp. 177–186, 2009.
[107] V. Stambolic *et al.*, “Negative regulation of PKB/Akt-dependent cell survival by the tumor suppressor PTEN,” *Cell*, vol. 95, no. 1, pp. 29–39, 1998.
[108] H. Sun *et al.*, “PTEN modulates cell cycle progression and cell survival by regulating phosphatidylinositol 3,4,5,-trisphosphate and Akt/protein kinase B signaling pathway,” *Proc. Natl. Acad. Sci.*, vol. 96, no. 11, pp. 6199–6204, 1999.
[109] W. Sui *et al.*, “Antitumor effect of a selective COX-2 inhibitor, celecoxib, may be attributed to angiogenesis inhibition through modulating the PTEN/PI3K/Akt/HIF-1 pathway in an H22 murine hepatocarcinoma model,” *Oncol. Rep.*, vol. 31, no. 5, pp. 2252–2260, 2014.
[110] Y. J. Zhu, B. Zheng, H. Y. Wang, and L. Chen, “New knowledge of the mechanisms of sorafenib resistance in liver cancer,” *Acta Pharmacol. Sin.*, vol. 38, no. 5, pp. 614–622, 2017.
[111] X. jun Dai *et al.*, “Ilexgenin A exerts anti-inflammation and anti-angiogenesis effects through inhibition of STAT3 and PI3K pathways and exhibits synergistic effects with Sorafenib on hepatoma growth,” *Toxicol. Appl. Pharmacol.*, vol. 315, pp. 90–101, 2017.
[112] H. Chen, Y. Huang, J. Huang, L. Lin, and G. Wei, “Gigantol attenuates the proliferation of human liver cancer HepG2 cells through the PI3K/Akt/NF-κB signaling pathway,” *Oncol. Rep.*, vol. 37, no. 2, pp. 865–870, 2017.
[113] L. Zhao *et al.*, “A blockade of PD-L1 produced antitumor and antimetastatic effects in an orthotopic mouse pancreatic cancer model via the PI3K/Akt/mTOR signaling pathway,” *Onco. Targets. Ther.*, vol. 10, pp. 2115–2126, 2017.

[114] X. Luo *et al.*, “The fatty acid receptor CD36 promotes HCC progression through activating Src/PI3K/AKT axis-dependent aerobic glycolysis,” *Cell Death Dis.*, vol. 12, no. 4, 2021.
[115] G. Fang *et al.*, “Inhibition of GSK-3β activity suppresses HCC malignant phenotype by inhibiting glycolysis via activating AMPK/mTOR signaling,” *Cancer Lett.*, vol. 463, no. August, pp. 11–26, 2019.
[116] E. J. Sun, M. Wankell, P. Palamuthusingam, C. McFarlane, and L. Hebbard, “Targeting the pi3k/akt/mtor pathway in hepatocellular carcinoma,” *Biomedicines*, vol. 9, no. 11, pp. 1–20, 2021.
[117] J. E. Darnell, I. M. Kerr, and G. R. Stark, “Jak-STAT Pathways and Transcriptional Activation in Response to IFNs and Other Extracellular Signaling Proteins Published by: American Association for the Advancement of Science Stable URL: http://www.jstor.org/stable/2884122,” *Adv. Sci.*, vol. 264, no. 5164, pp. 1415–1421, 1994.
[118] J. G. Williams, “STAT signalling in cell proliferation and in development,” *Curr. Opin. Genet. Dev.*, vol. 10, no. 5, pp. 503–507, 2000.
[119] J. N. Ihle *et al.*, “Signaling by the cytokine receptor superfamily: JAKs and STATs,” *Trends Biochem. Sci.*, vol. 19, no. 5, pp. 222–227, 1994.
[120] R. Morris, N. J. Kershaw, and J. J. Babon, “The molecular details of cytokine signaling via the JAK/STAT pathway,” *Protein Sci.*, vol. 27, no. 12, pp. 1984–2009, 2018.
[121] A. Basu *et al.*, “Microarray analyses and molecular profiling of Stat3 signaling pathway induced by hepatitis C virus core protein in human hepatocytes,” *Virology*, vol. 349, no. 2, pp. 347–358, 2006.
[122] B. Wang *et al.*, “STAT3 aggravates TGF-β1-induced hepatic epithelial-to-mesenchymal transition and migration,” *Biomed. Pharmacother.*, vol. 98, no. July 2017, pp. 214–221, 2018.
[123] D. F. Calvisi *et al.*, “Ubiquitous Activation of Ras and Jak/Stat Pathways in Human HCC,” *Gastroenterology*, vol. 130, no. 4, pp. 1117–1128, 2006.
[124] N. Raulf *et al.*, “Annexin A1 regulates EGFR activity and alters EGFR-containing tumour-derived exosomes in head and neck cancers,” *Eur. J. Cancer*, vol. 102, pp. 52–68, 2018.
[125] T. D. Barber, B. Vogelstein, K. W. Kinzler, and V. E. Velculescu, “ Somatic Mutations of EGFR in Colorectal Cancers

and Glioblastomas ," *N. Engl. J. Med.*, vol. 351, no. 27, pp. 2883–2883, 2004.

[126] R. A. Okimoto *et al.*, "new england journal," pp. 2129–2139, 2004.

[127] X. Tan, P. F. Lambert, A. C. Rapraeger, and R. A. Anderson, "Stress-Induced EGFR Trafficking: Mechanisms, Functions, and Therapeutic Implications," *Trends Cell Biol.*, vol. 26, no. 5, pp. 352–366, 2016.

[128] B. Singh, G. Carpenter, and R. J. Coffey, "EGF receptor ligands: Recent advances [version 1; referees: 3 approved]," *F1000Research*, vol. 5, no. 0, pp. 1–11, 2016.

[129] K. Komposch and M. Sibilia, "EGFR signaling in liver diseases," *Int. J. Mol. Sci.*, vol. 17, no. 1, 2016.

[130] P. Wee and Z. Wang, "Epidermal growth factor receptor cell proliferation signaling pathways," *Cancers (Basel).*, vol. 9, no. 5, pp. 1–45, 2017.

[131] Y. Ito *et al.*, "Expression and clinical significance of erb-B receptor family in hepatocellular carcinoma," *Br. J. Cancer*, vol. 84, no. 10, pp. 1377–1383, 2001.

[132] Z. Ezzoukhry *et al.*, "EGFR activation is a potential determinant of primary resistance of hepatocellular carcinoma cells to sorafenib," *Int. J. Cancer*, vol. 131, no. 12, pp. 2961–2969, 2012.

[133] M. J. Blivet-Van Eggelpoël *et al.*, "Epidermal growth factor receptor and HER-3 restrict cell response to sorafenib in hepatocellular carcinoma cells," *J. Hepatol.*, vol. 57, no. 1, pp. 108–115, 2012.

[134] N. Sueangoen, A. Tantiwetrueangdet, and R. Panvichian, "HCC-derived EGFR mutants are functioning, EGF-dependent, and erlotinib-resistant," *Cell Biosci.*, vol. 10, no. 1, pp. 1–15, 2020.

[135] M. Höpfner, A. P. Sutter, A. Huether, D. Schuppan, M. Zeitz, and H. Scherübl, "Targeting the epidermal growth factor receptor by gefitinib for treatment of hepatocellular carcinoma," *J. Hepatol.*, vol. 41, no. 6, pp. 1008–1016, 2004.

[136] E. Schiffer *et al.*, "Gefitinib, an EGFR inhibitor, prevents hepatocellular carcinoma development in the rat liver with cirrhosis," *Hepatology*, vol. 41, no. 2, pp. 307–314, 2005.

[137] R. A. Snyder and J. N. Vauthey, "Hepatobiliary cancers," *MD Anderson Surg. Oncol. Handbook, Sixth Ed.*, pp. 357–397, 2018.

[138] S. Pascual, I. Herrera, and J. Irurzun, “New advances in hepatocellular carcinoma,” *World J. Hepatol.*, vol. 8, no. 9, pp. 421–438, 2016.
[139] R. C. Jha *et al.*, “LI-RADS categorization of benign and likely benign findings in patients at risk of hepatocellular carcinoma: A pictorial atlas,” *American Journal of Roentgenology*, vol. 203, no. 1. 2014.
[140] M. Soresi *et al.*, “Usefulness of alpha-fetoprotein in the diagnosis of hepatocellular carcinoma,” *Anticancer Res.*, vol. 23, no. 2 C, pp. 1747–1753, 2003.
[141] S. H. Yim and Y. J. Chung, “An overview of biomarkers and molecular signatures in HCC,” *Cancers (Basel).*, vol. 2, no. 2, pp. 809–823, 2010.
[142] R. F. Schwabe and T. F. Greten, “Gut microbiome in HCC – Mechanisms, diagnosis and therapy,” *J. Hepatol.*, vol. 72, no. 2, pp. 230–238, 2020.
[143] R. Loomba *et al.*, “Gut Microbiome-Based Metagenomic Signature for Non-invasive Detection of Advanced Fibrosis in Human Nonalcoholic Fatty Liver Disease,” *Cell Metab.*, vol. 25, no. 5, pp. 1054-1062.e5, 2017.
[144] Q. Liu *et al.*, “Alteration in gut microbiota associated with hepatitis B and non-hepatitis virus related hepatocellular carcinoma,” *Gut Pathog.*, vol. 11, no. 1, pp. 1–13, 2019.
[145] S. Ryder, “Guidelines for the diagnosis and treatment of hepatocellular carcinoma (HCC) in adults,” *Gut*, vol. 52, no. Suppl 3, pp. iii1–iii8, 2003.
[146] C. Liu, K. Chen, and P. Chen, “Treatment of Liver Cancer,” vol. 315, no. 1, p. 934829, 2015.
[147] A. Vogel *et al.*, “Updated treatment recommendations for hepatocellular carcinoma (HCC) from the ESMO Clinical Practice Guidelines,” *Ann. Oncol.*, vol. 32, no. 6, pp. 801–805, 2021.
[148] J. M. Llovet *et al.*, “Sorafenib in Advanced Hepatocellular Carcinoma,” *N. Engl. J. Med.*, vol. 359, no. 4, pp. 378–390, 2008.
[149] X. Yang†, D. Wang†, J. Lin, X. Yang, and H. Zhao, “Atezolizumab plus bevacizumab for unresectable hepatocellular carcinoma,” *Lancet Oncol.*, vol. 21, no. 9, p. e412, 2020.
[150] D. Editor, “Metastatic occult breast carcinoma to gallbladder initially presenting as acute cholecystitis EGFR mutational landscape in nasopharyngeal carcinoma Management of multifocal HER-2 positive and hormone receptor negative microinvasive (T1mic) breast carcin,” vol. 26, no. 2, pp. 634–638, 2021.

[151] B. I. Rini *et al.*, “Atezolizumab plus bevacizumab versus sunitinib in patients with previously untreated metastatic renal cell carcinoma (IMmotion151): a multicentre, open-label, phase 3, randomised controlled trial,” *Lancet*, vol. 393, no. 10189, pp. 2404–2415, 2019.

[152] A. X. Zhu *et al.*, “Ramucirumab after sorafenib in patients with advanced hepatocellular carcinoma and increased α-fetoprotein concentrations (REACH-2): a randomised, double-blind, placebo-controlled, phase 3 trial,” *Lancet Oncol.*, vol. 20, no. 2, pp. 282–296, 2019.

[153] G. K. Abou-Alfa *et al.*, “Cabozantinib in Patients with Advanced and Progressing Hepatocellular Carcinoma,” *N. Engl. J. Med.*, vol. 379, no. 1, pp. 54–63, 2018.

[154] J. Bruix *et al.*, “Regorafenib for patients with hepatocellular carcinoma who progressed on sorafenib treatment (RESORCE): a randomised, double-blind, placebo-controlled, phase 3 trial,” *Lancet*, vol. 389, no. 10064, pp. 56–66, 2017.

[155] M. Kudo *et al.*, “Lenvatinib versus sorafenib in first-line treatment of patients with unresectable hepatocellular carcinoma: a randomised phase 3 non-inferiority trial,” *Lancet*, vol. 391, no. 10126, pp. 1163–1173, 2018.

[156] R. Dhanasekaran, S. K. Venkatesh, M. S. Torbenson, and L. R. Roberts, “Clinical implications of basic research in hepatocellular carcinoma,” *Journal of Hepatology*, vol. 64, no. 3. pp. 736–745, 2016.

[157] A. Cucchetti *et al.*, “Anatomic versus nonanatomic resection in cirrhotic patients with early hepatocellular carcinoma,” *Surg. (United States)*, vol. 155, no. 3, pp. 512–521, 2014.

[158] R. Ohlsson, R. Renkawitz, and V. Lobanenkov, “CTCF is a uniquely versatile transcription regulator linked to epigenetics and disease,” *TRENDS Genet.*, 2001.

[159] G. N. Filippova *et al.*, “An exceptionally conserved transcriptional repressor, CTCF, employs different combinations of zinc fingers to bind diverged promoter sequences of avian and mammalian c-myc oncogenes.,” *Mol. Cell. Biol.*, vol. 16, no. 6, pp. 2802–13, 1996.

[160] T. H. Kim *et al.*, “Analysis of the Vertebrate Insulator Protein CTCF-Binding Sites in the Human Genome,” *Cell*, vol. 128, no. 6, pp. 1231–1245, 2007.

[161] J. E. Phillips and V. G. Corces, “CTCF: Master Weaver of the Genome,” *Cell*, vol. 137, no. 7, pp. 1194–1211, 2009.

[162] E. Splinter *et al.*, “CTCF mediates long-range chromatin looping and local histone modification in the??-globin locus,” *Genes Dev.*, vol. 20, no. 17, pp. 2349–2354, 2006.

[163] and D. M. Y. Adam Moser, Kevin Range and A. Manuscript, “基因的改变NIH Public Access,” *Bone*, vol. 23, no. 1, pp. 1–7, 2008.

[164] A. A. Vostrov and W. W. Quitschke, “The zinc finger protein CTCF binds to the APBβ domain of the amyloid β-protein precursor promoter: Evidence for a role in transcriptional activation,” *J. Biol. Chem.*, vol. 272, no. 52, pp. 33353–33359, 1997.

[165] M. P. Murphy and H. Levine, “Alzheimer’s disease and the amyloid-β peptide,” *J. Alzheimer’s Dis.*, vol. 19, no. 1, pp. 311–323, 2010.

[166] T. Burton, B. Liang, A. Dibrov, and F. Amara, “Transforming growth factor-β-induced transcription of the Alzheimer β-amyloid precursor protein gene involves interaction between the CTCF-complex and Smads,” *Biochem. Biophys. Res. Commun.*, vol. 295, no. 3, pp. 713–723, 2002.

[167] A. A. Vostrov and W. W. Quitschke, “The Zinc Finger Protein CTCF Binds to the APBβ Domain of the Amyloid β-Protein Precursor Promoter: EVIDENCE FOR A ROLE IN TRANSCRIPTIONAL ACTIVATION,” *J. Biol. Chem.*, vol. 272, no. 52, pp. 33353–33359, 1997.

[168] E. M. Klenova *et al.*, “CTCF, a conserved nuclear factor required for optimal transcriptional activity of the chicken c-myc gene, is an 11-Zn-finger protein differentially expressed in multiple forms.,” *Mol. Cell. Biol.*, vol. 13, no. 12, pp. 7612–24, 1993.

[169] V. V Lobanenkov *et al.*, “A novel sequence-specific DNA binding protein which interacts with three regularly spaced direct repeats of the CCCTC-motif in the 5’-flanking sequence of the chicken c-myc gene.,” *Oncogene*, vol. 5, no. 12, pp. 1743–53, 1990.

[170] M. Lutz, L. Burke, G. Barreto, and F. Goeman, “Transcriptional repression by the insulator protein CTCF involves histone deacetylases,” *Nucleic acids*, 2000.

[171] A. Hurtado, K. A. Holmes, C. S. Ross-Innes, D. Schmidt, and J. S. Carroll, “FOXA1 is a key determinant of estrogen receptor function and endocrine response,” *Nat. Genet.*, vol. 43, no. 1, pp. 27–33, 2011.

[172] D. Wu, T. Li, Z. Lu, W. Dai, M. Xu, and O. Lu, “Effect of CTCF-binding motif on regulation of PAX6 transcription,” *Investig. Ophthalmol. Vis. Sci.*, vol. 47, no. 6, pp. 2422–2429, 2006.

[173] A. Y. Lai *et al.*, “DNA methylation prevents CTCF-mediated silencing of the oncogene BCL6 in B cell lymphomas,” *J. Exp. Med.*, vol. 207, no. 9, pp. 1939–1950, 2010.

[174] S. Renaud, D. Loukinov, F. T. Bosman, V. Lobanenkov, and J. Benhattar, “CTCF binds the proximal exonic region of hTERT and inhibits its transcription,” *Nucleic Acids Res.*, vol. 33, no. 21, pp. 6850–6860, 2005.

[175] A. C. Bell, A. G. West, and G. Felsenfeld, “The protein CTCF is required for the enhancer blocking activity of vertebrate insulators,” *Cell*, vol. 98, no. 3, pp. 387–396, 1999.

[176] A. T. Hark, C. J. Schoenherr, D. J. Katz, R. S. Ingram, J. M. Levorse, and S. M. Tilghman, “CTCF mediates methylation-sensitive enhancer-blocking activity at the H19/Igf2 locus.,” *Nature*, vol. 405, no. 6785, pp. 486–489, 2000.

[177] P. E. Szabó, S.-H. E. Tang, F. J. Silva, W. M. K. Tsark, and J. R. Mann, “ Role of CTCF Binding Sites in the Igf2/H19 Imprinting Control Region ,” *Mol. Cell. Biol.*, vol. 24, no. 11, pp. 4791–4800, 2004.

[178] J. Huang, I. L. Brito, J. Villén, S. P. Gygi, A. Amon, and D. Moazed, “Inhibition of homologous recombination by a cohesin-associated clamp complex recruited to the rDNA recombination enhancer,” *Genes Dev.*, vol. 20, no. 20, pp. 2887–2901, 2006.

[179] “American Association for the Advancement of Science,” *Nature*, vol. 60, no. 1560, pp. 515–516, 1899.

[180] V. Parelho, S. Hadjur, M. Spivakov, M. Leleu, and S. Sauer, “Cohesins functionally associate with CTCF on mammalian chromosome arms,” *Cell*, 2008.

[181] K. S. Wendt *et al.*, “Cohesin mediates transcriptional insulation by CCCTC-binding factor,” *Nature*, vol. 451, no. 7180, pp. 796–801, 2008.

[182] W. Chao, W. Chao, K. D. Huynh, and R. J. Spencer, “CTCF , a Candidate Trans -Acting Factor for X-Inactivation Choice,” vol. 345, no. 2002, 2014.

[183] J. T. Kung *et al.*, “Locus-specific targeting to the X-chromosome revealed by the RNA interactome of CTCF recruited in a locus-specific manner and implicates CTCF-RNA interactions in long-range chromosomal interactions,” *Mol. Cell*, vol. 57, no. 2, pp. 361–375, 2015.

[184] E. Aeby *et al.*, "Decapping enzyme 1A breaks X-chromosome symmetry by controlling Tsix elongation and RNA turnover," *Nature Cell Biology*, vol. 22, no. 9. pp. 1116–1129, 2020.
[185] A. L. Valton and J. Dekker, "TAD disruption as oncogenic driver," *Curr. Opin. Genet. Dev.*, vol. 36, pp. 34–40, 2016.
[186] Y. Qiu and S. Huang, "CTCF-mediated genome organization and leukemogenesis," *Leukemia*, vol. 34, no. 9, pp. 2295–2304, 2020.
[187] P. C. Taberlay *et al.*, "Three-dimensional disorganization of the cancer genome occurs coincident with long-range genetic and epigenetic alterations," *Genome Res.*, vol. 26, no. 6, pp. 719–731, 2016.
[188] J. R. Dixon *et al.*, "Topological domains in mammalian genomes identified by analysis of chromatin interactions," *Nature*, vol. 485, no. 7398, pp. 376–380, 2012.
[189] R. G. Arzate-Mejía, F. Recillas-Targa, and V. G. Corces, "Developing in 3D: the role of CTCF in cell differentiation," *Development*, vol. 145, no. 6, 2018.
[190] Y. Li *et al.*, "The structural basis for cohesin–CTCF-anchored loops," *Nature*, vol. 578, no. 7795, pp. 472–476, 2020.
[191] J. Dekker and L. Mirny, "The 3D Genome as Moderator of Chromosomal Communication," *Cell*, vol. 164, no. 6, pp. 1110–1121, 2016.
[192] G. Wutz *et al.*, "Topologically associating domains and chromatin loops depend on cohesin and are regulated by CTCF, WAPL, and PDS5 proteins," *EMBO J.*, vol. 36, no. 24, pp. 3573–3599, 2017.
[193] S. S. P. Rao *et al.*, "Cohesin Loss Eliminates All Loop Domains," *Cell*, vol. 171, no. 2, pp. 305-320.e24, 2017.
[194] F. Bastaki *et al.*, "Identification of a novel CTCF mutation responsible for syndromic intellectual disability – A case report," *BMC Med. Genet.*, vol. 18, no. 1, pp. 1–6, 2017.
[195] K. Higashimoto *et al.*, "Hypomethylation of a centromeric block of ICR1 is sufficient to cause Silver-Russell syndrome," *J. Med. Genet.*, vol. 58, no. 6, pp. 422–425, 2021.
[196] S. Berland *et al.*, "Evidence for anticipation in Beckwith-Wiedemann syndrome," *Eur. J. Hum. Genet.*, vol. 21, no. 12, pp. 1344–1348, 2013.
[197] L. Zhao *et al.*, "CTCF promotes epithelial ovarian cancer metastasis by broadly controlling the expression of metastasis-associated genes," *Oncotarget*, vol. 8, no. 37, pp. 62217–62230, 2017.

[198] J. C. Hillman *et al.*, “BORIS expression in ovarian cancer precursor cells alters the CTCF cistrome and enhances invasiveness through GALNT14,” *Mol. Cancer Res.*, vol. 17, no. 10, pp. 2051–2062, 2019.

[199] D. Takai, F. Gonzales, and Y. Tsai, “Large scale mapping of methylcytosines in CTCF-binding sites in the human H19 promoter and aberrant hypomethylation in human bladder cancer,” *Hum. Mol.*, 2001.

[200] T. Kondo, T. Oka, H. Sato, Y. Shinnou, and K. Washio, “Accumulation of aberrant CpG hypermethylation by Helicobacter pylori infection promotes development,” *Int. J. Oncol.*, vol. 35, pp. 547–557, 2009.

[201] A. Woloszynska-Read *et al.*, “Coordinated cancer germline antigen promoter and global DNA hypomethylation in ovarian cancer: Association with the BORIS/CTCF expression ratio and advanced stage,” *Clin. Cancer Res.*, vol. 17, no. 8, pp. 2170–2180, 2011.

[202] J. Hubertus *et al.*, “Selective Methylation of CpGs at Regulatory Binding Sites Controls NNAT Expression in Wilms Tumors,” *PLoS One*, vol. 8, no. 6, 2013.

[203] R. A. Irizarry *et al.*, “The human colon cancer methylome shows similar hypo- and hypermethylation at conserved tissue-specific CpG island shores,” *Nat. Genet.*, vol. 41, no. 2, pp. 178–186, 2009.

[204] J. Liu *et al.*, “Identification and validation of colorectal neoplasia-specific methylation biomarkers based on CTCF-binding sites,” *Oncotarget*, vol. 8, no. 69, pp. 114183–114194, 2017.

[205] T. Kawakami, C. Zhang, Y. Okada, and K. Okamoto, “Erasure of methylation imprint at the promoter and CTCF-binding site upstream of H19 in human testicular germ cell tumors of adolescents indicate their fetal germ cell origin,” *Oncogene*, vol. 25, no. 23, pp. 3225–3236, 2006.

[206] S. Sievers *et al.*, “IGF2/H19 imprinting analysis of human germ cell tumors (GCTs) using the methylation-sensitive single-nucleotide primer extension method reflects the origin of GCTs in different stages of primordial germ cell development,” *Genes Chromosom. Cancer*, vol. 44, no. 3, pp. 256–264, 2005.

[207] D. Höflmayer *et al.*, “Expression of CCCTC-binding factor (CTCF) is linked to poor prognosis in prostate cancer,” *Mol. Oncol.*, vol. 14, no. 1, pp. 129–138, 2020.

[208] Y. Guo, A. A. Perez, D. J. Hazelett, G. A. Coetzee, S. K. Rhie, and P. J. Farnham, “CRISPR-mediated deletion of prostate

cancer risk-associated CTCF loop anchors identifies repressive chromatin loops," *Genome Biol.*, vol. 19, no. 1, pp. 1–17, 2018.

[209] C. J. Walker *et al.*, "Patterns of CTCF and ZFHX3 mutation and associated outcomes in endometrial cancer," *J. Natl. Cancer Inst.*, vol. 107, no. 11, pp. 1–8, 2015.

[210] H. Cui, E. Niemitz, J. Ravenel, and P. Onyango, "Loss of imprinting of insulin-like growth factor-II in Wilms' tumor commonly involves altered methylation but not mutations of CTCF or its binding site," *Cancer Res.*, 2001.

[211] L. Sun *et al.*, "Gastric cancer mesenchymal stem cells regulate PD-L1-CTCF enhancing cancer stem cell-like properties and tumorigenesis," *Theranostics*, vol. 10, no. 26, pp. 11950–11962, 2020.

[212] R. C. Poulos, J. A. I. Thoms, Y. F. Guan, A. Unnikrishnan, J. E. Pimanda, and J. W. H. Wong, "Functional Mutations Form at CTCF-Cohesin Binding Sites in Melanoma Due to Uneven Nucleotide Excision Repair across the Motif," *Cell Rep.*, vol. 17, no. 11, pp. 2865–2872, 2016.

[213] C. F. Méndez-Catalá *et al.*, "A Novel Mechanism for CTCF in the Epigenetic Regulation of Bax in Breast Cancer Cells," *Neoplasia*, vol. 15, no. 8, pp. 898-IN14, 2013.

[214] G. Filippova, C. Qi, J. Ulmer, J. Moore, and M. Ward, "Tumor-associated zinc finger mutations in the CTCF transcription factor selectively alter its DNA-binding specificity," *Cancer Res.*, 2002.

[215] Y. Zhang *et al.*, "CCCTC-binding factor acts upstream of FOXA1 and demarcates the genomic response to estrogen," *J. Biol. Chem.*, vol. 285, no. 37, pp. 28604–28613, 2010.

[216] L. Huang *et al.*, "Transcriptional repression of SOCS3 mediated by IL-6/STAT3 signaling via DNMT1 promotes pancreatic cancer growth and metastasis," *J. Exp. Clin. Cancer Res.*, vol. 35, no. 1, pp. 1–15, 2016.

[217] L. Wei *et al.*, "Knockdown of CTCF reduces the binding of EZH2 and affects the methylation of the SOCS3 promoter in hepatocellular carcinoma," *Int. J. Biochem. Cell Biol.*, vol. 120, no. January, pp. 1–10, 2020.

[218] W. Gong, Y. Liu, H. Qu, A. Liu, P. Sun, and X. Wang, "The effect of CTCF binding sites destruction by CRISPR/Cas9 on transcription of metallothionein gene family in liver hepatocellular carcinoma," *Biochem. Biophys. Res. Commun.*, vol. 510, no. 4, pp. 530–538, 2019.

[219] B. Zhang *et al.*, “The CCCTC-binding factor (CTCF)–forkhead box protein M1 axis regulates tumour growth and metastasis in hepatocellular carcinoma,” *J. Pathol.*, 2017.

[220] N. E. Sanjana, O. Shalem, and F. Zhang, “Improved vectors and genome-wide libraries for CRISPR screening,” *Nat. Methods*, vol. 11, no. 8, pp. 783–784, 2014.

[221] O. Shalem *et al.*, “Genome-Scale CRISPR-Cas9 Knockout Screening in Human Cells,” *Science (80-.).*, vol. 343, no. 6166, pp. 84–87, 2014.

[222] O. Shalem *et al.*, “Genome-scale CRISPR-Cas9 knockout screening in human cells,” *Science (80-.).*, vol. 343, no. 6166, pp. 84–87, 2014.

[223] D. S. Chandrashekar *et al.*, “UALCAN: A Portal for Facilitating Tumor Subgroup Gene Expression and Survival Analyses,” *Neoplasia (United States)*, vol. 19, no. 8, pp. 649–658, 2017.

[224] M. Czarnek, K. Sarad, A. Karaś, J. Kochan, and J. Bereta, “Non-targeting control for MISSION shRNA library silences SNRPD3 leading to cell death or permanent growth arrest,” *Molecular Therapy - Nucleic Acids*, vol. 26. pp. 711–731, 2021.

[225] D. Tschaharganeh, V. Ehemann, T. Nussbaum, P. Schirmacher, and K. Breuhahn, “Non-specific effects of siRNAs on tumor cells with implications on therapeutic applicability using RNA interference,” *Pathol. Oncol. Res.*, vol. 13, no. 2, pp. 84–90, 2007.

[226] P. Mali *et al.*, “RNA-guided human genome engineering via Cas9,” *Science (80-.).*, 2013.

[227] S. W. Cho *et al.*, “Analysis of off-target effects of CRISPR/Cas-derived RNA-guided endonucleases and nickases,” *Genome Res.*, vol. 24, no. 1, pp. 132–141, 2014.

[228] J. G. Doench *et al.*, “Optimized sgRNA design to maximize activity and minimize off-target effects of CRISPR-Cas9,” *Nat. Biotechnol.*, vol. 34, no. 2, pp. 184–191, 2016.

[229] Y. Fu *et al.*, “High-frequency off-target mutagenesis induced by CRISPR-Cas nucleases in human cells,” *Nat. Biotechnol.*, vol. 31, no. 9, pp. 822–826, 2013.

[230] B. P. Kleinstiver *et al.*, “High-fidelity CRISPR-Cas9 nucleases with no detectable genome-wide off-target effects,” *Nature*, vol. 529, no. 7587, pp. 490–495, 2016.

[231] T. J. Cradick, P. Qiu, C. M. Lee, E. J. Fine, and G. Bao, “COSMID: A web-based tool for identifying and validating CRISPR/Cas off-target sites,” *Mol. Ther. - Nucleic Acids*, vol. 3, no. 12, p. e214, 2014.

[232] B. Zhang *et al.*, “The CCCTC-binding factor (CTCF)- forkhead box protein M1 axis regulates tumour growth and metastasis in hepatocellular carcinoma,” 2017.

[233] Q. Sun, S. Y. Zhang, J. F. Zhao, X. G. Han, H. Bin Wang, and M. L. Sun, “HIF-1α or HOTTIP/CTCF Promotes Head and Neck Squamous Cell Carcinoma Progression and Drug Resistance by Targeting HOXA9,” *Mol. Ther. - Nucleic Acids*, vol. 20, no. 1, pp. 164–175, 2020.

[234] C. Liu, L. Deng, J. Lin, J. Zhang, S. Huang, and J. Zhao, “Zinc Finger Protein CTCF Regulates Extracellular Matrix (ECM) -Related Gene Expression Associated With the Wnt Signaling Pathway in Gastric Cancer,” vol. 10, no. February, pp. 1–14, 2021.

[235] T. Brabletz, R. Kalluri, M. A. Nieto, and R. A. Weinberg, “EMT in cancer,” *Nat. Rev. Cancer*, vol. 18, no. 2, pp. 128–134, 2018.

[236] J. P. Thiery, H. Acloque, R. Y. J. Huang, and M. A. Nieto, “Epithelial-Mesenchymal Transitions in Development and Disease,” *Cell*, vol. 139, no. 5, pp. 871–890, 2009.

[237] D. A. Lauffenburger and A. F. Horwitz, “Cell migration: A physically integrated molecular process,” *Cell*, vol. 84, no. 3, pp. 359–369, 1996.

[238] 2 Anne J. Ridley, 1 Martin A. Schwartz, 6 Keith Burridge, 5 Richard A. Firtel, 3 Mark H. Ginsberg, 7 Gary Borisy, 8 J. Thomas Parsons, A. R. Horwitz4, and Cell, “Labrousse, A. M., Zappaterra, M. D., Rube, D. A., van der Bliek, A. M., Vater, C. A., Raymond, C. K., Ekena, K., Howald-Stevenson, I., Stevens, T. H., Hoepfner, D., van den Berg, M., Philippsen, P., Tabak, H. F., Hettema, E. H., Ridley, A. J., Schwartz, M,” *Annu. Rev. Plant Physiol. Plant Mol. Biol*, vol. 143, no. December, p. 1233, 1998.

[239] W. Skupiński, J. Mikosz, and S. Malinowski, “ESR investigation of the MgO-VCl4 system,” *React. Kinet. Catal. Lett.*, vol. 14, no. 3, pp. 363–366, 1980.

[240] U. Raudvere *et al.*, “G:Profiler: A web server for functional enrichment analysis and conversions of gene lists (2019 update),” *Nucleic Acids Res.*, vol. 47, no. W1, pp. W191–W198, 2019.

[241] Y. Zhu, J. Liu, J. Park, P. Rai, and R. G. Zhai, “Subcellular compartmentalization of NAD+ and its role in cancer: A sereNADe of metabolic melodies,” *Pharmacol. Ther.*, vol. 200, pp. 27–41, 2019.

[242] B. Vaitheesvaran *et al.*, “Role of the tumor suppressor IQGAP2 in metabolic homeostasis: Possible link between diabetes and cancer,” *Metabolomics*, vol. 10, no. 5, pp. 920–937, 2014.
[243] W. Kim *et al.*, “Polyunsaturated Fatty Acid Desaturation Is a Mechanism for Glycolytic NAD + Recycling,” *Cell Metab.*, vol. 29, no. 4, pp. 856-870.e7, 2019.
[244] H. Yang *et al.*, “ SIRT 3–dependent GOT 2 acetylation status affects the malate–aspartate NADH shuttle activity and pancreatic tumor growth ,” *EMBO J.*, vol. 34, no. 8, pp. 1110–1125, 2015.
[245] A. L. Jackson and P. S. Linsley, “Recognizing and avoiding siRNA off-target effects for target identification and therapeutic application,” *Nat. Rev. Drug Discov.*, vol. 9, no. 1, pp. 57–67, 2010.
[246] D. D. Rao, N. Senzer, M. A. Cleary, and J. Nemunaitis, “Comparative assessment of siRNA and shRNA off target effects: What is slowing clinical development,” *Cancer Gene Ther.*, vol. 16, no. 11, pp. 807–809, 2009.
[247] L. Peretz *et al.*, “Combined shRNA over CRISPR/cas9 as a methodology to detect off-target effects and a potential compensatory mechanism,” *Sci. Rep.*, vol. 8, no. 1, pp. 1–13, 2018.
[248] B. Evers, K. Jastrzebski, J. P. M. Heijmans, W. Grernrum, R. L. Beijersbergen, and R. Bernards, “CRISPR knockout screening outperforms shRNA and CRISPRi in identifying essential genes,” *Nat. Biotechnol.*, vol. 34, no. 6, pp. 631–633, 2016.
[249] Le Cong *et al.*, “Multiplex Genome EngineeringUsing CRISPR/Cas Systems,” *Science (80-.).*, vol. 339, no. 6121, pp. 816–819, 2013.
[250] P. Zhang *et al.*, “Altered cell differentiation and proliferation in mice lacking p57(KIP2) indicates a role in Beckwith-Wiedemann syndrome,” *Nature*, vol. 387, no. 6629. pp. 151–158, 1997.
[251] S. Matsuoka *et al.*, “is a candidate tumor suppressor gene,” pp. 650–662, 1995.
[252] C. Giovannini *et al.*, “CDKN1C/P57 is regulated by the Notch target gene Hes1 and induces senescence in human hepatocellular carcinoma,” *Am. J. Pathol.*, vol. 181, no. 2, pp. 413–422, 2012.
[253] J. Wade Harper, G. R. Adami, N. Wei, K. Keyomarsi, and S. J. Elledge, “The p21 Cdk-interacting protein Cip1 is a potent

inhibitor of G1 cyclin-dependent kinases," *Cell*, vol. 75, no. 4, pp. 805–816, 1993.

[254] T. Abbas and A. Dutta, "P21 in cancer: Intricate networks and multiple activities," *Nat. Rev. Cancer*, vol. 9, no. 6, pp. 400–414, 2009.

[255] G. J. Hannon and D. Beach, "P15INK4B is a potentiel effector of TGF-beta-induced cell cycle arrest," *Nature*, vol. 371. pp. 267–261, 1994.

[256] Y. Xia *et al.*, "Dominant role of CDKN2B/p15INK4B of 9p21.3 tumor suppressor hub in inhibition of cell-cycle and glycolysis," *Nat. Commun.*, vol. 12, no. 1, pp. 1–15, 2021.

[257] S. K. Balakrishnan, M. Witcher, T. W. Berggren, and B. M. Emerson, "Functional and molecular characterization of the role of CTCF in human embryonic stem cell biology," *PLoS One*, vol. 7, no. 8, pp. 12–15, 2012.

[258] L. Zhang *et al.*, "BMP4 administration induces differentiation of CD133+ hepatic cancer stem cells blocking their contributions to hepatocellular carcinoma," *Cancer Res.*, vol. 72, no. 16, pp. 4276–4285, 2012.

[259] A. R. Barutcu, P. G. Maass, J. P. Lewandowski, C. L. Weiner, and J. L. Rinn, "A TAD boundary is preserved upon deletion of the CTCF-rich Firre locus," *Nat. Commun.*, vol. 9, no. 1, 2018.

[260] C. Barrington, D. Georgopoulou, D. Pezic, W. Varsally, J. Herrero, and S. Hadjur, "Enhancer accessibility and CTCF occupancy underlie asymmetric TAD architecture and cell type specific genome topology," *Nat. Commun.*, vol. 10, no. 1, pp. 1–14, 2019.

[261] H. Agarwal, M. Reisser, C. Wortmann, and J. C. M. Gebhardt, "Direct Observation of Cell-Cycle-Dependent Interactions between CTCF and Chromatin," *Biophys. J.*, vol. 112, no. 10, pp. 2051–2055, 2017.

[262] T. Kim *et al.*, "Comparative characterization of 3D chromatin organization in triple-negative breast cancers," *Exp. Mol. Med.*, vol. 54, no. 5, pp. 585–600, 2022.

[263] S. K. Rhie *et al.*, "A high-resolution 3D epigenomic map reveals insights into the creation of the prostate cancer transcriptome," *Nat. Commun.*, vol. 10, no. 1, pp. 1–12, 2019.

[264] J. E. J. Rasko *et al.*, "Cell growth inhibition by the multifunctional multivalent zinc-finger factor CTCF," *Cancer Res.*, vol. 61, no. 16, pp. 6002–6007, 2001.

[265] F. Docquier *et al.*, “Heightened expression of CTCF in breast cancer cells is associated with resistance to apoptosis,” *Cancer Res*, vol. 65, no. 12, pp. 5112–5122, 2005.

[266] J. Y. Lee, M. Mustafa, C. Y. Kim, and M. H. Kim, “Depletion of CTCF in breast cancer cells selectively induces cancer cell death via p53,” *J. Cancer*, vol. 8, no. 11, 2017.

[267] M. G. V. Heiden, L. C. Cantley, and C. B. Thompson, “Understanding the warburg effect: The metabolic requirements of cell proliferation,” *Science (80-.).*, vol. 324, no. 5930, pp. 1029–1033, 2009.

[268] J. Feng *et al.*, “Emerging roles and the regulation of aerobic glycolysis in hepatocellular carcinoma,” *J. Exp. Clin. Cancer Res.*, vol. 39, no. 1, pp. 1–19, 2020.

[269] X. Yu *et al.*, “Knockdown of FOXO6 inhibits glycolysis and reduces cell resistance to paclitaxel in HCC cells via pi3K/Akt signaling pathway,” *Onco. Targets. Ther.*, vol. 13, pp. 1545–1556, 2020.

[270] Y. Y. Lee *et al.*, “Subcellular tissue proteomics of hepatocellular Carcinoma for molecular signature discovery,” *J. Proteome Res.*, vol. 10, no. 11, pp. 5070–5083, 2011.

[271] V. A. Schmidt, C. S. Chiariello, E. Capilla, F. Miller, and W. F. Bahou, “ Development of Hepatocellular Carcinoma in Iqgap2 -Deficient Mice Is IQGAP1 Dependent ,” *Mol. Cell. Biol.*, vol. 28, no. 5, pp. 1489–1502, 2008.

[272] C. S. Chiariello, J. F. LaComb, W. F. Bahou, and V. A. Schmidt, “Ablation of Iqgap2 protects from diet-induced hepatic steatosis due to impaired fatty acid uptake,” *Regul. Pept.*, vol. 173, no. 1–3, pp. 36–46, 2012.

[273] Y. A. Guo *et al.*, “Mutation hotspots at CTCF binding sites coupled to chromosomal instability in gastrointestinal cancers,” *Nat. Commun.*, vol. 9, no. 1, 2018.